



TAMPEREEN TEKNILLINEN YLIOPISTO
TAMPERE UNIVERSITY OF TECHNOLOGY

JAAKKO TAPIOLA
COLD METAL TRANSFER CLADDING OF WEAR AND CORROSION RESISTANT COATINGS IN ENGINE APPLICATIONS

Master of Science thesis

Examiners: Prof. Petri Vuoristo and
Dr.Tech Jari Tuominen
Examiners and topic approved by the
Faculty Council of Engineering Sciences on 8th June 2016

ABSTRACT

JAAKKO TAPIOLA: COLD METAL TRANSFER CLADDING OF WEAR AND CORROSION RESISTANT COATINGS IN ENGINE APPLICATIONS

Tampere University of Technology

Master of Science Thesis, 138 pages, 3 Appendix pages

January 2017

Master's Degree Programme in Material technology

Major: Coating technology

Examiners: Professor Petri Vuoristo and Dr.Tech Jari Tuominen

Keywords: CMT cladding, hardfacing, stellites, solid lubricants, sliding wear, hot corrosion

Wear and corrosion are severe problems in gas and diesel engine components and to prevent these problems, number of solutions are available. In this thesis one of the possible solutions, cladding of engine components is studied with a state-of-the-art welding process, Cold Metal Transfer. CMT is a rather new and cost-effective method of welding and cladding with a limited heat input and a large variety of available materials. During this thesis, a great number of cladding tests with different cobalt-base alloy filler materials on different metallic base materials were run. These tests aimed to optimize the cladding parameters for a cored Co-alloy filler wire. Another region of interest was to optimize the tribological properties of the coatings in order to reduce friction coefficient and increase the wear resistance of the components. In this thesis, a powder feeder was used to spray particles into the melt pool during cladding.

It was discovered that CMT is able to restrain problems traditional overlay welding processes exhibit: high heat input resulting in unwanted changes of the base material, which also leads to high dilution and large amount of spattering during the process. The to-and-fro movement of the filler wire reduces the heat input and the precise process control with mechanical droplet detachment reduces the amount of spattering greatly.

The CMT-process optimization was successful for Co-base filler wire, and optimal parameters were achieved by cladding tests and analyzation of the results. The optimization resulted in low-diluted (<5 %) Stellite-coating (450-500 HV₁) with a proper fusion bond and a narrow Heat Affected Zone (HAZ). These results were confirmed by optical and scanning electron microscopy (OM and SEM), hardness measurements, X-Ray Diffraction (XRD) and Energy-Dispersive X-Ray Spectroscopy (EDS). Unmelted particles of chromium and tungsten remained in the coatings because of the rather large particle size inside the filler wire. The particle size needs to be reduced by the wire manufacturer in order to achieve fully homogeneous clad with low dilution and higher hardness. Currently the heat input is insufficient to melt the particles but optimal in terms of dilution. Sliding wear tests were run to determine the wear behavior of the clads produced with CMT. The work-hardening ability of Stellite was clearly visible, as hardness of wear surfaces increased up to 58 % (Stellite –pin) at RT and 63 % at 300 °C. The coatings produced with CMT show predictable behavior and no cracking was detected. Some particles were successfully impregnated into the clad utilizing high-energy ball milling powder preparation in order to optimize the surface properties in terms of wear and friction, but the results of their effect on wear remain for future studies.

TIIVISTELMÄ

JAAKKO TAPIOLA: Kulutus- ja korroosiokestävien pinnoitteiden valmistaminen CMT-tekniikalla moottorisovelluksiin
Tampereen teknillinen yliopisto
Diplomityö, 138 sivua, 3 liitesivua
Tammikuu 2017
Materiaalitekniikan diplomi-insinöörin tutkinto-ohjelma
Pääaine: Pinnoitustekniikka
Tarkastajat: professori Petri Vuoristo ja TkT Jari Tuominen

Avainsanat: CMT-pinnoitus, kovapinnoitus, stelliitit, kiinteät voiteluaineet, kuluminen ja korrosio

Kuluminen ja korrosio ovat vakavia ongelmia kaasu- ja dieselmoottoreissa ja niiden osissa. Niiden aiheuttamien ongelmien ehkäisyyn on monia saatavilla olevia ratkaisuja, joista pinnoittaminen on tämän työn tutkimuksen kohde. Näiden pinnoitusta tutkitaan Fronius International GmbH:n kehittämällä Cold Metal Transfer, eli CMT-hitsauksella. CMT on verrattain uusi ja kustannustehokas tapa hitsata ja tuottaa pinnoitteita matalalla lämmöntuonnilla ja laajalla materiaaliskaalalla. Tässä diplomityössä tutkitaan CMT-pinnoitettuja koboltti-pohjaisia Stelliitti-materiaaleja eri pohjamateriaalien päällä. Näiden pinnoitustestien tavoitteena on optimoida CMT-prosessiparametrit Stelliitti-täytelangalle. Toinen työn tavoite on tutkia pinnoitteen ominaisuuksien optimointia, jotta kitkakerrointa voidaan tiputtaa ja pinnoitteen kulumiskesto parantaa. Tässä työssä partikkeleita lisättiin pinnoitteeseen käyttämällä jauhesyötintä, jolla aineita syötettiin hitsisulaan pinnoitustapahtuman aikana.

Työssä havaittiin, että CMT-menetelmällä onnistutaan vähentämään perinteisissä päällehit-sausmenetelmissä tiedettyjä ongelmia; korkeaa lämmöntuontia, joka aiheuttaa suuren seostu-man, sekä materiaaliroiskeita, joiden määrä voi olla suuri perinteisillä menetelmillä. CMT-prosessissa tapahtuva langan edestakainen liike vähentää lämmöntuontia ja tarkasti säädelty prosessi mekaanisella sulapيسان siirrolla vähentää roiskeiden määrää.

Prosessiparametrien optimointi onnistui Stelliitti-langalla suoritettujen testien ja näytteiden analysoinnin yhteistuloksena. Tuloksena saavutettiin niukkaseosteinen (<5 %) Stelliitti-pinnoite (~450-500 HV₁) vahvalla sulasadoksella ja kapealla lämpömuutosvyöhykkeellä. Nämä tulokset vahvistettiin optisella mikroskopiolla ja pyyhkäisyelektronimikroskoopilla (OM ja SEM), kovuusmittauksilla, röntgendifraktiolla (XRD) ja energiadispersiivisellä alkuai-neanalyysaattorilla (EDS). Pinnoitteisiin jäi melko paljon sulamattomia kromi- ja wolframipartikkeleita niiden verrattain suuren kokonsa takia. Tätä partikkelikokoa tulee pienentää langanvalmistajan toimesta, mikäli halutaan homogeeninen ja niukkaseosteinen pinnoite aikaiseksi suuremmalla kovuudella. Nykyisellä koostumuksella lämmöntuonti ei riitä partikkeleiden sulamiseen ja yhtäaikaaisesti matalaan seostumaan. Pinnoitteille suoritettiin kulutusko-keita niiden kulumisominaisuuksien testaamista varten pin-on-disk -laitteistolla. Stelliittien muokkauslujittuminen kävi ilmi testeistä selvästi, ja pinnoitteiden kovuus kulumispinnalta nousi 58 % Stelliitti-tapin osalta huoneenlämpötilassa; 300 °C asteessa nousu oli jopa suu-remppaa (63 %). Pinnoitteet osoittavat ennustettavaa käytöstä eikä säröilyä tai pinnoitteen ir-toamista havaittu. Pinnoitteen kulumiskäyttämisen optimointiin käytettyjä partikkeleita saatiin lisättyä pinnoitteeseen kuulamylytetyyn jauheseoksen avulla, mutta tämän vaikutukset kulumiseen jäivät tulevaisuudessa tutkittaviksi.

PREFACE

This work was conducted at Tampere University of Technology in the department of Material Science and it is a part of Northern European Interreg project. This was a very interesting project and an opportunity to study and create something new and hopefully useful. I got to know a lot of new interesting topics and people during this project.

I would like to thank my supervisor Dr. Tech. Jari Tuominen for the great support and help he gave during this project. He was always available and provided me with a lot of information, and was a huge help during the experimental part of this thesis. I would also like to thank my other supervisor, Prof. Petri Vuoristo for the assistance, literature and great ideas. I would like to acknowledge the help from the staff of Laboratory of Mechanical Engineering and Industrial Systems (MEI) I got concerning robotics and guidance with the CMT-equipment.

Many thanks to the people who helped me with my experiments and research and aided with the various research equipment I used. Everyone at the department was willing to help unselfishly.

Tampere, January 25th 2017
Jaakko Tapiola

CONTENTS

1.	INTRODUCTION	9
2.	OVERLAY WELDING AND CLADDING	10
2.1	Fusion welding	11
2.2	Welding consumables	14
2.2.1	Filler material transfer	14
2.2.2	Forces affecting material transfer	15
2.3	Arc	17
2.3.1	Arc types.....	18
2.3.2	Arc and melt temperatures and process efficiency	20
2.3.3	Polarity of the arc.....	21
2.4	Shielding gases	22
2.5	Common overlay welding methods.....	24
2.5.1	Plasma transferred arc welding (PAW/PTAW).....	24
2.5.2	Submerged arc welding (SAW).....	25
2.5.3	Gas metal-arc welding (GMAW)	27
2.5.4	Laser surface cladding (LSC)	28
2.5.5	Gas tungsten arc welding (GTAW)	30
2.6	Typical hardfacing materials	31
2.7	Parameters affecting the properties of the weld	32
2.8	Overlay welding of Stellite coatings.....	34
3.	COLD METAL TRANSFER – THE PROCESS	37
3.1	Different CMT-processes and their characteristics	38
3.1.1	CMT	38
3.1.2	CMT Pulse.....	39
3.1.3	CMT Advanced.....	40
3.1.4	CMT Pulse Advanced	41
3.1.5	CMT Dynamic	42
3.1.6	CMT Pin and CMT SynchroPuls.....	43
3.2	The use of CMT process in cladding	44
3.3	Synergic lines	46
3.4	CMT-process correction parameters.....	47
3.5	Pros and cons of CMT cladding	48
3.6	Other cold arc processes	49
4.	MATERIALS AND WEAR IN ENGINE COMPONENTS.....	52
4.1	Processes causing wear in engine valves	53
4.1.1	Corrosion and hot corrosion processes	54
4.1.2	The prevention of hot corrosion	56
4.2	Special materials in diesel engine valves.....	57
4.3	The coatings used in engine applications.....	59

4.3.1	Nickel-base alloys	60
4.3.2	Cobalt-base alloys	60
4.4	Solid lubricants	62
4.4.1	Lamellar solids	64
4.4.2	Halides, metal oxide based materials and others	67
5.	OBJECTIVE OF THE THESIS	70
	EXPERIMENTAL PART	72
6.	MATERIALS	73
6.1	Base materials	73
6.2	Stellite 21 wire consumable	73
6.3	Co-alloy wire consumable	74
6.4	Stellite 12 powder	74
6.5	Solid lubricants	75
7.	RESEARCH METHODS AND EQUIPMENT	77
7.1	CMT welding equipment	77
7.2	Powder feeder	79
7.3	Planetary mill	79
7.4	Sample preparation	79
7.5	Microscopy	81
7.5.1	Low-magnification images with optical microscopy (OM)	81
7.5.2	High-magnification images with Scanning Electron Microscopy	81
7.6	Composition and material phases	82
7.6.1	Energy-Dispersive X-Ray Spectroscopy (EDS)	82
7.6.2	X-Ray Diffraction (XRD)	82
7.7	Surface roughness	82
7.8	Vickers hardness measurements	83
7.9	Wear tests (Pin-on-disc, ASTM-G99)	84
8.	CLADDING TESTS	86
8.1	Basic cladding tests	86
8.1.1	Stellite 21 coatings	86
8.1.2	Co-alloy coatings	88
8.1.3	Stellite 12 coatings (reference)	94
8.2	Cladding tests with solid lubricant powders	95
8.3	Remarks during basic cladding tests	99
9.	RESULTS, DISCUSSION AND FURTHER ACTIONS	101
9.1	Characterization	101
9.1.1	Stellite 21	101
9.1.2	Co-alloy	103
9.1.3	Stellite 12 (reference)	110
9.1.4	Solid lubricant coatings	112
9.2	Hardness measurements	118
9.2.1	Stellite 21	119

9.2.2	Co-alloy	119
9.2.3	Stellite 12.....	121
9.3	Summary	122
9.4	Surface roughness.....	123
9.5	Wear tests.....	123
9.5.1	Co-alloy disc (CMT) vs. Co-alloy pin (CMT), RT.....	125
9.5.2	Co-alloy disc (CMT) vs. Nialloy pin, RT	128
9.5.3	Co-alloy disc (CMT) vs. CrNi pin, RT	132
9.5.4	Co-alloy disc (CMT) vs. Co-alloy pin (CMT), 300 °C.....	134
9.6	Further Actions.....	137
10.	CONCLUSIONS.....	138
	REFERENCES.....	140
	APPENDIX A. MINUTES OF CLADDING TESTS, STELLITE 21	147
	APPENDIX B. MINUTES OF CLADDING TESTS, CO-ALLOY	148

LIST OF SYMBOLS AND ABBREVIATIONS

A	Ampere
A_c	Molten area above the surface of the base material
A_m	Molten area below the surface of the base material
AC	Alternating Current
Al_2O_3	Aluminum oxide
ALC	Arc Length Correction
$^{\circ}C$	Celsius
C	Carbon
CaF_2	Calcium difluoride
$CaSO_4$	calcium sulfate
CMT	Cold Metal Transfer
Cr	Chromium
DC	Direct Current; Dynamic Correction
DCRP	Direct current reverse polarity
DCSP	Direct current straight polarity
E	Welding Energy
EDS	Energy-dispersive X-ray spectroscopy
F_N	The predetermined force of the wear test
FCC	Face-centered Cubic
FCW	Flux-cored Wire
GMAW	Gas Metal Arc Welding
GTAW	Gas Tungsten Arc Welding
HAZ	Heat Affected Zone
hBN	Hexagonal boron nitride
HCP	Hexagonal close-packed
HTHC	High-temperature Hot Corrosion
HV	Vickers Hardness
LSC	Laser Surface Cladding
LTHC	Low-temperature Hot Corrosion
MAG	Metal Active Gas
MIG	Metal Inert Gas
mm	Millimeter
MMAW	Manual Metal Arc Welding
MoS_2	Molybdenum disulfide
NaCl	Sodium chloride
Na_2SO_4	Sodium sulfate
Ni	Nickel
OM	Optical microscopy
PI	Polyimide
PTA	Plasma-transferred Arc
PTFE	Polytetrafluoroethylene
R	The pin contact distance from the center of the disk
r_0	The diameter of the disk
SAW	Shielded Arc Welding
SEM	Scanning electron microscopy
SFE	Stacking Fault Energy

SMAW	Shielded Metal Arc Welding
TiC	Titanium carbide
TIG	Tungsten Inert Gas
TUT	Tampere University of Technology
V	Volt
v	The sliding velocity $v = R\omega$
V ₂ O ₅	Vanadium pentoxide
W	Watt
WC	Tungsten carbide
WS ₂	Tungsten disulfide
wt%	Weight percent
XRD	X-ray diffraction
μm	Micrometer
ω	Rotational velocity

1. INTRODUCTION

The subject of this thesis is to investigate the use of Cold Metal Transfer –cladding in producing wear and corrosion resistant coatings in diesel and gas engines. The goal is to study the suitability of this relatively new and cost-effective process in overlay welding of cobalt-base alloy called Stellite and to optimize the parameters of the cladding process to certain base and filler wire materials. Another goal is to study the use of solid lubricant impregnation into the coating to improve wear and corrosion resistance of the coatings. The CMT-equipment is located in the Department of Mechanical Engineering and Industrial Systems (MEI) at Tampere University of Technology. This thesis is a part of collaboration project called Interreg involving Universities and companies from Northern Europe, mostly Scandinavia.

The goal of the thesis is to study the use of a “cold” process in cladding. Usually, the problem with traditional arc welding/cladding methods is the high amount of heat they transfer into the base material during the process. Heat alters the composition of the base material, which is not desirable, because of the possible changes in critical material properties. Another issue about traditional methods is the spattering of the filler material. This spatter around the weld usually needs to be cleaned and this consumes money and time. CMT exploits a technique developed by Fronius International GmbH, where the to-and-fro movement of the filler wire reduces heat input into the base material, and similarly it assists the mechanical, low current, transfer of the filler material.

The theoretical part of this work walks through the basics of fusion and arc welding from the perspective of coating and overlay welding. Different overlay welding methods and processes are introduced in order to the reader to fully understand the phenomena occurring during cladding. Some typical materials used in hardfacing are presented together with the materials in the focus of this work. The wear and corrosion of engine components are studied in the material point of view. Cold Metal Transfer, CMT, is introduced together with some CMT-cladding studies and other “cold” arc welding processes. High-temperature solid lubricants are studied, and the possibility of impregnating them into hardfacings to reduce wear and friction.

Experimental work includes cladding tests and the characterization of the specimens. Solid lubricant addition into the clad was attempted using a powder feeder. After parameter optimization and characterization, sliding wear test were conducted. All of the tests were done in order to find out the suitability of CMT to an industrial scale cladding applications.

2. OVERLAY WELDING AND CLADDING

This thesis focuses on cladding with fusion welding methods. Besides of these, there are a dozen other methods of that can be used to create a coating, such as thermal spraying, electrochemical methods, physical and chemical vapour deposition and painting for example. The main idea of a coating is to create a protective layer onto the surface of the work piece to extend its lifetime, providing it with improvement to its normal properties. This layer can add protection against corrosion, wear, high-temperature corrosion, erosion, fatigue or even improve many of these properties, depending on the coating material. Material can be cladded multiple times if necessary, for example adding thick wear resistant layers or adhesive layers, thermal barrier coatings and such.

Surface cladding, or overlay welding, often refers to a situation where a layer of material is applied to a carbon or low-alloy steel to provide a corrosion-resistant surface. Hardfacing refers to a slightly different situation, where a material layer with increased wear-resistance is deposited to protect the component from different kinds of wear (abrasion, impact, etc.). Material layer may also have other protective features e.g. against corrosion and/or oxidation. Battering is quite similar to a bond coat, and it is applied to the surface of a component before the final top coat. Usually, this is done for metallurgical reasons; if the metallurgical properties of the base material and the top layer are dissimilar and cladding would not be successful [1]. Additive manufacturing/welding has increased its potential and the variety of applications in the last years, meaning adding extra material layers on top of each other to achieve demanded dimensions for a piece.

The obvious pros of overlay welding are the enhancements of material surface properties, including e.g. hardness, resistances to wear, corrosion and hot corrosion, erosion and such. The fusion/metallurgical bond between the coating/clad and the substrate material is the biggest benefit; the coating does not separate from the base material. The thickness of the coating is rather easy to control depending on the coating method, and multiple layers can be added to boost certain properties even further. There might be some negative side effects including the changes in the base material. The heat of the process alters the composition of the base material in the heat affected zone (HAZ). The width of the HAZ is dependent on the energy brought by the cladding technique. This results in changes of composition which affects e.g. hardness and strength of the HAZ. Too high dilution and penetration may result in lack of hardness in the coating and thus complicating the prediction of the lifetime of the component. An example of HAZ is shown in Figure 1. Cracks caused by transformations and heat may result in unexpected corrosion or wear behavior. This is why overlay cladding is quite sensitive to different parameters control-

ling the process and thorough tests are required when applying coatings to new applications. The high heat input may also cause geometrical changes, like bending, especially in thin components.

In Figure 1, the different zones can be clearly seen. This overlay has been manufactured with plasma transferred arc welding (PTA) with a nickel-based powder with tungsten carbide particles on a cold-worked tool steel. The dilution and penetration are quite high and the HAZ extends quite deep into the material. [2]

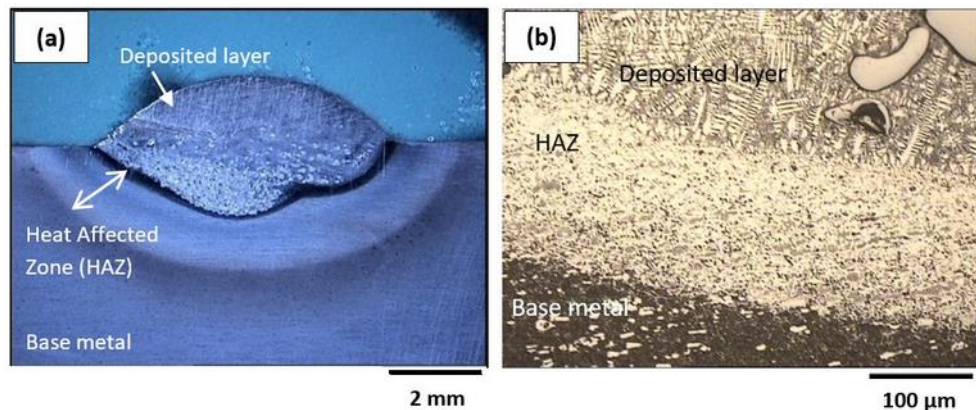


Figure 1. (a) Macrostructure, (b) Microstructure of one weld overlay bead with different zones visible. Manufactured with Plasma Transferred Arc welding (PTA). [2]

In this chapter the basic principles of electrically-powered arc-processes used in overlay welding are reviewed together with the most common welding processes used in manufacturing coatings.

2.1 Fusion welding

Fusion welding is defined as a process that uses thermal energy to create a weld pool by melting the metallic materials to be joined. This thermal energy brought into the process causes physical state changes, metal movement and metallurgical phase transformations in the work pieces. Weld pool creates a metallurgical bond between the metals when solidified, as the melting process allows these materials to intermix with each other. Usually a filler material with suitable material composition is added to add more strength to the bond. To create a weld pool and melt the filler material a powerful heat source is needed. Figure 2 presents fusion welding tree diagram. In this thesis, electrically powered arc-processes are taken under closer inspection along with laser-welding process under radiation-assisted welding. These two are marked with dark background colour. [3,4]

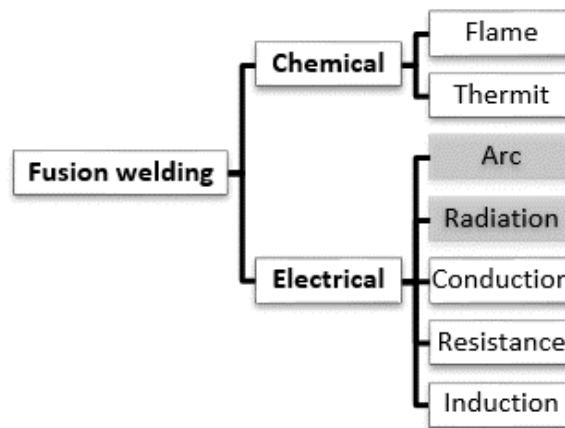


Figure 2. Fusion welding processes [3]

In arc welding the heat required to melt metal is produced by an electric arc. To form an arc a power source is needed, and this power source provides the welding voltage and current needed. Typically, current is DC (Direct Current); AC (Alternating Current) is used far less. DC means that the polarity of electricity remains unchanged during the whole process; cathode remains cathode and anode remains the anode at all times. The arc itself is formed between the base material and an electrode. To create an arc, the welding electrode lead must be connected to the power source (fixed connection, sliding contact). The work piece lead must be connected to the work piece with a clamp or such. These connections and the basic SMAW (shielded metal arc welding) graph is presented in Figure 3. The electrode is usually in a form of stick or wire, and it can be either consumable (gas metal arc welding, GMAW) or non-consumable (Gas Tungsten Arc Welding, GTAW). GMAW-processes include metal inert gas/metal active gas (MIG/MAG) -welding and GTAW-process include tungsten inert gas (TIG) -welding. For example, CMT is categorized under GMAW-processes. [3,5]

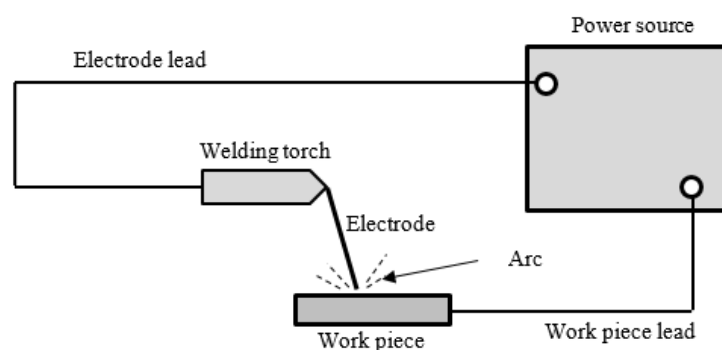


Figure 3. Simplified arc welding graph

In Figure 4 different arc welding methods are listed. The ones most used in industries and comparable to CMT-process are presented in this thesis.

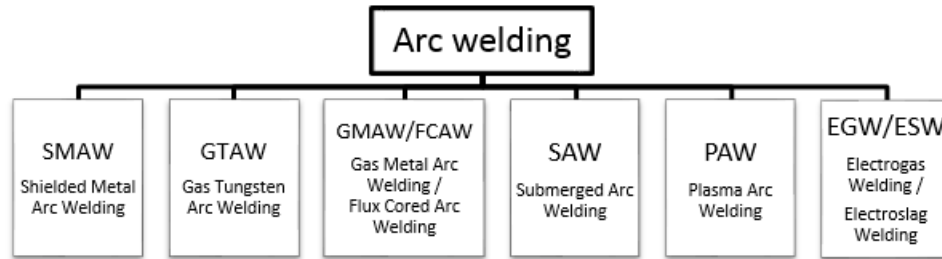


Figure 4. Arc welding processes [3]

Figure 3 presents a simplified arc welding assembly. The power source generates alternating or direct current, which is transferred to the welding torch via electrode lead. An arc is created between the electrode and the work piece, which creates enough heat to melt them together and thus creating a weld pool. As the weld pool solidifies, a weld bead is created. This bead can join pieces of metals together or in overlay cladding, create a coating. The differences of arc modes are presented in Figure 5.

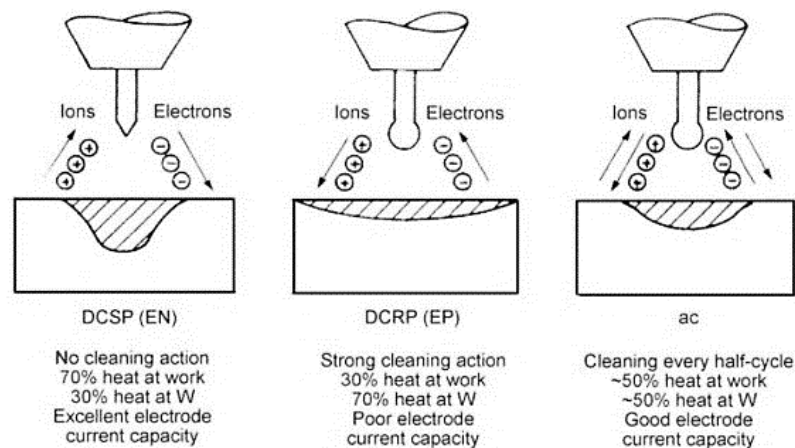


Figure 5. Characteristics of operating modes for GTAW. DCSP (EN), direct current straight polarity (electrode negative); DCRP (EP), direct current reverse polarity (electrode positive); ac, alternating current [5]

Besides arc welding, there are also other processes exploiting electrical power supply. In resistance welding, the pieces to be joined act as resistance units, and when pressing pieces together while current flows through them, heat is generated in the junction melting the pieces together. Induction welding generates heat with an external induction coil via eddy currents. Surfaces heat up and join together as they are pressed together. Induction welding is typically used in pipe manufacturing. In this thesis the focus is on the processes which can be used in cladding, presented in chapters 2.5 and 3. [6]

2.2 Welding consumables

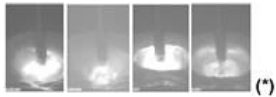
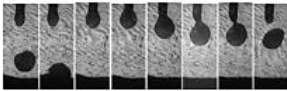
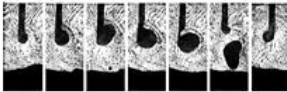
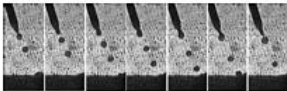
There are a number of different kind of welding consumables for different purposes and processes. Term “welding consumable” comprises both filler material and welding aid/adjuvant material. Filler material is the substance brought into the welding zone in the welding process, which creates the joint between the two surfaces, or which creates the coating in cladding process. Filler materials include for example wire electrodes, welding rods, powders and strips. Welding wire electrodes can be solid or cored. Welding adjuvant is the substance which enables the welding to take place or makes the welding process easier. Some example adjuvants are protective gases (argon, carbon dioxide and gas mixes) used in GMAW-processes and flux powders in SMAW. In MMA (SMA) welding the shell of the covered electrode can be thought as an adjuvant, because it contains materials generating protective gases and slag. Some problems might be encountered when using FCWs (flux-cored wires) as they always bring more oxygen into the weld and may have some issues with e.g. toughness. In addition, the powder inside the wire is never 100 % homogenous, as every step in the manufacturing process decreases the constancy inside the wire. [6]

It is also important to understand the difference between an electric conducting filler material (for example wire electrode) and non-conducting filler material (for example welding rod, welding filler wire). Filler material can be categorized with many different ways, based on properties of the wire; material, welding process, conductivity, structure etc. Also overlay filler materials can be categorized as a separate group. Some welding processes can use multiple types of filler materials simultaneously, for example Submerged Arc Welding (SAW), which uses both wire and flux powder. [6]

2.2.1 Filler material transfer

There are many types of material migration processes depending on the welding method. The transfer mode is also greatly dependent on the filler material, shielding gas and the values of current and voltage used in welding. In arc welding the migration happens via the high temperature of the arc. Typically, the material transfers in the shape of a drop, or in other words the transfer mode is thus globular transfer. Droplet is formed at the tip of the filler material under high heat, and with the help of various forces, is migrated into the weld pool. The modes of transfer can be separated into three categories; contact transfer, free-flight transfer and slag-protected transfer. Different material migration modes in arc-welding are presented in Table 1. Fast solidifying of the weld and the fact that forces affecting the droplet migration are greater than gravity, enable welding to be done in various positions. In CMT-welding the to-and-fro movement of the wire also assists the droplet detachment mechanically in addition of the factors mentioned in this chapter. [4–7]

Table 1. GMA-welding material transfer modes [7]

Group of modes	Transfer mode	Appearance	Main governing force (effect)
Contact transfer	Short-circuiting		Surface tension and electromagnetic pinch effect
	Bridging		Surface tension
	Forced short-circuiting		Strongly pronounced electromagnetic pinch effect
Free-flight transfer	Globular		Gravitational force
	Repelled globular		Gravitational force and repelling forces
	Projected spray		Electromagnetic force
	Streaming spray		Electromagnetic force
	Rotating spray		Electromagnetic force
	Explosive		Electromagnetic force and chemical reactions

2.2.2 Forces affecting material transfer

The forces affecting material transfer are presented next. These forces impact the transfer mode of the droplet listed in the table above.

Viscosity and surface tension

Droplet is the most advantageous shape for fluids, because fluids tend to keep their volume so that the outer area is as small as possible. Viscosity and surface tension affect the size of the filler material droplet at the tip of the filler. As temperature and oxygen level decrease, both viscosity and surface tension increase. High surface tension and viscosity values make the droplet size smaller. [6]

Gravity

Welding in “normal” position gravity pulls the droplet downwards as the size of the droplet grows high enough. Usually gravity is not a significant force affecting the migration,

because if it were, “inverted” position welding would not be possible (inverted meaning migration happens upwards). [6]

Plasma flow

Plasma flow enables the migration to happen at opposite direction than gravity. The arc is shaped like a cone downwards to the direction of the work piece. Power density is greater closer to the filler material in the arc, which causes the constrictive force of the magnetic field to bring about an additional force parallel to the filler material. This results in a powerful arc plasma flow inside the arc. These forces, and expanding gases in the arc, cause a strong plasma flow with a velocity close to the speed of sound. In consequence of these phenomena a suction is created to ease the droplet shedding. [6]

Pinch-force

Pinch-force, or Lorenz-force, is created as the current in the filler material causes a transverse magnetic field; this field creates a force that pinches the molten tip of the wire and detaches a droplet. This is presented in Figure 6. Another force, to the direction of the wire, impels the detached droplet to the direction of the work piece. Pinch-force is directly proportional to the square of the welding current. Pinch-force is the most important force in MIG/MAG-welding with inert protective gas (argon, argon-mix). This force is so strong that the droplets are very small and the migration happens almost jet-like with no short-circuiting. [6]

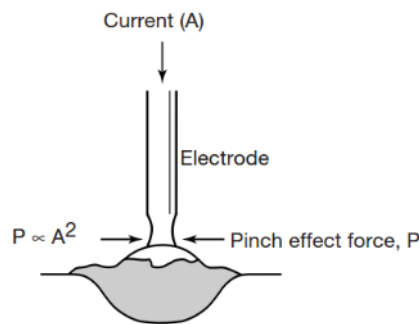


Figure 6. Pinch-effect during short-circuiting transfer [8]

There are also two forces opposing the separation of the droplet from the electrode. Arc located directly underneath the droplet can create a force directed upwards which supports the droplet and prevents the separation of it. An arc can also overheat the droplet causing the metal to vaporize creating a steam-jet, which may support the droplet upwards or even cause the droplet to be thrown out of the arc. These forces are relevant in MAG/CO₂-welding with high welding currents. [6]

2.3 Arc

It is vital to understand the basics of the arc in order to comprehend the CMT-process, since the whole process depends on the precise control of the arc. The arc converts electrical energy into heat during the welding process. An arc is capable of producing temperatures and heat inputs high enough to melt any material. Arc is the most important energy source in welding industry because it is easy to create and maintain, and also for its high power density. Short, it is a burst of electrically charged particles in a gas medium. Air is a bad conductor but with certain preconditions current can travel in it; if the air gap is small enough and the voltage is high enough. Also, the air gap must be ionized. There are always some conducting particles in air and when they are exposed to the electric field of the welding circuit, particles travel towards the opposite pole. Negatively charged electrons travel towards the positive pole (anode) and positively charged ions towards negative pole (cathode). The voltage regions of the arc are presented in Figure 7. [5,6]

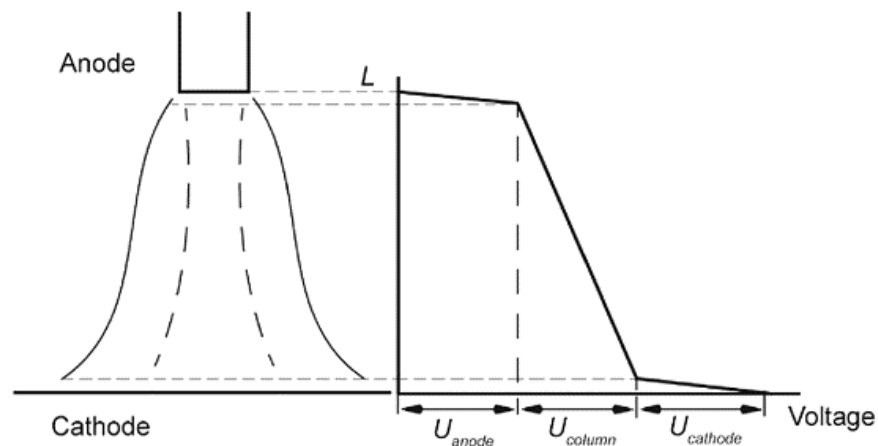


Figure 7. Voltage distribution in the arc. [9]

The kinetic energy of the electrons is controlled by the voltage. While travelling towards the anode electrons collide with gas molecules, whose electronic balance is disturbed by these collisions and they disintegrate into atoms. This phenomenon is called disassociation. This process continues, as in the collision new electrons are being released from the atom orbits and new collisions take place over and over again. Remaining atoms, or now ions, are positively charged and move towards cathode. This whole process of gas becoming conductive is called ionization, which leads to current flow in the arc of the welding circuit. The metallic substrate also has an electron cloud surrounding it and by the effect of the electric field with high temperature the electrons travel towards the anode. The kinetic energy of the electrons and ions is transferred into heat in the collisions at anode and cathode. [6]

Two types of arcs can be categorized in the field of arc welding; arc between non-consumable electrode and work piece (in TIG and plasma welding) and arc between consumable electrode (filler material) and work piece (MIG/MAG, CMT, SAW, stick/SMAW welding). The length of the arc varies greatly depending on the welding process and parameters. Typically, it varies approximately from 1 to 10 mm. Accurate measurements can be difficult to state as part of the arc occurs in the melt and cannot be seen. [6]

The ignition of the arc can be done with either short circuit or by an external ignition system, or spark-ignition. Short circuit ignition occurs by touching the work piece with a conducting filler material. At the point of contact very high local densities of current are created due to the small area. This causes high local heating and melting and overheating of the metal. This produces metal steams which ionize easily. The hot cathode surface begins to emit electrons. At the time of the short circuit, voltage drops close to zero for a very brief period of time. After the short circuit, the filler material is lifted slightly and the arc ignites. This short-circuit method is used in stick welding, MIG/MAG-welding, SAW, and sometimes in TIG-welding. Usually TIG-welding arc ignition is done with spark-ignition. [6]

2.3.1 Arc types

There are different types of arc which affect the material transfer mechanisms. Figure 8 shows the voltage and current regions of each arc type. The characteristics of each type of arc are presented in this chapter.

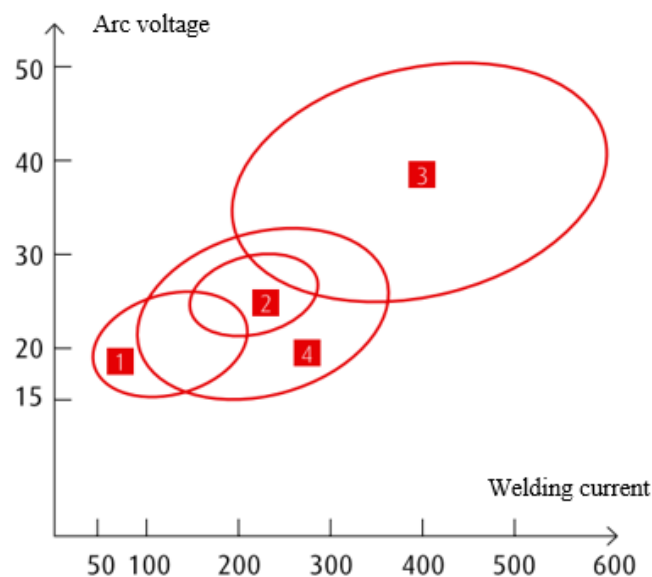


Figure 8. Arc types in fusion welding. 1=short arc, 2=intermediate arc, 3=hot arc, 4=pulsed arc. [10]

In short-arc welding the filler material is transferred via short circuits. Filler wire creates a short circuit as the droplet migrates into the weld. The number of short-circuits varies between 20 to 200 per second depending on shielding gas and other factors. Heat input is moderate because the arc is extinguished during the short circuits. Short-arc welding is suitable for thin sheet welding because of the low heat input. In intermediate arc-welding the filler material transfers as droplets and via short-circuiting, but because the big size of the droplet and arc forces cause high amounts of spattering and fumes, this region should be avoided. Figure 9 presents filler material migration of short-arc and intermediate arc-welding. [10]

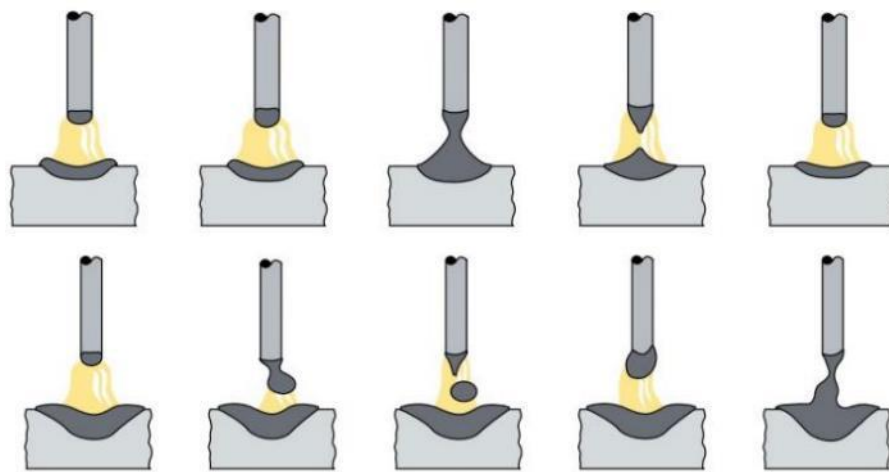


Figure 9. Short-arc welding (top) and medium arc-welding (latter) [10]

In hot arc welding the material transfer occurs as small droplets without short-circuiting. This method requires the use of Argon-based shielding gas, which maintains the stability of the arc. CO₂-based gases cause unstable arc and lots of spattering, and thus cannot be used. Hot arc welding provides high welding speed with low spattering, smooth weld bead, good penetration and a stable arc. The filler material migration in hot arc welding is presented in Figure 10. [10]

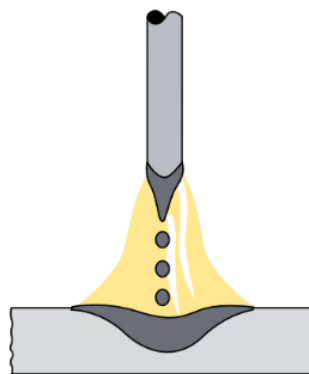


Figure 10. Material transfer in hot arc welding [10]

In pulsed arc welding the welding current is being pulsed to achieve steady arc and filler material transfer together with low heat input. Penetration is even along the weld and spattering is low, and it is easier to achieve pore- and crack-free weld bead. Filler material is transferred in fairly large droplets without short-circuits. Pulsed arc enables the use of thick filler wires with reasonably low voltage. The material transfer mechanism is presented in Figure 11. [10]

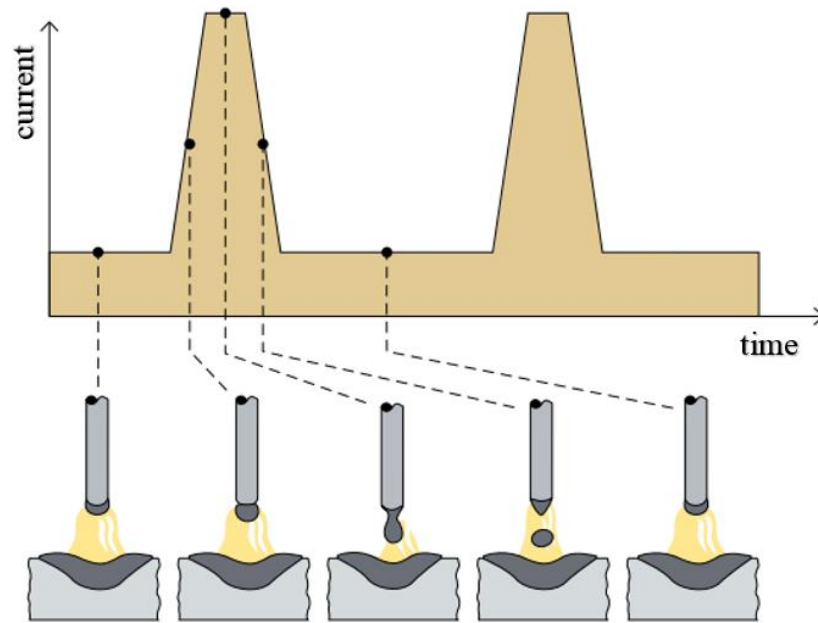


Figure 11. Material transfer in pulsed-arc welding [10]

2.3.2 Arc and melt temperatures and process efficiency

The temperature in the arc is higher in the anode than the cathode. This is because the electrons collide at high speeds into the anode, and some of the power at the cathode is consumed into the emission of the electrons. The temperatures in both anode and cathode depend vastly, among other things, on arc type, protective gas and filler material. Temperatures set mainly between 2500-3500 °C. Anode temperature is usually around 500 °C higher than cathode. This concerns an arc between non-consumable electrode and work piece. When the other pole is consumable the situation might be different. [6]

The core temperature of the arc is significantly higher than the temperatures at either of the poles. Approximate temperatures in different welding processes according to literature: stick welding 5000-6000 °C, SAW around 6000 °C, MIG over 8000 °C, TIG 10000-30000 °C and plasma welding over 20000 °C. [6]

With traditional welding methods the temperature in the weld pool in steel welding, depending on the process and protective gas, is around 1600-2200 °C. Accurate measurements are difficult to achieve, as many factors affect the temperature and measuring it is

not an easy task. Arc temperature may exceed the boiling point of metal (e.g. low-alloy steel ~ 2700 °C), which mean the metal can vaporize and release harmful steams. Weld pool is in a molten state from 1 to 10 seconds with traditional methods. This time has been reduced with less heat input using CMT-process. [6]

Another way of estimating the heat and efficiency of welding processes is to take a look at power densities. Generally, it is stated that to melt most metals, a heat-source power density of approximately 10 W/mm² is needed. As the intensity goes to a level of 10^4 – 10^5 W/mm² it is enough to vaporize most metals in only a few microseconds. Figure 12 presents the power density spectrum and some intensity levels of typical welding processes. High power densities mean that the processes are able to produce deeper and narrower welds with small HAZ. [5]

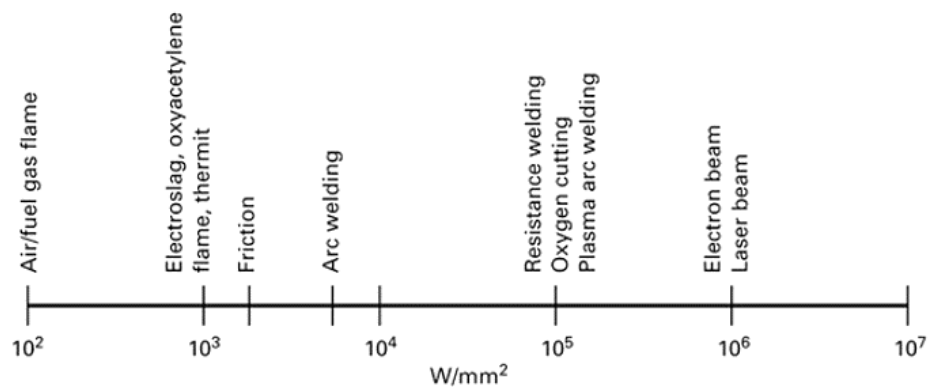


Figure 12. Power densities of welding heat sources [5]

Efficiency of the process relates to the power density, and typically the higher the power density, the better the process efficiency, because the heat conduction losses remain low. In keyhole laser welding the process efficiency is high, but with laser cladding the efficiency is typically only around 10 %; vast amount of the laser light is reflected off the melt pool. With MIG/MAG-welding the efficiency is stated to be 70-80 % depending on process parameters. Pépe et al. [11] studied process efficiencies of controlled gas metal arc welding processes that CMT-process has a process efficiency around 90 %. Other GMAW-variables also achieved values over 80 %.

2.3.3 Polarity of the arc

Newer CMT-processes (CMT Advanced, CMT Pulse Advanced) exploit the changes in the arc polarity to improve the properties of weld and to reduce the heat input of the process. Polarity has a big effect on the penetration and deposition rate of the process and it also affects the melting speed of the filler material. The effects depend strongly on the welding process. Penetration, the melting speed of the filler material and deposition rate depend on other things than the heat (difference) of the poles. Usually is stated that in

TIG-welding the +pole is slightly hotter than the –pole, but this does not necessarily apply to other welding processes. The effect of polarity when using consumable electrode on deposition rate and penetration can be seen in Figure 13. [6,9]

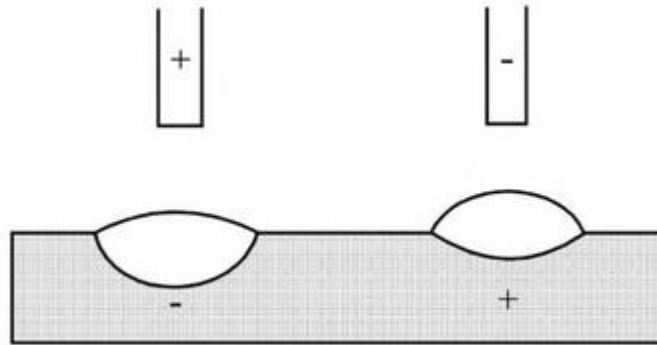


Figure 13. Positive electrode gives good penetration with lower deposition rate than the use of negative electrode [9]

Usually it is stated that penetration is greater in the +pole and deposition rate is higher in the –pole with no thorough reasoning. It is presumed that penetration depends on the forces in the melt pool caused by the arc, which grow stronger with higher welding powers. The arc forces affect the behavior of the melt pool by transferring it mechanically. In MIG/MAG-welding less heat is being generated in the +pole than –pole. One explanation to the lower penetration in the –pole is that the melting speed of filler material is greater which makes the weld pool bigger. This prevents the penetration of arc in the pool and thus makes the pool also a bit colder. Polarity also affects the spattering and the stability of the arc. In MIG/MAG welding, using solid wire, spattering is higher if –pole is used due to a moving cathode point at the end of the wire. The greatly increased spattering is why the 20-30 % bigger deposition rates provided by the use of -pole cannot be exploited and +pole is mostly used in MIG/MAG-welding. This is not a big problem in cladding applications which benefit in higher deposition rates, as the surface is usually machined after cladding. [6]

2.4 Shielding gases

The main objective for protective gas is to protect the heated and molten metal from the surrounding atmospheric air and to provide propitious circumstances to the stability of the arc. If the oxygen in air gets in touch with the molten metal it tends to oxidize it and the surroundings, where nitrogen and humidity of air cause pores in the weld. The composition of the protective gas affects the migration of material from the filler into the weld pool which has an impact on the amount and size of spatters around the weld. In addition, the gas has also effects on several properties of the weld and the process: looks, shape,

welding speed, strength (via combustion of additives), corrosion properties and slag formation on top of the weld. [12]

There are active and inert gases tailored for different applications and materials. Protective gas can be either inert or active; inert gas does not react with the substances in the weld pool and active does. Active gas is typically a mix of argon and carbon dioxide (CO_2), argon and oxygen, or argon, oxygen and CO_2 . Pure CO_2 is also used. Inert gases are argon, helium or mix of these two. Argon is usually the main component in MIG/MAG and TIG-welding. Pure argon is not suitable for MAG-welding of steels because the arc becomes unstable. CO_2 , O_2 or the mix of these two is usually used as an oxidizing component to stabilize the arc and to provide more stable migration of filler material into the weld. The effects of different components in shielding gases are presented in Figure 14. [6,12]

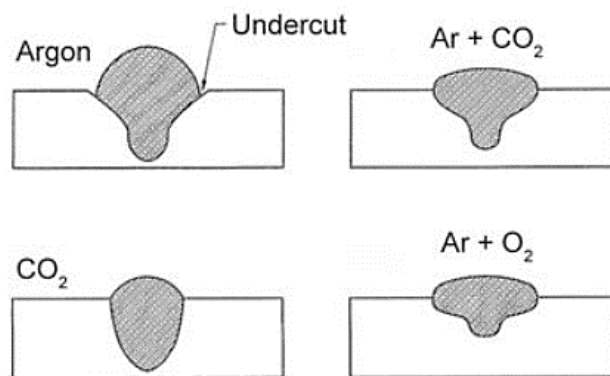


Figure 14. Effect of shielding gas type on weld penetration and shape for steel [5]

Carbon dioxide is more beneficial than oxygen as an oxidizing element. Some of the benefits are better looks and geometry of the weld bead. This is due to the changes of fluidity caused by surface tensions and the amount of oxidization in the weld pool. When using CO_2 , oxidization level and slag formation both decrease, and the weld requires less machining afterwards. CO_2 also provides higher penetration than oxygen. This is mainly due to higher arc voltage and energy inputs compared to argon-oxygen gas mixes. [5,12]

Helium is used with argon together with a few percent of CO_2 or O_2 addition in MAG-welding of stainless steels. Pure helium (or Ar-He mix) is used in TIG- and MIG-welding. Compared to argon-based gas, helium provides slightly better side penetration and an increase in welding speed due to higher arc energy, although the arc becomes more sensitive to length changes. Helium also provides better wettability of the material. Downside of helium is the high price. [12]

Other components of a protective gas can be hydrogen (H_2), nitrogen (N_2) and nitrogen monoxide (NO). Hydrogen can be used as a component when TIG-welding austenitic stainless steels. Hydrogen addition makes the arc hotter and more concentrated providing

greater welding speed and better penetration into the substrate. H_2 also makes the geometry of the weld bead smoother and reduces oxidation. Nitrogen is not a common component, but it can be used in TIG-welding of nitrogen-alloyed austenitic and super duplex steels to recover some of the nitrogen lost from the steel during the welding. Nitrogen monoxide (NO) is used to reduce the amount of ozone (O_3) generated in the welding process. Ozone is generated during the welding process, when ultraviolet light caused by the arc reacts with oxygen molecules, O_2 , splitting them into two. Oxygen atoms then react with oxygen molecules generating ozone, O_3 . Ozone can cause various harms to your health and therefore the amounts of it must be kept minimum (below 0,05 ppm (health regulations in 2009)). NO reacts easily with ozone generating NO_2 and O_2 . [5,12]

2.5 Common overlay welding methods

In the following chapters some welding processes for overlay cladding/hardfacing are presented briefly. This is to give some type of comparison between the CMT and the processes already widely spread in the industries. The review includes plasma-, arc-, TIG- and laser-welding processes. These methods are all used for producing wear and corrosion resistant overlays, such as nickel-tungsten carbide (Ni-WC), chromium carbide and Stellite coatings, although they can be used to produce most types of metallic coatings. CMT-process can be categorized under GMAW-processes since it has been developed from MIG/MAG-process.

2.5.1 Plasma transferred arc welding (PAW/PTAW)

Plasma transferred arc welding is a similar process with the GTAW; tungsten electrode and the base metal form an arc between them while shielding gas is being flooded to protect the weld pool from contaminants. A water-cooled arc constrictor is used to increase the energy density in the arc. Temperature of the plasma jet can reach up to 20000 °C. To be more precise, there are two types of arcs in plasma welding: transferred arc and non-transferred arc. In transferred arc the plasma arc transfers from the electrode into the work piece, which is a part of the electrical circuit. Heat is also generated via the anode spot in the work piece in addition to the arc. Non-transferred arc means that the arc is formed between the electrode and the nozzle of the burner and the work piece is not part of the circuit. Plasma jet is the only source of heat. Transferred-arc is typically used in welding and cladding, and non-transferred arc in cutting and spraying applications. Plasma arc welding process is presented in Figure 15. [6,13]

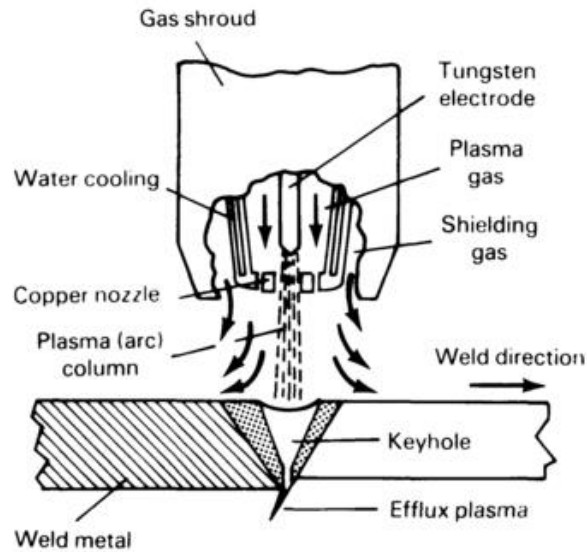


Figure 15. Plasma arc welding process. Figure shows constriction of the transferred-arc by copper nozzle and a keyhole through the plate [4]

Separating this process from GMAW and SAW-processes, PTAW usually utilizes consumables in powder form. The consumable is fed into the process with the help of carrier gas through the welding gun. As the consumable is in powder form, as high HI (Heat Intensity) is not needed to reach deposition rate of the same level as other arc based overlay methods. PTAW can be used in cladding as well. [13]

PTAW process has a restrained dilution into the substrate (<10 %) compared to other arc based processes. The overlays have very good adhesion to the surface with metallurgical bonds and have usually low number of defects. The powder consumable also provides the possibility to customize the composition of the coating by mixing different powder with each other, as long as the size of the particles in the powders are somewhat equal. Typical deposition rates range between 1-10 kg/h with automated systems; the process is not done manually. [13]

2.5.2 Submerged arc welding (SAW)

Submerged Arc Welding (SAW) is an arc welding process where the arc burns between the filler material and the work piece under a powder flux. Flux protects the weld from atmospheric contamination and some of it melts creating a protective slag layer on top of the weld. The arc burns in an arc cavity which is formed inside the flux caused by gases and metal fumes created in the process. Its “walls” are melted substrate, weld pool and melted flux slag layer in front, behind and on top of the arc, respectively. This means the arc is not visible to the observer which is beneficial for the working environment. The flux powder is fed through the flux inlet in front of or centrifugally on top of the arc. The final composition of the weld can be quite easily adjusted by additives in the flux powder.

For example, when using SAW in CCOs (chromium carbide overlay) the flux typically contains elements such as chromium, carbon, manganese and molybdenum. Excess powder is recovered and re-used in the process. SAW provides very good deposition rates even up to 23 kg/h with single wire, some references mention that even 70 kg/h can be achieved. Multiple SAW wire systems are available to further increase the deposition rate and efficiency of the process; literature know values up to 100 kg/h. Wires used in SAW overlay welding are thick. Also strip consumables are used, providing lower penetration. Typically strips are soft and ductile alloys because of manufacturing reasons. Strips are mainly used for corrosion protection. Figure 16 presents the schematic of typical weld pool dynamics. [6,13,14]

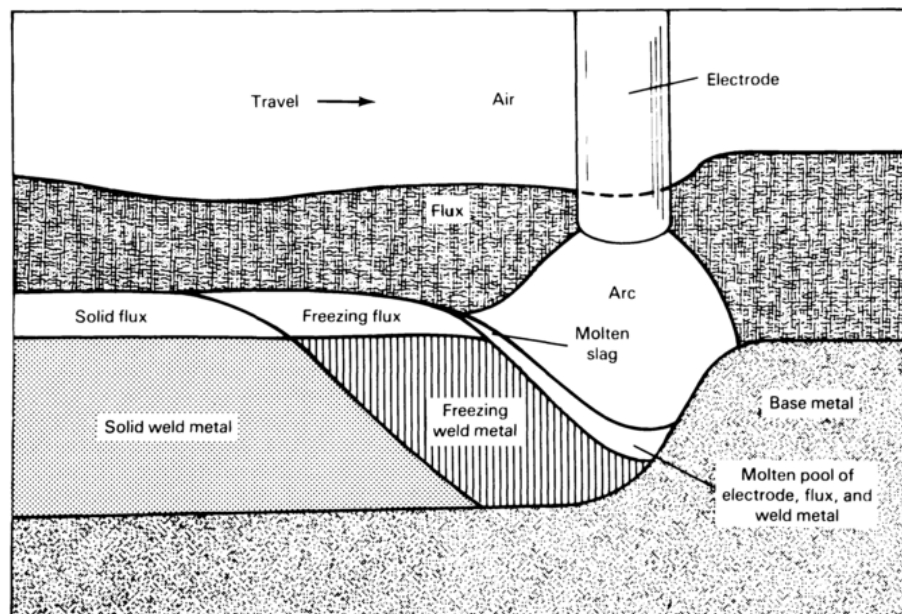


Figure 16. Schematic of SAW-process, weld pool dynamics [4]

Flux powder and slag are efficient in stopping radiation and in heat insulation. This means higher amount of the welding energy is being used in melting the filler and work piece than in processes using open arc. SAW process is typically automated, either the welding torch or the work piece is being moved during the welding. Welding current varies from 300 A to 1200 A, which is more than in typical arc welding processes. This, together with high welding energy, causes SAW to have high penetration depths, which again cause higher amount of melted base material. This can be an issue because HAZ is very large and the properties can be unpredictable (e.g. fragility). Typically, direct current (DC) is used, but alternating current (AC) is used in multiple-wired systems. [6,13]

Quality of the weld bead is usually consistent and good without pores or closures because of the slow solidification times of the weld. The slag and flux also provide good protection to the weld. In cladding solutions most common product manufactured by SAW are CCOs when wear resistance is wanted. Tungsten carbide overlays suffer from dissolution of the carbides because of the high temperature in the weld pool caused by the process. The high

amount of dilution related to high amount of HI can also cause various challenges, like decrease in wear resistance in some coatings and altering the behavior of some overlays. High heat input also causes large amounts of distortion in the work pieces. SAW can only be performed in flat position and cannot be used to repairs on-site because of the size and other restrictions of the process. [6,13]

2.5.3 Gas metal-arc welding (GMAW)

GMAW is general name for metal-arc active gas welding (MAG) and metal-arc inert gas welding (MIG). It is the most commonly used welding processes industrially. MIG/MAG welding is a metal-arc welding process, where an arc is created between a wire electrode and work piece, while the arc is being protected with protective gas. Melt is transferred from the tip of the wire electrode in droplets into the weld pool. Wire is fed by a wire feeder through the welding torch into the arc at a constant rate. Welding current is transferred from the power source via power cable to a contact tip in the welding torch and into the wire. Protective gas protects the arc and weld pool from atmospheric contamination. Typically, it is stated that MAG is related to welding of steels and MIG is welding of non-ferrous metals. The GMAW-system consists of a welding gun, a wire feed unit, a power supply, electrode and shielding gas-system. The basic principle is presented in fig. 17. [6]

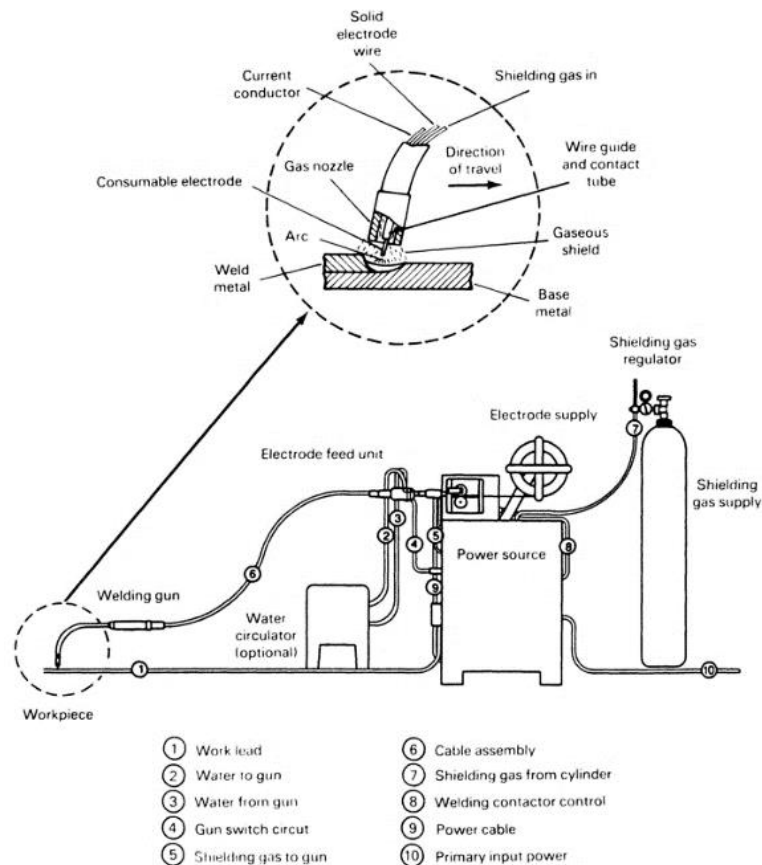


Figure 17. Schematic of GMAW process [4]

Arc ignition happens, when the tip of the wire touches the surface of the work piece: a short circuit is thus created and a strong short-circuit current melts and evaporates the tip of the wire lighting the arc. Protective gas helps to make the conditions propitious for a steady arc. Process can be either automatized and/or robotized, or done manually. Typically, current values range from 80 A to 350 A, depending on the diameter of the wire and the type of the arc. High current densities are typical to GMAW-processes because of thin filler wires. This enables high penetration values increasing with high power values. Usually DC-power source is used, but there are also AC-welding equipment for especially for thin plate welding. GMAW-processes are versatile and are capable of producing different types of welds and clads, they are easy to use, compact in size and typically quite inexpensive. Typical deposition rates vary between 2-7 kg/h, but can be up to 10 kg/h. Value is strongly dependent on current, wire diameter, distance between nozzle and work piece and the quality of the wire. [6,12–14]

2.5.4 Laser surface cladding (LSC)

Probably one of the most important invention of modern times is laser (light amplification by stimulated emission of radiation). It is used widely across all industries and it is also applied in producing coatings. The basic idea of LSC is that a new layer of material (metallic, composite) is fused onto the surface of the material by using a coherent and high-intensity laser beam irradiation. The laser beam itself is created by bringing energy in the form of electricity or light into a medium. The electrons in the medium become excited and begin to release energy in the form of photons. After this, the electromagnetic energy created is focused into the surface of the material. The energy absorbed by the material turns into heat via the interactions between atoms in the lattice. Interactions create vibrations which create localized heat energy. This causes melting and/or evaporating in the material and creates a melt pool. [15]

Lasers can be divided by the medium; it can be gas, liquid or solid. Most common types of lasers used for cladding are CO₂-lasers, Nd-YAG lasers and diode-lasers, although fiber lasers have mostly replaced both CO₂ and Nd-YAG-lasers. The substantive difference between different types of lasers is the wavelength of the light produced (CO₂: 10.6 μm; Nd-YAG: 1.06 μm; diode: 0.8-1.0 μm). Figure 18 presents absorption of different wavelengths to different metals; the amount of beam power that is absorbed by the work piece instead of reflecting from it. [16]

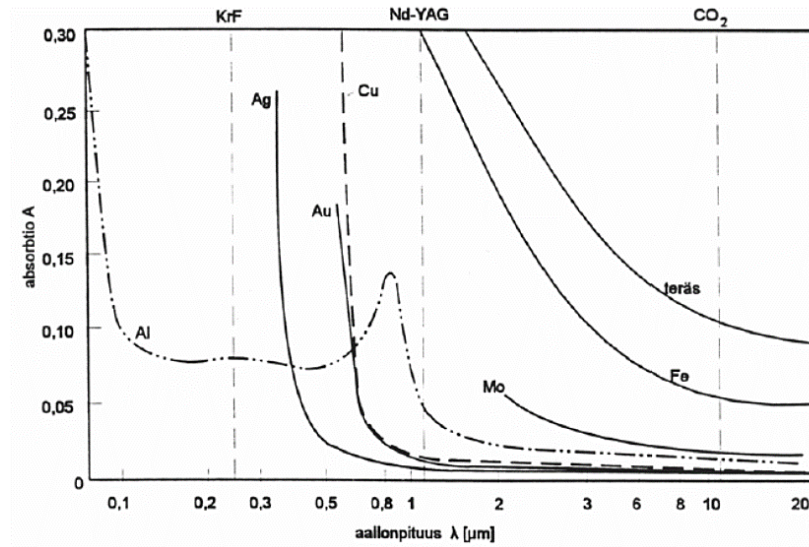


Figure 18. Absorption of different lasers in some materials [16]

When cladding, the additive material can be pre-placed onto the surface (2-step laser cladding) or added into the process, and usually the additive material is in a powder-form, although also a wire can be used (1-step laser cladding). The additive material can be fed off-axis or coaxial. These methods are presented in Figure 19. This process can be applied with different material surfacing applications, such as surface property modification, repairing and manufacturing complex three-dimensional components. It can be easily automated, it's fast and very accurate. Relatively thin coatings can be produced by laser coating, starting from 0,1 mm up to 5 mm. High power laser cladding is able to deposit up to 9 kg/h, but such values require expensive equipment. Typically, deposition rates vary between 1.5 and 4.5 kg/h with conventional LSC processes. [15–19]

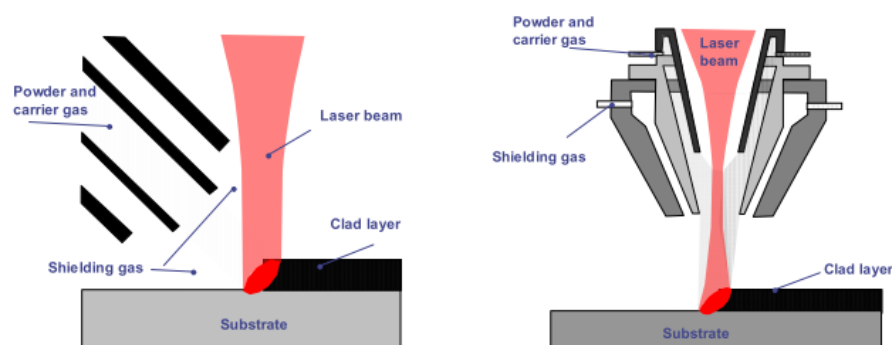


Figure 19. 1-step laser cladding; off-axis and coaxial powder feeding [19]

The effect of wavelength in laser cladding is significantly higher than in laser welding. The most efficient laser is the one with the shortest wavelength. For example, to reach the same cladding efficiency as with a 2.5 kW diode-laser, a 6 kW CO₂-laser or a 3 kW Nd:YAG-laser is needed. All the lasers are capable of producing high quality coatings.

Laser cladding equipment typically consists of the laser, a manipulator, powder feeder and a cladding nozzle. Capital costs for laser cladding equipment can vary from 300 000 – 1 000 000 €, which is remarkably higher than for example arc welding equipment. A proper welding equipment can be bought with less than 100 000 €. [16]

High-power laser cladding exploits newly commercialized laser technologies, like high power diode lasers (HPDL) up to 20 kW and fiber lasers up 100 kW. With fiber lasers the laser energy can be focused to a tiny area, meaning much higher power densities can be reached. By enlarging the beam to a decent level for cladding ($100\text{-}1000\text{ W/mm}^2$), deposition rates of 10-16 kg/h have been achieved with combination of off-axis and coaxial powder feeding. [20]

2.5.5 Gas tungsten arc welding (GTAW)

GTAW, also known as tungsten inert gas (TIG) welding, relies on non-consumable tungsten electrode with an inert (argon, helium or a mix) shielding gas. Both AC and DC power sources are used. The filler material can be a solid or a filler wire. TIG welding of close-fit joints can also be done without filler materials. The arc, protected by the shielding gas, is created between the non-consumable tungsten electrode and the work piece (transferred arc). Shielding gas is important for the protection against oxidation of the filler material and molten metal. It also provides a conducting path for the current. The wire is fed into the arc from the side. The basic schematic is presented in Figure 20. The direction of welding in the figure is to the left. If higher currents are used the torch is usually water-cooled. [5,21]

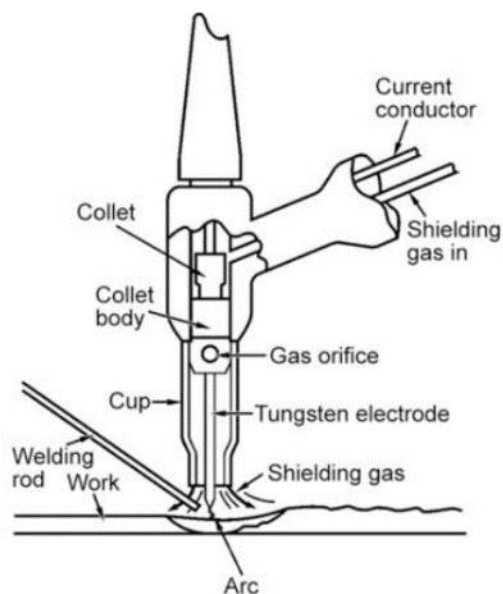


Figure 20. Schematic of TIG-welding [5]

GTAW can be automatized or done manually. TIG welding/cladding is required in applications, where high-quality welds are needed and atmospheric contamination needs to be minimized. Material examples are reactive and refractory metals like titanium, zirconium and niobium. In these metals the tiniest amounts of oxygen, nitrogen or hydrogen can reduce ductility and corrosion resistance. TIG welding can be applied in joining of stainless steel, nickel-base alloys, magnesium and aluminum. The advantages of GTAW process include high-quality welds, minimal amount of spatter, applicability with or without of filler wire over a wide range of power supplies, suitability for almost all metals, and the welding heat can be precisely controlled. The disadvantages include lower deposition rates than consumable electrode arc welding processes, possible tungsten inclusion (if the electrode is allowed to contact the weld pool), low tolerance on filler/base material contaminants and contamination of the weld metal if proper shielding of the filler metal is not maintained. [5]

The deposition rate can be increased if hot-wire systems are used instead of the regular cold-wire. Also, different advanced TIG welding systems, applying multi-cathode and multi-wire into the process have further increased to efficiency of the GTAW-processes. Different advanced applications and their efficiencies have been studied by Egerland et al. [22]. With cold-wire systems the deposition rates are typically less than 1 kg/h, but with hot wire systems the deposition rates can be comparable to GMAW [23]. The dilution in TIG can be controlled, and in a study by Shanmugan et al. [24] valve seat rings were cladded with Stellite 6- alloy with dilution rates ranging from 6-17 %. This application they studied is very similar than the one studied in the experimental part of this thesis, although the cladding method is different.

2.6 Typical hardfacing materials

The selection of suitable hardfacing (coating) material depends on the application and the environment. By correct material selection the lifetime of a component can be increased greatly, and vice versa. In Table 2 some common steels, steel alloys and Ni- and Co-base alloys and their properties as hardfacings are presented. Different carbides (Cr, W, V or B) in an iron, cobalt or nickel matrix are used when resistance to abrasive wear is needed. Work hardening alloys with austenitic structure (e.g. austenitic manganese steel) are used if impact resistance is the property to be enhanced. [14]

Table 2. Hardfacing materials and properties [14]

	Material type	Properties of deposits	Type of duty for which deposits are most appropriate
Increasing abrasion resistance ↓ Decreasing toughness	Austenitic manganese steels	Tough, crack resistant and soft. Ability to work harden	High stress, heavy impact
	Martensitic and high speed steels	Good combination of abrasion and impact resistance. Abrasion resistance increases with carbon and chromium content at expense of impact resistance.	Non-lubricated metal-to-metal wear.
	Nickel- and cobalt-base alloys	Wear, corrosion and heat resistant, with good all round strength but low ductility.	Abrasive conditions accompanied by high temperature and/or corrosion.
	Martensitic and high chromium irons	Excellent resistance to wear by most minerals. Brittle.	Highly abrasive conditions.
	Tungsten carbide composites	Extreme resistance to sliding abrasion by hard minerals. Worn surfaces become rough.	Extremely abrasive conditions where extra cost is warranted.

Heat and corrosion resistances are also vital aspects when selecting hardfacing materials. Cobalt and nickel-based alloys are considered to have excellent resistance to both heat and corrosion, as martensitic alloy steels and manganese steels quickly corrode under corrosive environments. Figure 21 presents relative wear, impact, heat and corrosion resistances of different materials and hardfacings.

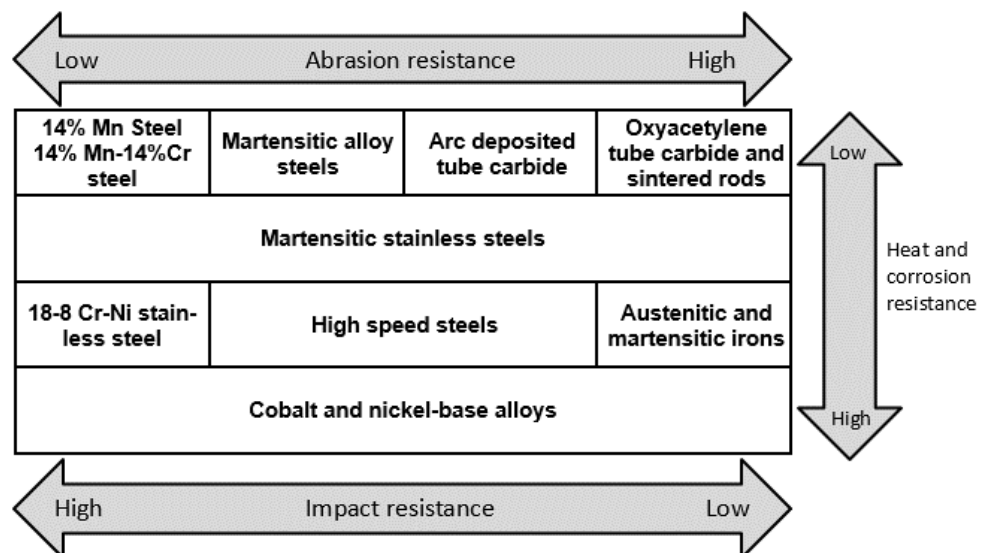


Figure 21. Relative abrasion, impact, heat and corrosion resistance of hardfacing alloys [14]

2.7 Parameters affecting the properties of the weld

Dilution, the mixing of base material and the filler material, is a vital aspect of overlay cladding. It defines the final composition and microstructure of the fusion zone and therefore affects greatly the properties of the weld and the efficiency of the processes. Dilution can be controlled in many ways and usually it is kept as low as possible to keep the chemical composition of the clad and HAZ within optimal limits. If dilution rate is below 5 %, the adhesion between base material and the coating may become uncertain, and if dilution

is over 20 %, the costs of filler material rise and the composition of the surface region can become unwanted. CMT-cladding is so adaptable that the dilution rate can be anywhere from 0 % upwards. Figure 22 presents how the dilution rate can be calculated. [5,25]

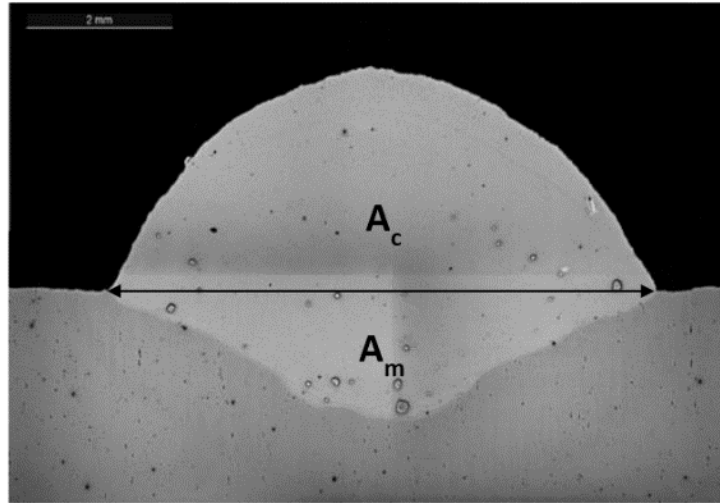


Figure 22. Weld bead with areas to calculate dilution rate (calculated value 31.6 %)

Dilution rate is calculated with the following formula:

$$Dilution = \frac{A_m}{A_m + A_c} \times 100\%$$

where

A_m = molten area below the surface of the base material

A_c = molten area above the surface of the base material.

Below is listed some dilution rates for welding processes according to literature. [25]

- Laser cladding 2-5 %
- GTAW (TIG) 5-20 %
- CMT 0-40 %
- MIG/MAG-pulsed 10-20 %
- Stick welding 15-25 %
- MIG/MAG 20-40 %
- SMAW (wire) 40-70 %

Important welding parameters and how they affect the dilution and penetration of the weld are presented next. The things listed pertains mainly to single bead-on-plate welds. Volumetric filler-metal feed rate and arc power are the primary factors that control dilution in fusion welding. [1,5]

Welding current: Current has the strongest influence on penetration and dilution rate. As the current increases, so do penetration and dilution. Pulsed welding has lower dilution than continuous steady current welding. [25]

Polarity: Welding with DC electrode positive gives greater penetration and dilution than DC electrode negative. AC positions itself between these two. [1]

Diameter of the filler material: With larger diameter wires the current is usually higher, which leads to greater dilution. If similar welding current is used, penetration with smaller diameter wire is greater because of the higher current density. [25]

Length of the free wire: The shorter the distance between the nozzle and base material, the greater are both current and penetration, which leads to greater dilution. [25]

Welding travel speed: As travel speed increases, usually penetration and thus dilution also increase up to a certain level of speed; after this penetration decreases. Similarly, the amount of filler material per weld length decreases which means dilution increases. [5,25]

Oscillation: As the length of the oscillation movement grows wider, dilution decreases. The growing frequency of the movement also decreases dilution. [25]

Overlapping of weld beads: The more the weld beads overlap the smaller is the dilution. With bigger overlapping, dilution rates can be decreased significantly compared to the values stated on page 25. [25]

Travel angle of the nozzle: The angle of the welding wire in the direction of the motion has a significant effect on the dilution. If the angle is dragging ($<90^\circ$) penetration and dilution increase, and with pushing angle ($>90^\circ$) the penetration decreases. [25]

Protective gas: Gases have effects on the dilution rate, for example in MIG/MAG welding. With CO_2 dilution rate is higher than with gas mixtures due to higher penetration.

If wire feed speed is increased, the dilution is decreased because it decreases the penetration and increases the amount of filler material. Welding position also affects the dilution; if the weld pool stays ahead or under the arc, penetration and dilution are smaller. [25]

2.8 Overlay welding of Stellite coatings

This chapter reviews studies presented in literature and reports concerning Stellite alloy coatings produced by various welding methods, mostly GMAW-processes but also some reports with TIG-welded overlays are included as they are more common.

Fouilland et al. [26] studied the friction behavior of MIG-welded Stellite 21 hardfacings and friction-induced work-hardening (FIWH) of the multilayer coatings produced. Coatings were deposited using gas shielded arc welding (GSAW) using hot-working steel 55NiCrMoV7 as the base material (pre-heated to 400 °C). The filler material was flux-cored Stellite 21 wire with 1.6 mm diameter. The hardfacings were produced in four layers using argon as the protective gas. They used different types of welding programs, P1 and P2 with semi-automatic (S.A.) and full-automatic (A.) process control. P1-program, with less welding energy, was able to reach dilution levels of approximately 7.7 % (S.A.) and 16 % (A.) with the first deposited layer, while the P2-program resulted in higher dilution levels of 37 % (A.) and 40 % (S.A.) with the first layer. The highest FIWH rates were observed by the lowest diluted top layers. This behavior increases wear resistance of the coatings.

In another study by Fouilland et al. [27] studied the microstructural variations in Co-based superalloy caused by welding process energy. The process and the materials are the same as mentioned above [26] with similar dilution rates. Microhardness levels of 350-400 HV0.2 were reached. Chemical microanalysis shows that eutectic precipitates are located between primary dendrites of a cobalt-rich fcc phase. Cored dendrites with higher content of Mo and Cr at their surfaces are formed during solidification with both low and high welding energies. It was discovered that the welding energy seems to have a greater influence on the secondary precipitation, which occurs in the deposition of successive layers as it requires high temperatures for a sufficient amount of time. Dendritic zones rich in Mo and Cr precipitate and fine cuboid-shaped particles of Cr_{23}C_6 can be observed within dendrites around eutectic precipitates. P2-welding program with higher welding energy seems to produce coarser sized precipitates. It was discovered that the presence nor the size of Cr_{23}C_6 carbides affect the microhardness levels.

GTAW is used in the hardfacing of smaller sized valves. Shanmugam et al. [24] studied the effects of process parameters using GTAW in the cladding of valve seat ring with Stellite 6 alloy. GTAW was studied because of its advantages like superior weld quality, low equipment cost and high accuracy. Stellite 6 has great resistance to corrosion and erosion even at higher temperatures. A Stellite 6 rod of 3.15 mm in diameter was used with argon as the shielding gas. They concentrated on optimizing the process parameters to predict weld properties like dilution and weld bead geometry. They also created a mathematical model to predict the dilution and the bead width. They did 20 tests and the dilution rates varied from 6 % to 17.5 %. Penetration into the base material varied from 0.17 mm to 0.37 mm. This shows that the dilution is very limited with TIG.

Motallebzadeh et al. [28] studied the sliding wear characteristics of PTA deposited Stellite 12 and Stellite 12 with a 10 wt% molybdenum addition in elevated temperatures. Both of the materials, Stellite 12 and molybdenum, were used in powder form. Five mm thick

clads were deposited and ground to a thickness of 2.5 mm. They discovered that the molybdenum addition not only increased the hardness of the clad but also enhanced the wear resistance at all temperatures. The average hardness of Stellite 12 coatings was 490 ± 10 HV₂ while the coating with Mo-addition had average hardness of 621 ± 8 HV₂. The Mo-addition encouraged the eutectic reaction to form Co₆Mo₆C carbide and Co₃Mo intermetallic as well as Cr₂₃C₆ which resulted in solid solution hardening of the Co-rich dendritic matrix. Wear track areas were reduced with the 10 wt% addition in all of the wear testing temperatures. Coefficient of friction (COF) values were also slightly decreased with the Mo-addition. The relative wear rates were significantly lowered in the clads with Mo-addition.

3. COLD METAL TRANSFER – THE PROCESS

As mentioned earlier, CMT-process is a relatively new method of fusion welding. It is very versatile process capable of welding, brazing, cladding and additive manufacturing. It has gained a market share in the welding business for its low heat input properties, dissimilar metal welding (joining steel and aluminum) and nearly spatter-free welding. It has proved to be an alternative for almost any type of welding or cladding methods. This chapter presents the CMT-process and its variables and some results of investigations done concerning CMT-cladding.

The birth of CMT process was inspired by the study of welding aluminum and steel, which was found impossible with traditional welding methods in the early 1990's. To achieve this, the heat input needed to be significantly lowered. This “cold” process, compared to traditional MIG/MAG welding, has been achieved with alternation of hot and cold phases during the welding. Fronius Internation GmbH has introduced variants to the traditional CMT-process for different applications. Comparison of the technologies among other arc welding processes are presented in Figure 23. The basic CMT-Arc process has its upper limit at a point, where the transition arc begins to appear. CMT process relies on the short-circuiting effect and for higher currents this phenomenon does not occur anymore. [29–31]

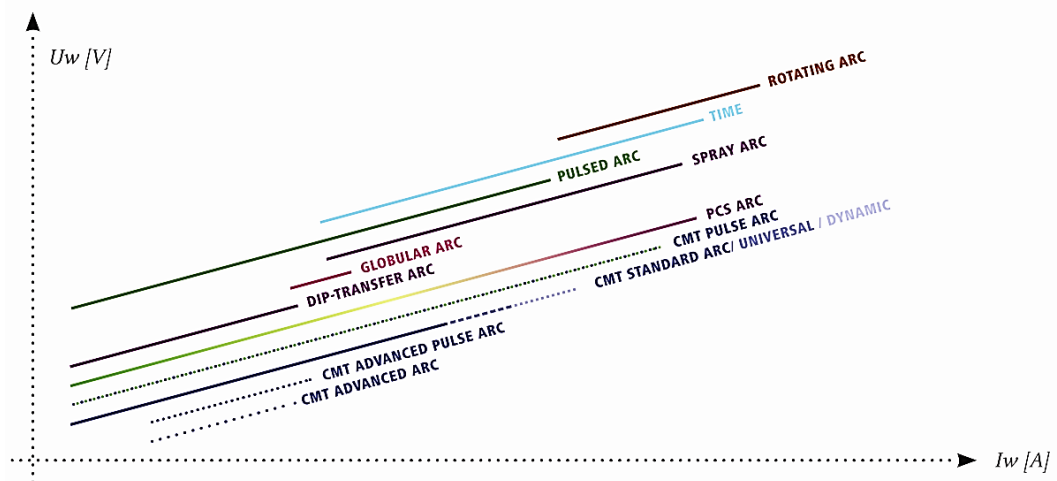


Figure 23. Comparison of arc welding technologies by current and voltage [30]

Inspecting CMT welding in general, the whole process relies on the integrated wire motion. This motion is made possible by using two separate wire-drives; one in the wire feeder (rear drive) and one in the welding torch (front drive). These are separated by a wire buffer. The rear drive pushes wire from the filler spool constantly, while the front drive moves the wire in a back and forth motion. The wire buffer helps with this process

by compensating the motion of the wire. The process is digitally controlled and the wire motion varies from 70 Hz (basic CMT) up to 130 Hz with CMT Dynamic. This frequency, with the help of new synergic lines and a new design of the welding torch, will increase up to 160 Hz. What this precise process control does along with the wire motion, is the careful detachment of the droplet. As compared to traditional MIG/MAG-process where the wire motion is only towards the work piece, this provides the lower heat input and also significantly lower spattering during the welding. The arc is also adjusted mechanically, so it adapts to the changes in the surface and the speed of the welding. The different variants of CMT process and their characteristics are explained in more detail in the following chapters. Also CMT-Twin systems are available to further increase the productivity of the process. [29,30]

3.1 Different CMT-processes and their characteristics

In this chapter the different variations of the CMT process are explained.

3.1.1 CMT

The basic CMT-process is based on the wire motion, which helps with the detachment of the molten droplet. This allows the arc to be extinguished periodically, which lowers the heat input of the process. One cycle of the CMT-process is presented in Figure 24. In the first phase, or the arcing period, the filler metal is moved towards the weld pool created by the arc. When the filler metal enters the weld pool, arc is extinguished and the welding current is lowered. The droplet detachment comes next, assisted by the rearward motion of the wire, during the short circuit. In short-circuit phase the current is kept low. After this the cycle begins again as the arc is ignited and the wire pushed towards the weld pool. The length of this cycle is not predefined; it is optimized live according to predetermined arc characteristics. So the movement of the wire controls what happens in the weld pool and vice versa. This is why the exact value of frequency of the wire movement cannot be stated, but the mean value is approx. 70 Hz. [3,29,30]



Figure 24. Basic CMT process, one cycle [30]

Below, in Figure 25, are the characteristic curves for CMT-process. At the top is the curve for wire feed rate. The back and forth motion can be seen from the curve during short-

circuit phase. The numbers indicate multiple variables that can be adjusted to optimize the welding process, such as power and current adjustments and the lengths of each phase in the cycle. [32]

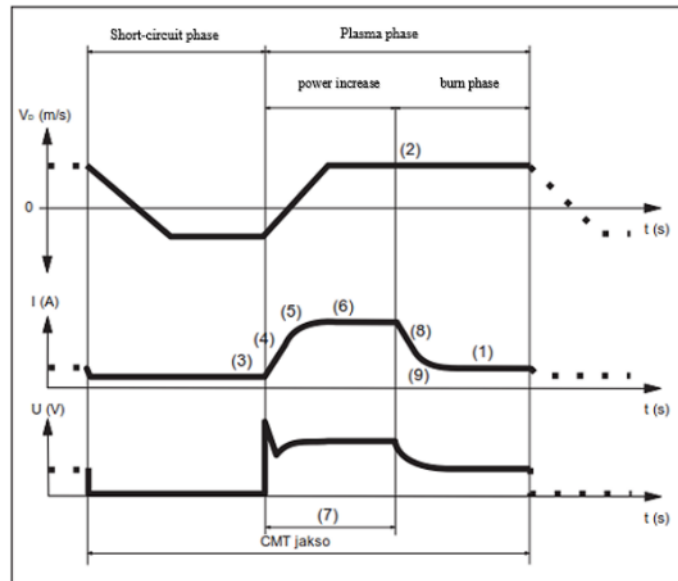


Figure 25. Wire speed rate, current and voltage curves during a CMT cycle [32]

The basic CMT-process is an all-around welding method and can be used widely among different kinds of applications, including cladding because of the limited heat input.

3.1.2 CMT Pulse

In CMT Pulse a pulsed cycle is added into the process; this also means more heat input. This adds an extra droplet detachment to each cycle which leads to higher deposition rates. In the first phase the wire is retracted while the arc being positive, like in CMT-process. Then comes the pulsed-arc phase, where the wire is moved towards the work piece while detaching a droplet simultaneously. The arc is extinguished at this point and a normal CMT cycle continues again. This CMT Pulse cycle is presented in fig. 26. [30,33]

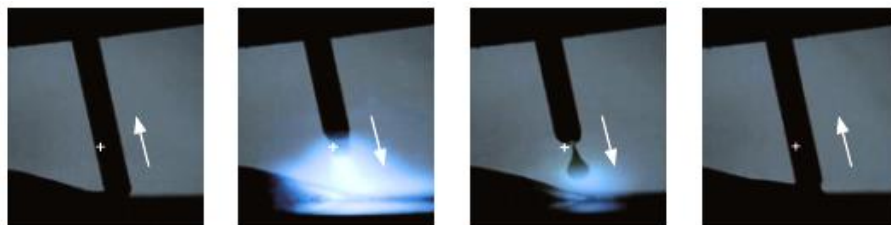


Figure 26. CMT Pulse cycle [30]

Figure 27 presents the characteristic curves for CMT Pulse cycle. The pulses take place in between the CMT cycles, in this example there are two pulses. The number of CMT cycles and pulse cycles can be selected between 0-500. [32]

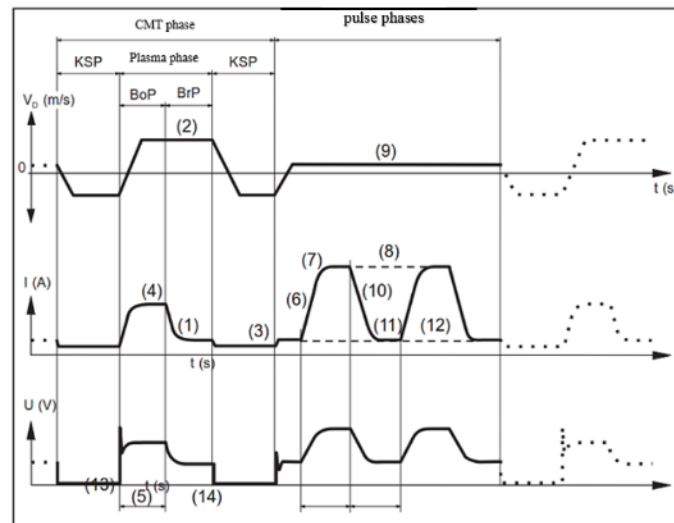


Figure 27. Wire speed rate, current and voltage curves during a CMT Pulse cycle. KSP = short-circuit phase, BoP = power ramping phase, BrP = burning phase [32]

CMT Pulse gives a very narrow bead and is mainly used for aluminum welding. For cladding purposes, it is not recommended as the heat input is greatly increased which affects the dilution and thus the composition of the coating. It enables higher welding speeds with the increased heat input.

3.1.3 CMT Advanced

Recent development in the CMT-technology is the CMT Advanced, and the principle of this variant is shown in fig. 28. The process flows with positive and negative CMT cycles and combines these two, in other words introduces alternative current (AC) into the process. This makes the process even cooler than the normal CMT process. The polarity reversal of the welding current takes place in the short-circuit phase, which results in lower thermal input, high gap bridgeability and bigger deposition rates. [30,34]

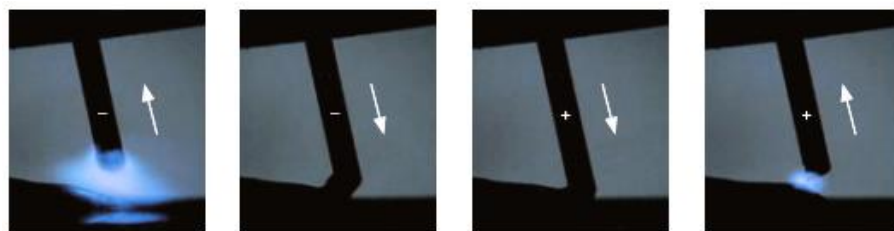


Figure 28. CMT Advanced cycle [30]

As can be seen in fig. 11. below, the polarity of the cycle changes after normal CMT-phase in the CMT Advanced process.

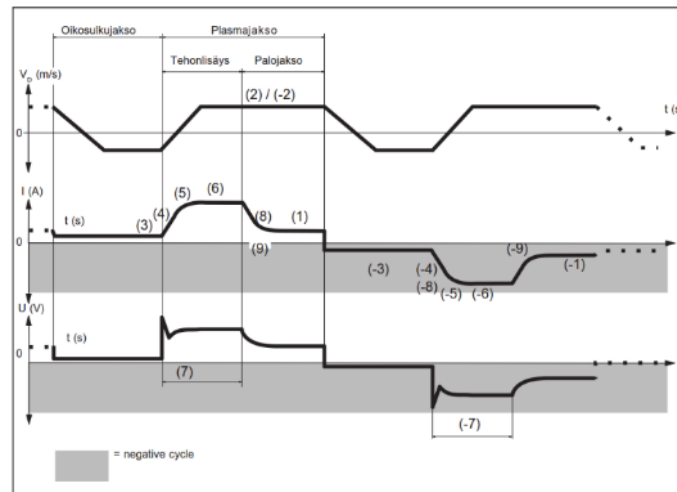


Figure 29. Wire speed rate, current and voltage curves during CMT Advanced cycle. [32]

CMT Advanced enables the use of higher WFR values, and because the droplets produced by the negative cycle are bigger, also higher deposition rates can be achieved.

3.1.4 CMT Pulse Advanced

Yet another CMT-process is the CMT Pulse Advanced. This combines negatively poled CMT cycles and positively poled pulsing cycles. This combination is presented in Figure 30. First comes the CMT negative phase where the wire moves towards the work piece. It is followed by initialization phase where the wire is retracted and cycle is positively poled, which is continued to positively poled pulsed-arc cycles.

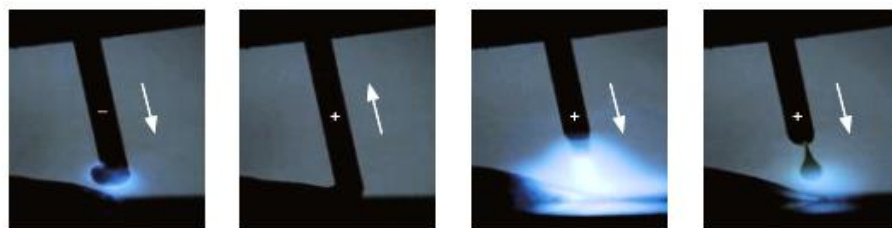


Figure 30. CMT Pulse Advanced cycle [30]

In Figure 31 the CMT Pulse Advanced cycle is presented. As can be seen, only the CMT-phase is negatively poled, and the pulses are positively poled as in CMT Pulse. The described pole difference is in fact the only thing separating the CMT Pulse from the CMT Pulse Advanced process. CMT Pulse Advanced is designed for special applications such as the need for bridge-gaping.

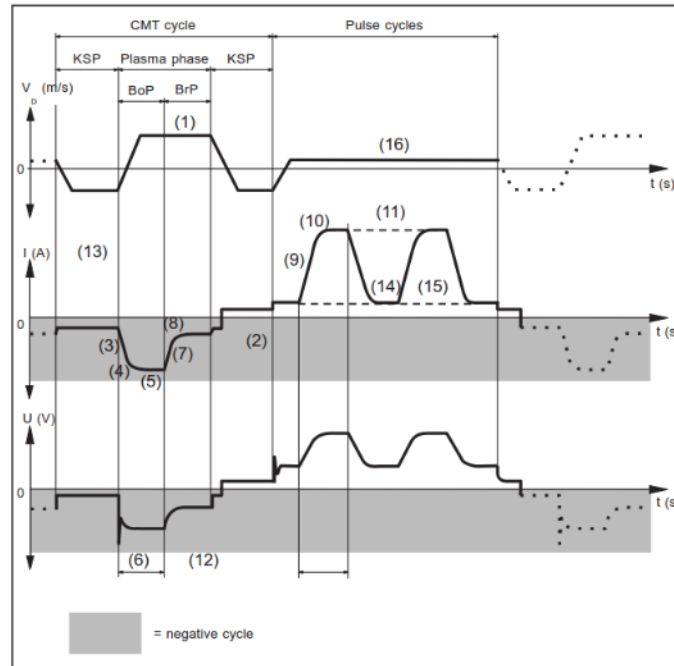


Figure 31. Wire speed rate, current and voltage curves during CMT Pulse Advanced cycle. KSP=short-circuit phase, BoP=power ramping phase, BrP=burning phase [32]

3.1.5 CMT Dynamic

CMT Dynamic is the latest development in the CMT-family. It has been designed in the welding of thicker plates. The to-and-fro wire movement has been increased up to 130 Hz which raises the operating limit of the process. This increase in the wire motion provides deeper penetration and enables higher welding speed with higher wire feed rate; thus increasing deposition rates. CMT Dynamic has more heat input, increased arc pressure and thus more energy. These reasons mean that it is not designed for cladding. [30]

The different arc modes and their differences can be seen in Figure 32 where arc current and voltage waveforms have been collected. These results were obtained by Cong et al. [35] using an AA2319 wire consumable on a wrought AA2219 alloy plates. Argon was used as a protective gas.

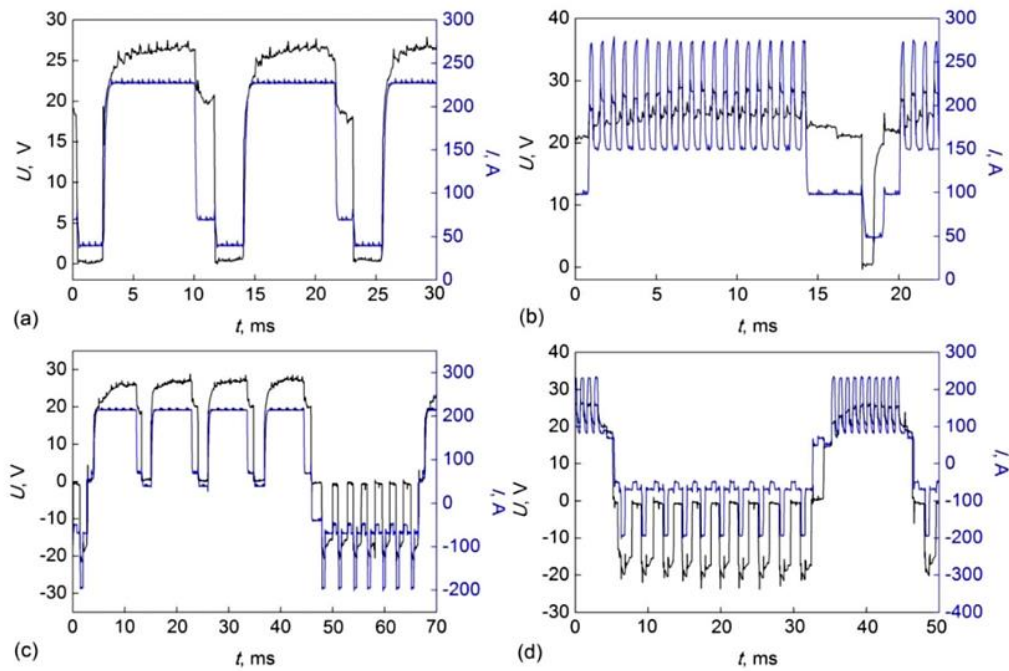


Figure 32. Comparison of different CMT-alternatives; (a) CMT, (b) CMT Pulse, (c) CMT Advanced, (d) CMT Pulse Advanced (WFS=7,5 m/min) [35]

3.1.6 CMT Pin and CMT SynchroPuls

These processes are designed for very specific applications and are not relevant to this thesis and are thus only explained briefly. In CMT Pin small brads of wire are welded onto a metal surface. This method is based on resistance heating and deposition of the free wire. Different shapes and geometries can be achieved, as can be seen in Figure 33. With CMT Pin different adhesive/non-slip surfaces can be manufactured and more applications are discovered as we speak. [36]

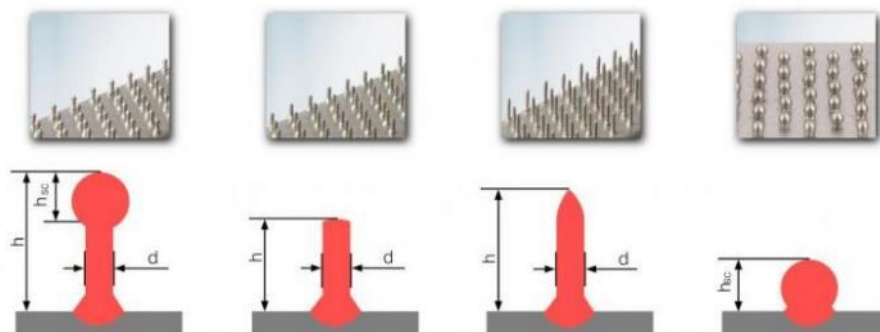


Figure 33. Pin variants produced with CMT-Pin [37]

CMT SynchroPulse combines two power ranges in a single welding process. It uses two WFR values and combines them so that high and low WFR values alter by turns. These two process phases are divided into individual CMT processes. This is used e.g. when joining plates to control the burn-through. It is used in joining applications and not recommended for cladding. [36]

3.2 The use of CMT process in cladding

So far, CMT has been applied in the cladding of Ni-base superalloys and Al alloys. Some studies are reviewed in this chapter. CMT reaches deposition rates up to 5,5 - 6 kg/h with single-wire unit depending on the process parameters and the materials in question. This number is comparable to other similar overlay cladding methods even exceeding some. Dilution and penetration of the process can be precisely controlled by changing the synergic line and adjusting the corrections parameters. [29]

Lorenzin et al. [29] investigated the use of CMT producing Inconel 625 alloy (1.2 mm diameter wire) surface facings on carbon-manganese steel sheeting. They used the CMT Pulse, classic pulsed arc and CMT Arc welding processes. They used a weld speed of 250 mm/min with 10 mm oscillation movement, argon as the protective gas and a stick-out of 20 mm. All methods produced solid, defect-free coatings. They came into a conclusion that the pure CMT process produced the less diluted coating, which is critical e.g. concerning the iron content in the clad. Inconel typically withholds 1-1.7 % iron, and the coating manufactured with pure CMT-process had a maximum iron content of 2.5 %. As a comparison the coating manufactured with the Pulsed-Arc (non-CMT)-method had an iron content of 13-14 %. Increasing dilution affects the chemical composition of the coatings and can have a negative effect in e.g. hardness values, corrosion and wear properties. Low dilution also indicates a low heat input, which is beneficial concerning possible changes in the microstructure and geometrical distortions.

Ola et al. [38] studied repair-CMT-cladding of Inconel 718 superalloy with an 0.89 mm Inconel 718 wire. They investigated the geometrical and microstructural characteristic of the clads. They used Argon, a contact tip-to-work piece distance of 14 mm with different push angles, wire feed rates and weld speeds. The CMT-process was found suitable for repair-cladding of Inconels as defect-and crack-free clads were able to be produced with low dilution. They also made calculations of heat input values corresponding to the various wire feed speeds used. The results suggest a linear relationship between heat input and wire feed speed, as shown in Figure 34. Further calculations and statistical analysis were used to create regression models. These models proved to be adequate in predicting the width, depth and weld metal dilution ratio of the clads; this can prove to be very helpful in optimizing welding process parameters. They also stated that a contact angle

of the weld bead greater than 115° helps the overlapping of weld beads when adding multiple successive passes.

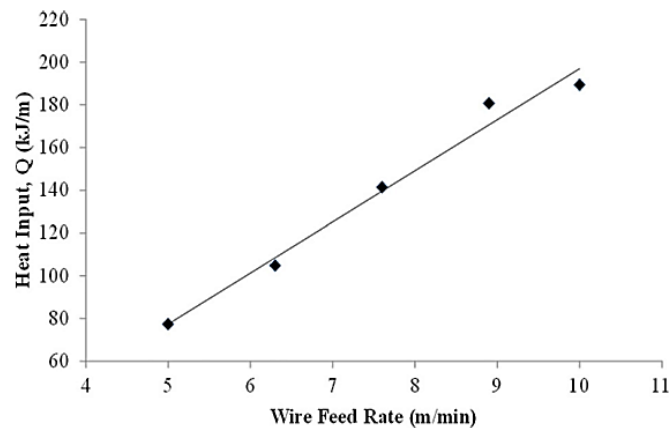


Figure 34. A plot of heat input Q versus wire feed speed using Inconel 718 as wire and substrate [38]

Pickin et al. [39] explored the use of CMT in low dilution cladding of Al alloy 2024 with Al-2319 filler wire. This alloy system has a tendency to solidification cracking, but CMT-process was able to extinguish this unwanted feature. They were able to control dilution quite precisely which is more difficult with pulsed MIG welding normally used in this application. In a study by Rajeev et al. [40] a commercially pure, 3 mm thick aluminum plate was cladded with an Al-Si-Mn coating. Low dilution and pore-free coatings were able to be produced with significantly increased hardness compared to bulk material. They used Argon as the protective gas and cladded with different weld speeds to study the effects on weld dilution, geometry and characteristics. They found CMT to be good, low-energy process for weld repairing of aluminum alloy components and able to produce thick coatings even with single pass.

Rozmus-Górnikowska et al. [41] studied Inconel 625 coatings on a ferritic-perlitic steel substrate. It is stated that one requirement for Ni-based overlays is an iron content below 5 wt%. The Inconel 625 filler material has an iron content of about 0.3 wt%, and the applied coating had iron content of 2-3 %, which indicates low dilution. The coatings produced were defect-free and otherwise successful as well. Zhang et al. [42] studied the effects of welding speed on microstructures on AZ31 magnesium alloy clad. The substrate material and the filler wire were both of the same nominal composition. Al-4043 synergic program was used. They discovered that welding speeds at range of 10-12 mm/s produced the best quality coatings due to the effects of welding speed into the cooling rates and heat input values. Higher cooling rate give precipitates less time to nucleate and grow which leads to less precipitates. Lower heat input results a narrower HAZ area.

Liang et al. [43] studied a CMT/TIG hybrid cladding of 6061 aluminum alloy. This hybrid method was executed in such a way that the arcs of these processes were not interacting

with each other. Both torches were perpendicular to the weldment and the TIG-torch was clamped in front of the CMT-torch to the welding direction. It was found that the addition of TIG improves the wettability of molten metal and thus contributes multi-passes welding and cladding of aluminum alloy. TIG was used to preheat the base metal and has a big influence into the contact angle and dilution of the weld bead by increasing the value of both of these.

Dutra et al. [44] studied Inconel 625 coatings produced by MIG/MAG Pulsed +DC, Pulsed AC and CMT –processes to a steel plate using a 45° welding position. The coatings were produced starting from bottom and then moving upwards on the plate. Weaving motion was used and the wire-electrode (1.0 mm in diameter) velocity was used with each process. Pulsed +DC exhibited the highest average welding power, 4127 W, and the dilution was high at 28 %. The CMT process was the “coldest” and the dilution was only 3 %, which is low and the fusion might not be adequate. The AC-version had a dilution of 8 % and the result was the best in terms of runoff and the quality of coating. The welding power with CMT was not high enough for the process the manufacture a good quality coating, as the weld beads remained quite narrow and had not enough wettability. In other words, the power reduction of the CMT was too great.

3.3 Synergic lines

Fronius constantly develops and publishes new synergic lines for different filler materials and filler material diameters, most of these lines are made for the demand of customers. Synergic lines are probably the most important aspect in CMT-welding because they give the basic parameters automatically to each filler material and thus, in theory, correct program should enable the manufacturing of good quality welds. Of course, especially in robotic welding, there are a number of parameters controlled by the robot and these need to adjusted correctly in order to obtain good results. Synergic lines containing databases need to be uploaded into the remote control from computer and selected prior to welding. Apart from the equipment with synergic welding there are more basic CMT-equipment with less automation and adaptivity. With these machines the user also needs to adjust the voltage in addition to wire feed rate. Also the amount of synergic lines available might be more limited because of the design of the equipment.

Synergic lines are designed with the help of an oscilloscope and a high speed camera to optimize the process and to see the different characteristics in more detail. Basically, the process of creating a new synergic line starts with a low value of Wire Feed Rate (WFR), and to that value a functioning voltage region is then defined with the help of the equipment mentioned. This method is then repeated to each WFR-value until the maximum is reached. In Figure 35 this method is illustrated; this “synergic line” is not based on any

real line. In the figure also the effects of Arc Length Correction are presented. ALC is used to finesse the voltage of each WFR-value selected from -30 % to +30 %. This gives the working area of each synergic line marked with yellow color. [36]

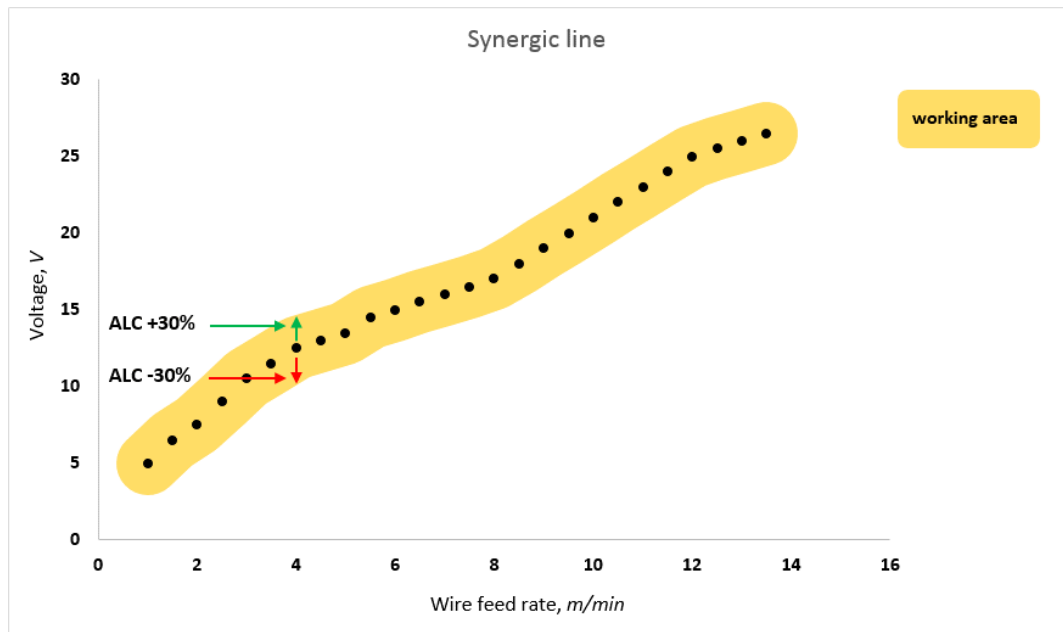


Figure 35. An illustration of a synergic line

These synergic lines can be altered with the RCU-controller by adding characteristic points. These modifications can be used to e.g. increase the maximum ALC-value of a certain WRF-value to reach a higher voltage. This requires more training and knowledge of the system and is usually not recommended or necessary.

3.4 CMT-process correction parameters

Although choosing the correct synergic line for the right material should give a decent welding result, some parameters usually need to be adjusted to gain an optimal result. Arc Length Correction, ALC, is used to set the spatial elongation of the arc plasma column. Shorter arc has a favorable effect on welding speed and against undercuts, and a long arc has positive effects in terms of formation of wide weld seam and edge formation. In traditional processes ALC controls the voltage and WFR, but in CMT-process the connections are more complex. [36]

ALC can be adjusted from -30 % to +30 %. Reducing the arc length, the wire return time decreases and similarly the process frequency increases. Negative value of ALC also increases the forward acceleration of the wire, decreases heat input and average voltage. The droplets become smaller and the amount of them increases. By increasing the arc

length, the return time increases and process frequency decreases. This also means smaller amount of bigger droplets. Longer arc also “loses” more energy than a shorter one, affecting the efficiency of the process. [36]

Another important process correction is Dynamic Correction, DC. The correction simulates inductance and it is used to adjust the duration and property of the short-circuit break. In other words, DC controls the arc pressure by adjusting the reignition current. Reduction of the arc-force dynamic correction produces a higher reignition current and thus a higher arc pressure. When DC value is set to -5, it gives 60 % higher current during the short circuit. This makes the droplet “explode” away from the tip of the wire and more spattering can be observed. Negative value also gives more penetration, higher contact angle of the weld bead and more stable arc. If DC is set to +5, 60 % lower current in short circuit is gained as a result. This leads to reduced heat input, lower stability of the arc, less penetration and less spatter. Positive DC value is recommended for cladding purposes, but this recommendation depends greatly on the materials. [36]

Stick-out of the wire, in other words the distance from the contact tip to the weld pool, has also effects on the properties of the weld. While stick-out changes in CMT do not affect the stability of the arc, shorter stick-out leads to smaller penetration into the base material, decreases deposition rate and thus gives a flatter weld bead.

3.5 Pros and cons of CMT cladding

There are many benefits of CMT cladding. The equipment is rather inexpensive when compared to e.g. laser-cladding, which by the properties is probably the most similar process. CMT has good energy efficiency and the process is flexible and capable of producing fine coatings regardless of the material. It is a cold process; dilution and penetration can be controlled easily which leads to good coating properties and composition. CMT has good productivity and with single-wire systems deposition rates of around 5 kg/h can be reached. With twin wire systems this rate can be doubled. There are also many different materials available with wire diameters varying from 0.8 mm to 1.6 mm covering both solid and cored wires.

There are not many negative aspects concerning CMT according to literature. CMT is not as accurate dimensionally as e.g. laser system but rather thin beads can be produced with e.g. thin aluminum wire. Also the coating thicknesses are rather high. It seems that it is not possible to manufacture 1.0 – 1.5 mm thick clad with low dilution and fusion bond. When going below this thickness area, the heat of the process is insufficient which causes defects and lack of fusion.

3.6 Other cold arc processes

Heat input reduction can be identified as a trend in the welding industry and many “cold” processes are available currently. These processes rely on power source regulation, short-circuiting, polarity controlling and tuning the wire motion to decrease heat input by optimizing molten material transfer. The birth of these innovations and techniques has been made possible by digitalization which enables the integration of software into the equipment. The driving force for these low heat input process developing lie in big industries like automotive and aerospace applications. Joining dissimilar metals like aluminum and steel with welding processes and thin-sheet welding are some of the significant benefits these new technologies have made possible. In this chapter some advanced gas metal arc welding processes are reviewed. There are several different approaches to decrease the heat input, mostly based on the filler material transfer and power regulation. Some of these processes are listed below by functionality of the process. [34]

Advanced power source regulation

These processes rely on the power source regulation during the short circuiting phase by adjusting the shape of the arc curve. This is usually done by digitalized power source control which monitors and adjust the arc in real time resulting in predictable short circuiting and thus minimal amount of spattering. Below is listed processes that use this kind of power source regulation. [34]

- WiseRoot™ by Kemppi (2005)
- STT™, Surface Tension Transfer by Lincoln Electric (patented 1988, launched 1994)
- RMD™, Regulated Metal Deposition by Miller Electric Mfg. Co (2004)
- Cold Arc™ by EWM Hightec Welding GmbH (2004)
- Cold MIG by Merkle
- IAC™, Intelligent Arc Control by Migatronik (2010)
- SP-MAG, Super-imposition™ by Panasonic
- CBT, Controlled Bridge Transfer™ by Panasonic Co
- Cold Weld™ by CLOOS

Mechanically assisted droplet transfer

Processes of this functionality can also be described as dynamic as the whole welding equipment, including power source, wire feeder and shielding gas flow, act as a one single unit to optimize the result. The wire movement, not only forwards but also backwards, helps the droplet transfer and the process adapts to minimize spattering and limit the heat input. [34,36]

- CMT, Cold Metal Transfer™ by Fronius International GmbH (2004)

- MicroMIG™ by SKS Welding Systems Co (2009)
- CSC-MIG™, Controlled Short-Circuit MIG by Jetline

AC-MIG (variable polarity) or variable polarity GMAW

Variable polarity means that the processes have both electrode positive (EP) and electrode negative (EN) cycles, and the ratio between them can be controlled to obtain certain results, mostly to control the heat input. For example, with CMT Advanced the gap bridging ability increases with variable polarity and it is also good for joining dissimilar materials, e.g. aluminum and steel.

- AC-MIG™ by OTC-Daihen (2008)
- CMT Advanced™ by Fronius International GmbH (2009)
- Cold Process™ by CLOOS

Hybrid metal transfer

This process is also called GMAW-P and it combines the positive transfer mode characteristics of spray transfer and short arc metal transfer mode. This is done by pulsing of the current using lower background current and high-level peak current, but holding the mean current less than the level in which spray transfer occurs. Background current preserves the arc as the peak current helps with the detachment of the droplet. [34,45]

- Pulse/pulse™ Arc Process by ESAB (2003)

Kah et al. [34] have put together a review of these new cold welding processes, their discoveries are presented in Table 3. No comparative studies of these different processes have yet to be made, main reason for this might simply be funding; lot of the information gathered in the table is from the manufacturers. In addition, the table has been put together with thin sheet welding in the scope of view. These results do not recognize differences between manual, semi-automatic and robotized processes.

Table 3. Comparison of low heat input welding processes (thin sheet metal) [34]

Group	Features processes	Welding speed vs MIG/MAG	Thermal input	Material and thickness			Gap -bridging and position (mm)	Productivity
				Steel (\geq mm)	Stainless steel (\geq mm)	Al (\geq mm)		
Advanced controlled	WiseRoot	10 % faster	10–15 % less	0.6	Yes	–	6	Good Different position
	STT	High welding speed	Lower than TIG	0.9	Yes	0.9	5 ^a	High productivity
	RMD	Increase 2 or 3 times faster ^a	Reduce heat input ^a	3.17 or less	Yes	3.1 or less	4.7	High productivity for root pass
	Cold Arc	Can improve	Minimised	0.3	Yes	1.3	+ Possible ^a	All position ^a
	Cold MIG	Increase	Minimised	0.6	Yes	0.6	Can+	All position,
	IAC	15 % faster	Reduce heat input ^a	0.6 ^a	Programme include	0.6 ^a	+ Possible ^a	Increase productivity ^a
Mechanically assisted	SP-MAG	Faster	Lower	Tested on 1.2	Yes	– ^b	Possible	Increase productivity
	CBT	Faster	Reduce	0.8	Yes	No	1.4	++
	CMT	50 % Slightly twice faster ^a	30 %	0.3	Yes	0.3	2.5	++
AC-MIG modified	CMT Advanced	50 % Slightly twice faster ^a	30 %	0.3	Yes	0.3	2.5	+++
	Micro MIG	Same as	Less ^a	0.6	Yes	0.6	No exp	++
	AC-MIG	+ Increased	–Reduction 30–40 % ^a	Thinner	Yes	Less than 0.8 ^a	No exp ^b	+++ Good because of melting rate
Hybrid metal transfer	CP	++ Increased	Reduction – –	0.5	Yes	0.8	2	+++
	Pulse/short arc	++ Increased	Reduce – –	0.6	Yes	0.6	No ^b	High productivity root pass
Conventional MIG/MAG	Short circuit	Slower	Moderately higher	0.6	–	–	Difficult	Thin sheet all position
	pulse	Moderately slower	Higher	0.6	Yes	Yes	Difficult	Thin and medium

– Decrease of feature, + increase in feature

^a Indication from the manufacture^b No information

4. MATERIALS AND WEAR IN ENGINE COMPONENTS

There are many aggressive elements attacking materials in combustion engines. Constant motion, friction, heat and different corrosive and abrasive particles can cause serious damage in different parts of engines. That is why special materials and coatings are used in diesel and petrol engines, especially in valves and parts related with the combustion process. By applying suitable coatings for components, the lifetime and maintenance intervals can be remarkably increased. Different lubricants are usually present in an engine both in liquid and in solid phase. The trend recently has been towards more aggressive operation environments (pressure, temperature) in automotive and aerospace engines, and liquid lubricants cease to perform the higher the temperature in the environment goes. This is why an alternative, solid lubricants, have been found to have potential in these kinds of applications. Solid lubricants form no paste with dust or adhesive particles, require no pump or cooling systems and are not affected by the pressure or heat in the system. This chapter goes through materials and coatings used in engine components, specifically valves and valve seats. In addition, wear and corrosion processes are reviewed. The basic principle of a four-stroke engine is presented in Figure 36. On the top of each picture are the valves; left one is the inlet valve and on the right is the exhaust valve. [15]

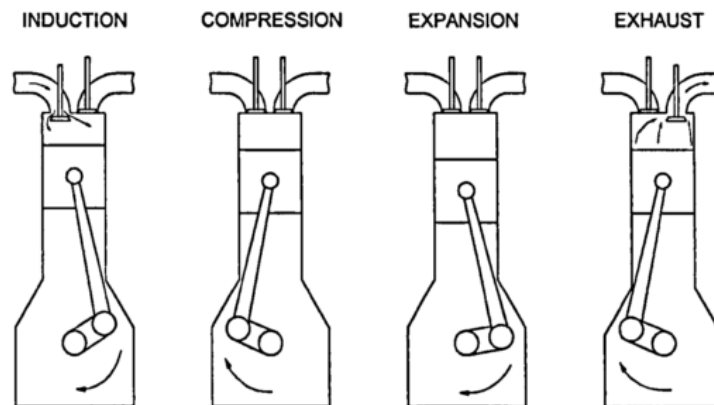


Figure 36. Four stroke engine cycle [46]

During the induction stroke the inlet valve is open and the piston is moved down in the cylinder as a charge of air is drawn in. Next, the inlet valve is closed as the piston moves up. When the piston reaches its top position in the cylinder, ignition occurs. As combustion takes place during the expansion stage, pressure and temperature push the piston down. At the end of this stroke the exhaust valve opens. It stays in an open position as the

piston pushes the exhaust gases out of the cylinder. Exhaust valve closes and the cycle starts from the beginning. [46]

4.1 Processes causing wear in engine valves

Valve wear mechanisms are generally quite difficult to characterize and investigate. They are a combination of abrasive, adhesive and oxidative wear together with residues from valves, fuels and combustion gases forming tribofilms on surfaces. This residue is mostly soot and it acts as a solid lubricant in the system. The environmental concerns and legislations are changing the conditions in the chamber towards higher pressures and higher temperatures, and also affect the fuels in many ways, for example resulting in reduction in the amount of soot formed. In the 1970s when lead fuel was still in use, the lubrication of valve components was partly because the lead in the fuel formed oxides on the surfaces of valves and valve seats. This effect was not known back then. When lead was removed from fuels together with catalytic converters were introduced, this lubricating effect of lead disappeared. This resulted in heavy wear of combustion chamber components as brittle iron oxides replaced the lubricating lead oxides and led to flaking of the oxide film and to abrasive wear. Seat surface hardening and new designs in valve seat inserts using more suitable materials appeared to be the solutions. Figure 37 presents a valve, valve seat and insert, that are very prone to wear and corrosion. [47,48]

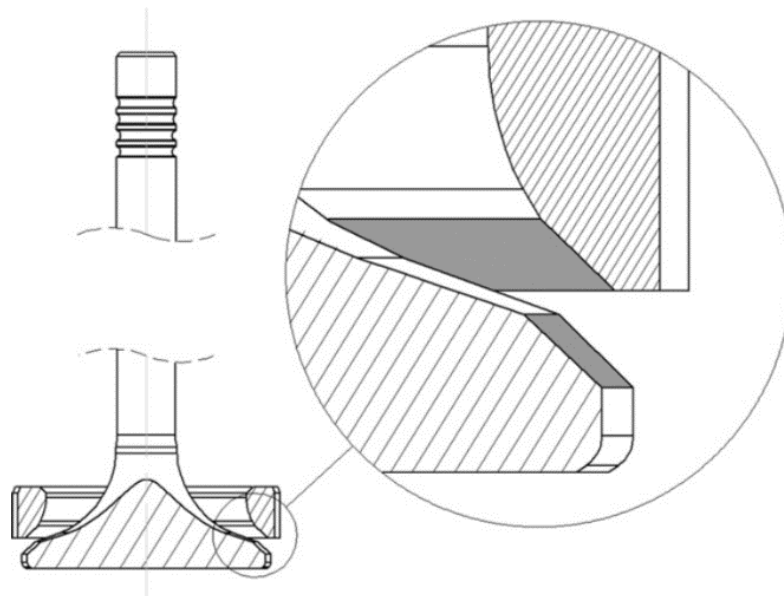


Figure 37. Valve seat and insert, contact angle 45°. Contact surfaces marked grey in the magnification. [47]

There are also other kinds of factors affecting the valve, including oxidation, adhesive wear, micro sliding, varying temperatures, exhaust gas flow and particulates. Valves must endure as long as possible in these difficult, harsh conditions that makes the material

selection vital. The sources of stresses affecting valve head are different temperature gradients, seating pressure due gas pressure and valve closing, manufacturing processes and distortions in the valve or cylinder head. The manufacturing process or e.g. the hardfacing of the valve, especially with traditional welding processes where the heat input is relatively high, cause residual stresses. Residual stresses can be attenuated with heat treatments and heat input controlling. Low cycle stresses relate to the starting and stopping of the engine when the stress and load change is sudden. The “normal” engine cycle when the load is constant is not normally the cause of engine failure, but these low of high cycle situations cause high thermal stresses and load the valve more. [47,48]

One of the most critical factors concerning the lifetime of combustion chamber components, especially exhaust valves, is the operating temperature. Valve temperature controlling is one of the most efficient ways to reduce hot corrosion and thus prolong the lifetime of the valves and the combustion system. During the combustion period, the heat input comes via the valve flame face and during the exhaust period gases flow in high velocity transferring heat to the surfaces of the valve head. Heat transfers away from the valve through a small seat contact area, and lesser portion via the valve stem guide at the end of the opening period of the valve. The deposits caused by hot corrosion can disturb the heat transfer away from the valve and in that way raise the temperature in the valve. [47,48]

A list of design changes in the valve system and solutions for wear reduction has been composed by Forsberg et al. [47] and Lewis [46]. These include structural and dimensional changes such as increased seat width, positive rotation of the valve, reduction of the speed of valve impact and reduction of the seating face angle. The latter of these, angle change from 45° to 30° decreases the frictional movement and can lead to great wear reduction according to S.K. Schaefer et al. [49]. Changes involving material technical aspects are hardening of the seat, seating face cladding (hardfacing), rigidity improvements of valve system and valve head, use of hardened valve seat inserts and lubrication, especially between valve and seat.

4.1.1 Corrosion and hot corrosion processes

In high temperature ($650 - 950^\circ\text{C}$) environments, molten salt compounds can form molten deposits, which consume the protective oxide layer on metal surfaces. This process called hot corrosion, or accelerated corrosion, can be quick, hard to predict and causes wear of motor components especially in diesel engines. The salt contaminants responsible can be e.g. sodium sulfate (Na_2SO_4), calcium sulfate (CaSO_4), sodium chloride (NaCl) and vanadium pentoxide (V_2O_5). Hot corrosion is divided into two types based on the form of the attack; Type I or high-temperature hot corrosion (HTHC), and Type II or low-temperature hot corrosion. The development of these forms are driven by many param-

ters, such as alloy composition, thermomechanical condition, temperature and temperature cycles among other factors. Damage caused by hot corrosion on a valve can be seen in Figure 38. Severe material loss has occurred in the valve. [48,50,51]



Figure 38. Hot corrosion damage on a valve from a GM 149 V16 diesel electric generator, less than 2000 service hours [52]

Type I hot corrosion takes place in temperature region of 850 – 950 °C when fused alkali metals start a series of chemical reactions attacking the oxide film on the material surface. This leads to depletion of chromium from the substrate and escalates the oxidation by formation of a porous scale. Because of its thermomechanical stability, Na_2SO_4 is the prevailing salt. Marine atmosphere, containing Na_2SO_4 and NaCl , is the most salient source of the sodium, but it is also found in the fuel. Fuel and air contains also impurities like vanadium, phosphorus, lead, chlorides and sulfur, which form different salts to enhance hot corrosion by lowering the melting point via eutectic formation. For example, melting point of Na_2SO_4 decreases from 884 °C to 620 °C in eutectic formation. Na_2SO_4 is also formed via the reaction between sodium chloride, sulfur oxide and oxygen. [51,53]

The presence of vanadium is practically unavoidable when using certain liquid fuels and it is a major factor in accelerated hot corrosion. In specific circumstances, very harmful liquid vanadium phases can form at low as 535 °C, and together with Na_2SO_4 , it enhances the solubility of the oxide layer. HTHC can be observed and characterized by color changes and peeling of the metal. Typically, a greenish color indicates the formation of nickel oxide (NiO) in the area where hot corrosion affects. Microscopic scale inspections reveal sulfidation and regions of depletion in the metal beneath the porous scale and oxide precipitates dispersed in the salt film. [48,51]

Type II hot corrosion occurs at a temperature range of 650 – 800 °C and it can be characterized as localized pitting because of local chloride attack, thermal cycling or erosion. In cobalt-base alloys, Na_2SO_4 forms mixtures with CoSO_4 , the latter one being a corrosion

product of cobalt from the base material and SO_3 from the combustion products. Similarly, in nickel-based alloys Na_2SO_4 forms harmful salts with NiSO_4 . These mixtures form localized deposits of salts in crevices and pits in scale cracks. In contrary to HTHC, high partial pressure of gaseous SO_3 is required for LTHC to occur. In addition, microscopic sulfidation and chromium depletion observed in HTHC are not present in LTHC. [51,53]

In big diesel engines, the components in the combustion chamber are the ones exposed to the possible hot corrosion. These parts include intake and exhaust valves, fuel and water nozzles, cylinder liner, cylinder head and piston crown. Most severe sites are flame faces of piston crown and exhaust valves where deposits can form over long period of time and the temperature is high. According to literature, temperature of the piston crown during combustion period rises up to 340 – 400 °C [54] and the face of the valve up to 650-705 °C. [50,55]

4.1.2 The prevention of hot corrosion

There are several methods and approaches to prevent and control hot corrosion, for example material selection, alloying, coatings, and fuel cleanliness and fuel composition controlling. Alloying can be quite difficult with certain elements, as e.g. tungsten, vanadium and molybdenum enhance the mechanical properties but predispose the superalloy to hot corrosion. Chromium has proven to be the main element in hot corrosion prevention in quantities between 15 and 20 wt% depending on the material its alloyed into. The effect of Cr in hot corrosion prevention is based on its capability to stabilize the melt chemistry and thus inhibiting the dissolution of the protective oxide scale. Cobalt-based superalloys have a higher resistance against HTHC than Ni-based alloy, but are more apt to LTHC. Other beneficial alloying elements against hot corrosion are e.g. zirconium, yttrium and scandium (improve the adhesion of the oxide layer), silicon, platinum, titanium, aluminum and niobium. Alloy microstructure also has a profound effect on hot corrosion resistance. For example, NiCoCrAlY alloy demonstrated better hot corrosion resistance with increasing microstructural refinement. The reason behind this was found to be Al-rich scale, which formed a barrier protecting the alloy from the salt thus preventing transient oxidation and liquid salt formation. One other factor that may lead into an accelerated attack are secondary phases in the microstructure. Coarse refractory metal carbides should also be avoided to prevent hot corrosion. [51,53]

Surface engineering is an efficient approach to protect components from hot corrosion. Protective, high-temperature coatings are common in forms of diffusion, overlay and thermal barrier coatings. Different types of metallic and ceramic coatings are potential in engine combustion chamber component protecting, and some even have the potential to increase the efficiency in motors by decreasing heat losses. Thermal Barrier Coatings (TBCs) act as an insulator between the substrate and the harmful gases and salts. Usually, they have a composite structure with an outer ceramic layer on a bond coat. The outer

layer can be e.g. stabilized zirconia and the bond coat some type of MCrAlY overlay (M = some metal). Thermal barrier coatings have showed some unwanted behavior like spalling and reactivity of some components of the alloy (yttria (Y_2O_3), magnesia) with sulfur, sodium and vanadium. Post-laser treatment can be used to extend the life of TBCs. [50,51]

In addition, other, more simple methods can be used in preventing hot-corrosion and its propagation. The usage of high-efficiency air filters can be used in order to drop the content on sodium in engines. Fuel cleanliness is also important, and the near-future exhaust emission restrictions decrease the sulfur content of fuels, which will most likely decrease corrosion problems. Simultaneously, operating temperatures and pressure have increased in the combustion chamber in order to raise the efficiency of the engine, and as a result, this demands more endurance from the materials used. [50,51]

4.2 Special materials in diesel engine valves

There are two types of valves in engine: intake and exhaust valves. Both valves undergo a lot of mechanical and thermochemical stresses but the environments of these can vary widely. This is why different types of materials and coatings are used depending on the valve type. Alloys are usually martensitic or austenitic with various carefully planned heat treatments to optimize the mechanical and structural properties of the valves. Intake valves operate in an environment with much lower temperatures and the high temperature properties are not as vital as in the exhaust valves. An alloy with good high temperature strength and corrosion resistance used in the exhaust side may not have the desired properties in lower temperatures and this why the different valve types can be made from different alloys. Intake side suffers more from wear-related issues and not so much from hot corrosion as exhaust side valves. [56]

Exhaust valves must withstand very harsh environments including aspects like hot corrosion; hot exhaust gases like nitrous oxides and different fumes. That is why normal steel is not fit for the purpose, because low carbon alloyed steels lose their strength and hardness as temperatures rise above 500-600 °C. Intake valves can be made of these kinds of steels because temperatures usually stay below this temperature area. There are also various other properties required from a material to be suitable for exhaust valve operation. Material must be able to resist the salt attacks, in other words hot corrosion. This ability can be improved with cladding. The material must be hard enough to resist indentations even in high temperatures. Thermal expansion coefficients of the base material and the hardfacing should be low and close to one another, because temperatures affecting the exhaust valve are strongly place dependent. This way stress gradient is kept low and thermal stress levels will also stay low. Material should have a high fatigue resistance in the

temperature range of the operation. It is beneficial if the seat area of the valve is high in conductivity. Some typical valve materials used in operation are listed next. [48,56]

- Steel valve (austenitic, martensitic) with Stellite 6/12/20 hardfacing
- Nimonic 80A without hardfacing
- Nimonic 81 with Deloro Alloy 60 hardfacing
- Nimonic 81 with Colmonoy 6 hardfacing

In Table 4 is shown the valve materials typical to certain engines. Although this list may seem to be outdated as it is from the 1990s, the materials listed are still very much in use. The manufacturing and cladding methods have made some progress but the base materials remain very similar. As can be seen, the most common valve materials are nickel-based alloys, Nimonic, clad with different Stellites. The reason why Nimonic alloys are preferred over steel valves is the failure mechanism, as Nimonic does not fracture like steel, and cause damage to the piston, liner and turbocharger with the resulting pieces. [48]

Table 4. List of engines and the valve materials used [48]

Engine	Valve	Hard facing
Deutz	NIMONIC 80A	–
Mirrlees K Major	NIMONIC	Alloy 60
Mark 3		
Mirrlees E Major 2	Alloy Steel	Colbalt based
Mirrlees MB 275	NIMONIC 81	–
SEMT PA6	Martensitic steel (changed in service to NIMONIC)	Stellite 20
SEMT PC4	Not given	Stellite 12
SEMT PC2-6	NIMONIC	–
Bergen (for IFO)	NIMONIC 81	Deloro Alloy 60
SWD F240	NIMONIC	–
SulzerZ40	NIMONIC 80	–
Sulzer AS25	NIMONIC	–
Sulzer A20 (for HFO)	NIMONIC	–
Sulzer RTA	NIMONIC	–
Sulzer S35P	NIMONIC	Alloy 60
B and W K84 EF	Austenitic steel	Stellite 6
B and W L23/30	NIMONIC	–
GMT A420	45CrNiW austenitic steel x 80 CrSiNi Martensitic steel	–
BL 230 12	NIMONIC A	–
Akaska A Series	Not given	Stellite faced
Daihatsu DS-26	SUE3	Stellite welded
Daihatsu DL series	NIMONIC or heat resistant steel	–
Fuji H32	NIMONIC	Colomony
Hanshin EL series	Not given	Stellite faced
Yanmar T240	Not given	Stellite 12
MaK 240 bore	Not given	Colomony 6
M282 M332		
Nohab F.30 (250)	NIMONIC	–
Wartsila Vasa 32	NIMONIC	–
Lindholmen CN275	NIMONIC	–
Caterpillar 3600 series	Not given	Stellite faced
{Engine A	NIMONIC 80A	–
{ or	NIMONIC 81	Deloro alloy 60
{Engines B, C, D	NIMONIC 81	–

The following Table 5 lists the composition of valve materials, both base and coating materials. As can be seen, nickel and chromium are the most important elements in exhaust valves. They provide corrosion resistance and ductility into the alloy among other things.

Table 5. Chemical composition of valve materials (base and coating) [48]

	C	Si	Mn	Cr	Ni	Fe	Al	W	Ti	Co	Mo	B
NIMONIC 81	0.05	0.5	0.5	30	bal	1	0.9	–	1.8	2	–	–
NIMONIC 80A	0.1	–	–	20	bal	5	1	–	2	2	–	–
X45CrNiW189	0.45	2.50	1.20	18	9	bal	–	1	–	1	–	–
X45CrSi93	0.45	3.10	0.45	9	–	bal	–	–	–	–	–	–
X80CrNiSi20	0.80	2.25	0.40	20	1.5	bal	–	–	–	–	–	–
En52	0.45	3.5	0.5	8.5	0.5	bal	–	–	–	–	–	–
Stellite 6	1	–	–	26	–	–	–	5	–	bal	–	–
Stellite 12	1.8	–	–	29	–	–	–	9	–	bal	–	–
Stellite 20	2.5	–	–	33	–	–	–	18	–	bal	–	–
Deloro alloy 60	0.5	4.5	–	16	bal	4.5	–	–	–	–	–	–
21-12(N)	–	0.2	1	1.25	21	11.5	bal	–	–	–	–	–
Colmonoy 6	0.75	1.0	–	15	70	4.5	–	–	–	–	–	3.5
Inconel X 750	0.08	<0.06	<1.0	15.5	bal	7	0.8	–	2.5	<1.0	–	–
VMS 513	0.08	0.5	11	27	39	bal	1.0	–	2.5	–	–	–
Pyromet 31	0.04	<3	<10.2	22.7	55.5	bal	1.3	–	2.3	–	2.0	–
Tribaloy 800	–	3	–	17	–	–	–	–	–	bal	28	–
Tribaloy 700	<.08	1.0	–	15	50	–	–	–	–	–	32	–

The materials are designed and selected to enhance the lifetime and overhaul period of both the valves, and therefore, the critical engine components. Different approaches have been developed to make the materials last as long as possible, including design changes and surface engineering. Cladding and hardfacing are one of the most important methods to provide the much-needed properties for the valves.

4.3 The coatings used in engine applications

Valve stems and heads are often coated to prolong the lifespan of valves. Chrome-plating is used in stock valves which reduces wear and protects the stem from galling. Also thin film coatings (diamond-like carbon, DLC; titanium nitride, TiN; chromium nitride, CrN) are used in order to add wear resistance and lubrication, dry films help to reduce the build-up of carbon deposits. In some valves thermal barrier coatings (TBC) can be used to reduce the heat transfers into the valve and reflect some of it back into the combustion chamber. In theory, this enhances the lifespan and also improves burning efficiency and power. Black nitride can be used as a replacement for chrome plating, as it protects the stems from various kinds of wear by creating a hard surface layer. Stellite is an often-

used hardfacing material for heavy-duty applications, especially in diesel engine exhaust valves. It provides protection against wear, oxidation and corrosion. Laser clad Inconel 625 is used in piston crowns against hot corrosion. [56]

In the next chapters, Ni- and Co-base alloys are reviewed.

4.3.1 Nickel-base alloys

Nickel-based alloys are typically cheaper than cobalt-based alloys. Nickel-based hardfacing alloys can be divided into three categories based on the composition; boride-containing, carbide-containing and Laves-phase-containing alloys. Nickel-based alloys containing carbides with similar properties as cobalt-base hardfacing alloys have been developed in nuclear industry, as cobalt-base alloys are sources of highly radioactive ^{60}Co isotope after their use in the nuclear industry. These exhibit excellent abrasion, galling and corrosion resistances, but their impact strength are generally quite poor. Compared to cobalt-based alloys, Laves-phase alloys (e.g. T-700) are quite similar to Stellite 6 and 12; however the hot corrosion resistance is mildly worse at 650 °C. [1]

4.3.2 Cobalt-base alloys

Properties including excellent high temperature hardness, corrosion and galling resistance are reasons why Co-base hardfacing alloys are often used in difficult environments where sliding wear, together with elevated temperatures and the presence of corrosive media tend to cause problems. Typical alloying elements include C, Cr, Mo, W, Ni and Si. These elements together with the allotropic nature of Co enable the properties mentioned. Co-base alloys are subdivided to solid solution strengthened, intermetallic and carbide type alloys. Solid solution strengthened and carbide type alloys are known as Stellites and intermetallic alloys are called Triballoys. Alloys with lower carbon content are relatively soft and ductile, which makes them easy to machine. Ductility also makes cladding possible without pre-heating the components. [19]

Some of the alloys work-harden during machining, which is dependent on the alloying elements. The phase transformation for work hardening happens via the change in crystalline structure of Co (face-centered cubic $\gamma\text{-Co}$ to hexagonal close-packed $\epsilon\text{-Co}$). This transformation occurs at 417 °C, if cobalt is cooled extremely slowly. Usually, the fcc structure is retained at room temperature because of the nature of the transformation, and hcp transformation is only caused by mechanical stress or time at high temperatures. The low stacking fault energy (SFE) of the unstable fcc structure leads to material properties like high yield strength, high work-hardening rate and makes the material less predisposed to fatigue under cyclic stress. These attributes lead to material capability of preventing damage during sliding wear and are the reasons behind the resistance to erosion-corrosion and cavitation of cobalt. Alloying element including Cr, Mo, W and Si favor

the phase transformation and work hardening by deducting SFE of Co matrix, whereas elements such as Fe, Ni and Mn stabilize the metastable fcc-structure by promoting the stacking fault energy. [19,57]

Stellite alloys are used for their high wear resistance, excellent chemical and corrosion performance especially in hostile environments. Range of applications is wide from gas turbine to cutting tool coatings. Stellite is trademarked name of Deloro (Kennametal) for these kinds of alloys. Stellite alloys consist of complex carbides in a cobalt-chromium matrix with components like molybdenum, tungsten and carbon. Other alloying elements can be titanium, silicon, sulfur, phosphorus, manganese, boron, aluminum, iron and nickel. Usually Stellites contain 4-8 of these components. Stellites are non-magnetic alloys that can be tailored for specific applications. Because of their hardness, machining is usually quite difficult and some special methods may need to be used. [58,59]

Cobalt and chromium combined provide a high melting point for the alloys. Chromium also provides high corrosion resistance properties and is a predominant carbide former, which means it provides strengthening in the matrix as a solute. It forms metal carbides M_7C_3 and $M_{23}C_6$. Mo and W have similar roles in the alloys, forming primarily M_6C and MC carbides, and also inter-metallic phases like $Co_3(Mo, W)$. They also hinder the movements of dislocations and slips due to their large atomic size. Most of tungsten remains in solid solution. Nickel stabilizes the face-centered cubic structure of the solution matrices. Carbon content, which controls the carbide volume, is essential to the performance of Stellites, and the alloys can be grouped by carbon content. The effect of carbon content to hardness values of Stellite alloys is presented in fig. 39. [58,59]

- High carbon for high wear applications
- Low carbon for high temperature applications
- Low carbon, higher chromium for corrosion resistance [58]

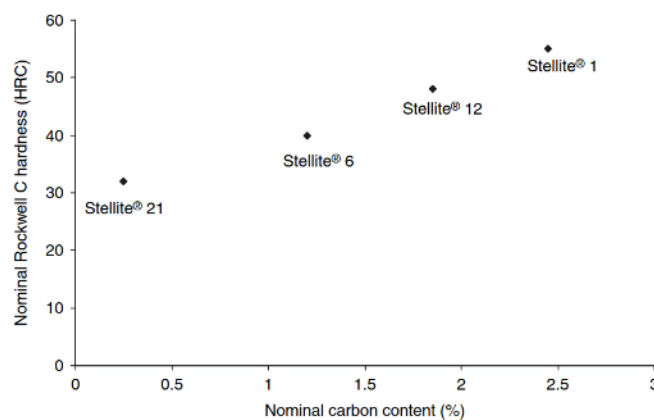


Figure 39. Nominal Rockwell C hardnesses of some Stellite alloys as a function of their nominal carbon content [1]

When the tungsten content of a Stellite alloy increases, it can enhance the high temperature hardness stability of the solid solution of the alloy. Carbides are less temperature dependent; their hardness remains almost unchanged to up to 650 °C. At room temperatures carbon content and tungsten are the most important elements affecting the wear resistance of Stellites. At elevated temperatures the carbon content is not as significant to wear resistance as at room temperature, but material oxidation takes an important role concerning the wear resistance. Higher chromium content improves the high-temperature oxidation resistance; as higher tungsten content reinforces the stability of performance at high temperatures of Stellite alloys. [59]

Studies indicate that Stellite exhibits good tribological properties at elevated temperatures. During wear tests, it was discovered that Stellites form oxide films with Co_3O_4 and CoCr_2O_4 on surfaces that increase wear resistance. [60,61]

4.4 Solid lubricants

Lubrication is one of the most vital solutions in the area of surface engineering in controlling wear and friction in different applications. In many industries, the operating conditions (temperature, pressure) have become more severe in mechanical systems in the pursuit of the higher process efficiency. Conditions may be severe in terms of temperature ($>1000^\circ\text{C}$), high stress, corrosion, friction etc. Conventional lubricants, like oil and grease, have limitations concerning in applying them, e.g. sealing problems, production of harmful paste, weight and environmental conditions. Liquid lubricants have a rather limited operating range concerning temperature, as they vaporize in temperatures above 523 K. In addition, some solidify at low temperatures and cease to lubricate the system. This malfunctioning in the lubrication can cause severe damage and that is why solid lubricants are the only solution in some demanding applications (cylinder liners, exhaust valves and components, nuclear valves etc.). In many cases, liquid lubricants can cause contamination (e.g. food industries) and thus are forbidden. Solid lubricants simplify lubrication and applying them can be often cheaper than the use oils and greases. Some types of wear, for example reciprocating motion in gears and chains, cause the liquid lubricants to be squeezed out whereas solid lubricants do not escape the system. [15,62,63]

Classification of different solid lubricants is based on their chemistry, crystal structure and lubricity. Most widely used and recently developed solid lubricants are presented in Table 6. The wide ranges of friction coefficients per material can be explained with environmental factors; friction is very sensitive to test environment, conditions, temperature and other factors. Also the form and shape of the lubricants (for example thin film, powders, composites, etc.) affect the frictional properties. That is why no single accurate value

can be given to each type of lubricant. The friction coefficient ranges in the table are compiled from measurements under various different environments and test conditions. [64]

The most common lubricants in polymer solid lubricant category are polyimide, PI, and polytetrafluoroethylene, known as PTFE or by its trade name Teflon. Both of these have a rather high temperature resistivity (PTFE 260°C, PI 350 °C) and low friction coefficients PTFE offers one of the lowest friction coefficient known, which is based on small adhesion and low shear strength. These enable PTFE-PTFE slide surfaces to form when PTFE migrates on both surfaces of the sliding system. For engine applications, polymers are not functional because of the much higher temperatures that are reached inside engines. That is why only high-temperature solid lubricants are reviewed on this thesis. [64]

Table 6. Solid materials with self-lubricating capability [64]

Classification	Key Examples	Typical Range of Friction Coefficient ^a
Lamellar solids	MoS ₂	0.002–0.25
	WS ₂	0.01–0.2
	HBN	0.150–0.7
	Graphite	0.07–0.5
	Graphite fluoride	0.05–0.15
	H ₃ BO ₃	0.02–0.2
	GaSe, GaS, SnSe	0.15–0.25
Soft metals	Ag	0.2–0.35
	Pb	0.15–0.2
	Au	0.2–0.3
	In	0.15–0.25
	Sn	0.2
Mixed oxides	CuO–Re ₂ O ₇	0.3–0.1
	CuO–MoO ₃	0.35–0.2
	PbO–B ₂ O ₃	0.2–0.1
	CoO–MoO ₃	0.47–0.2
	Cs ₂ O–MoO ₃	0.18
	NiO–MoO ₃	0.3–0.2
	Cs ₂ O–SiO ₂	0.1
Single oxides	B ₂ O ₃	0.15–0.6
	Re ₂ O ₇	0.2
	MoO ₃	0.2
	TiO ₂ (sub-stoichiometric)	0.1
	ZnO	0.1–0.6
Halides and sulfates of alkaline earth metals	CaF ₂ , BaF ₂ , SrF ₂	0.2–0.4
	CaSO ₄ , BaSO ₄ , SrSO ₄	0.15–0.2
Carbon-based solids	Diamond	0.02–1
	Diamond-like carbon	0.003–0.5
	Glassy carbon	0.15
	Hollow carbon nanotubes	—
	Fullerenes	0.15
	Carbon-carbon and carbon-graphite-based composites	0.05–0.3
Organic materials/polymers	Zinc stearite	0.1–0.2
	Waxes	0.2–0.4
	Soaps	0.15–0.25
	PTFE	0.04–0.15
Bulk or thick-film (>50 μm) composites	Metal-, polymer-, and ceramic-matrix composites consisting of graphite, WS ₂ , MoS ₂ , Ag, CaF ₂ , BaF ₂ , etc.	0.05–0.4
Thin-film (<50 μm) composites	Electroplated Ni and Cr films consisting of PTFE, graphite, diamond, B ₄ C, etc., particles as lubricants	0.1–0.5
	Nanocomposite or multilayer coatings consisting of MoS ₂ , Ti, DLC, etc.	0.05–0.15

Selecting a suitable solid lubricant(s) is very vital in obtaining high temperature tribological and mechanical properties. The biggest reason for this is that usually a combination of a low temperature lubricant and a high temperature lubricant is used, since no single material is able to offer decent lubricating effect over a wide temperature range. The lubricant is either cladded onto the surface or mixed with coating material creating a composite coating. It is crucial to find an optimum content for the lubricant; too high content decreases the friction coefficient, but also softens the coating. This can make the coating to wear faster than intended. [64]

In engine applications, the operating temperature is the most crucial factor, as lubricants need to withstand temperatures exceeding 500 °C. Some of the common lubricants, including molybdenum and tungsten disulfides (MoS_2 , WS_2), silver and graphite are classified as low temperature lubricants meaning the preferred operating temperature for them is below 500 °C. Lubricants surpassing this 500 °C limit include compounds like hexagonal boron nitride (hBN) and calcium difluoride (CaF_2). The problem of many lubricants is the impregnation of them as the original chemical compounds; most of the lubricants tend to oxidize and/or decompose below the melting temperature during the cladding process. With some materials, this is not an issue, depending on the mechanism of the wear reduction possessed by the lubricant. For example, MoS_2 (powder with 70 wt% MoS_2 , 20 wt% TiC, 10 wt% Ni) particles pre-placed using laser cladding with Ni led to the dissociation of MoS_2 and formation of various sulfides in the matrix material, but low friction was still obtained as a result ([19,65]). Different approaches have been executed to solve this issue for example in laser cladding. [19]

4.4.1 Lamellar solids

The most typical mechanism of lubrication of solid lubricants is the layered or lamellar crystal structure. These layered lubricants are the most common solids used among different industries. This structure is presented in Figure 40. As illustrated, it shows that the atoms in the same layer are tightly packed and strongly bonded with each other, but between the atomic layers the bonds are relatively weak (van der Waals forces and such) because they are rather far apart. This enables the layers to align parallel in the direction of relative motion and decrease friction by sliding over one another easily. This layered structure also helps in wear damage reduction. [64]

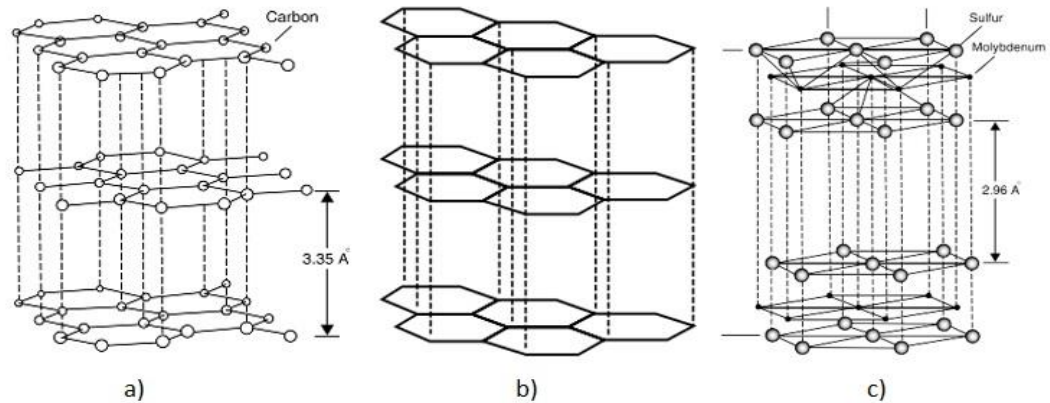


Figure 40. Schematic illustration of layered crystal structures of a) graphite, b) hexagonal boron nitride and c) molybdenum disulfide [64]

In this chapter the lamellar solid lubricants which possess high temperature lubrication properties are reviewed.

Tungsten disulfide, WS₂

The lubrication properties of tungsten disulfide (WS₂) is based on the lamellar structure and low shear strength, which under tribological contact cause the forming of lubricious transfer film. WS₂ has a rather high oxidation temperature (539 °C) compared to graphite (325 °C) and MoS₂ (370 °C), which enables it to preserve its lubrication ability also in a bit higher temperatures. Several studies show the lubrication properties of WS₂ are still good at 300 °C, but the lubricating phase oxidizes at temperatures approaching 600 °C and the lubricative property will reduce significantly. [15,66]

Yang et al. [67] studied the a laser clad NiCr/Cr₃C₂-WS₂ high temperature composite coating and its wear resistance and self-lubricating properties. They used 30 wt% of WS₂ in the powder and 0Cr18Ni9 austenitic stainless steel as the substrate material. It was noticed, that WS₂ significantly decomposed during the cladding process due to its rather low decomposition and oxidation temperatures, 510 °C and 539 °C, respectively. Although the WS₂ was decomposed, it formed compounds with Cr (CrS) which also have lubricating properties. They tested friction and wear properties of coatings with and without of WS₂ at elevated temperatures. Although friction coefficients of both coatings decrease as temperature was risen from 17 °C to 600 °C, wear rates of both increase at this same range. Wear rate of the coating with WS₂ is lower at 300 °C but higher at 600 °C compared to coating without WS₂. Thus, it can be drawn from the results that WS₂ is an effective lubricant from RT to approximately 300 °C, but above this temperature the effectiveness decreases.

Hexagonal Boron Nitride, hBN

Hexagonal Boron Nitride, hBN, is a white, clean lubricant. It has high chemical inertness, oxidation resistance and thermal conductivity. It has a lamellar structure like graphite and MoS₂, meaning the bonds between molecules within each layer are strong covalent, but only weak van der Waals forces held the layers together. The applications for hBN lie in high-temperature applications, since it is less effective in lower temperatures. It has applications like nuclear-based valves and pipe fittings, aerospace industry and metalworking. [15,68]

Erdemir [64] has joined together some results of the use of hBN as a solid lubricant. It can withstand the heat of plasma spraying and thus be incorporated into different coatings (e.g. Ni-based coatings), resulting in excellent frictional and wear properties even under high temperature applications, as hBN does not oxidize until about 1000 °C. There are also some issues in the synthesis of hBN because of its poor wetting property and low density (2.27 g/cm³). This results in inhomogeneous distribution of hBN, as the particles stay on top of the melt pool. In addition, a higher content of hBN impairs the surface roughness. Yan et al. [69] used nano-Ni powder to encapsulate the nano-sized h-BN particles trying to solve this issue on interfacial compatibility. This proved to be successful using Ni60-10 wt% hBN mixture, as wear test results with non-capsulated vs capsulated Ni-hBN powders were compared. Friction coefficient values decreased from 0.5-0.6 to approximately 0.35 and mass loss from 28.5 mg to 6.3 mg. Capsulation also resulted in a more uniform distribution of the hBN particles. The friction coefficient value achieved, 0.35, is still rather high, but a vast improvement compared to surfaces without solid lubricants.

Zhang et al. [70] prepared Ni/hBN (70 wt% Ni-coated hBN, 30 wt% Ni) coating on 1Cr18Ni9Ti base material with laser cladding and ran a series of wear tests in elevated temperatures. In this study, the hBN powders were also electroplated with Ni to improve wettability and sinterability. It was discovered, that the coatings produced exhibited good wear resistance and gradually reducing friction coefficients as the temperature rose at a range of 100-600 °C. In addition, wear rate improved as temperature was increased from 100 °C to 600 °C, where it reached its minimum value, 24 times lower than value at 100 °C. It was found, that the coatings with electroplated hBN performed better than electroless coatings at elevated temperatures. Some softening of the coating was noticed at approximately 300 °C which resulted in hBN wear debris transfer onto the counter body reducing abrasive wear. As a conclusion, laser cladding of Ni/hBN coating is a good method to prevent wear and add protection to stainless steel up to 800 °C. Zhang et al. [71] also studied NiAl/hBN coatings on Ni-based superalloy and the results were similar; tribological properties were excellent up to 1000 °C.

Molybdenum disulfide, MoS₂

The lubricative effect of MoS₂ is based on the same shearable lamellar structure which enhances sliding properties of counter-bodies. MoS₂ exhibited decomposition and reactions with other elements during laser cladding tests executed by Yiwen Lei et al [72]. MoS₂/Ni-based composite coating have also been prepared by Xu et al [65] on AISI 1045 steel. They managed to reduce the friction coefficient from 0.82 to 0.37, but this situation was untenable as the lack of hardness in the cladding caused the cladding to wear off in minutes and resulted in high wear. As TiC was added into to mix of MoS₂/Ni, the properties including wear resistance, hardness and load-bearing capacity increased greatly, although friction coefficient was slightly increased compared to MoS₂/Ni-coating. This was due higher sulfide content and hard particulate TiC reinforcement. After wear tests, the worn surface was smooth which indicates resistance to groove formation. This was verified by the 6 times better wear resistance it exhibited, compared to hardened AISI 1045 steel. [15]

4.4.2 Halides, metal oxide based materials and others

The use of alkali fluorides, like CaF₂, as solid lubricants is based on the low shear strength and their thermochemical and thermophysical stability at elevated temperatures.

Titanium dioxide, TiO₂

The lubrication properties of certain oxides in elevated temperatures, including TiO₂, is based on softening of the compounds and thus becoming more easy to shear. Oxides provide good levels of friction coefficients in terms of wear and thus enhance the wear life. Downsides are that oxide-based lubricants wear out quickly because of their brittle nature and also do not provide lubrication in room temperature. Oxides are used as lubricants in high temperature applications like seals, valves, valve seats and gears for example. [64]

The effects of TiO₂-doping as a solid lubricant have not been studied vastly. The effect on nickel-based hardfacing composite coating, G112, using laser cladding on carbon steel with TiO₂-doping shows, that it has potential in adding wear resistance by lubrication. This was studied by Chao et al. [73]. The composition of G112 is shown in Table 7. With a proper amount of TiO₂ (~3-4 wt%) it was shown that good quality coatings with no pores and cracks could be created. Cracking sensitivity and wear resistance were greatly improved, although some decrease in hardness was measured. The decrease of hardness can be explained with increase of eutectic amounts. Eutectic amounts also provide better cracking sensitivity. TiO₂-doping affected the microstructure of the coating by refining grain size and in making grain distribution more homogenous in the coatings. The refinement of grain size can be explained with generation of new phases like TiB₂ and TiC meaning more nucleation sites in the matrix. In TiO₂-doped G112 coating the grain sizes

of dendritic phases were approximately 2 orders of magnitude smaller than in pure G112 coating.

Table 7. Composition of hardfacing G112 powder

Alloy (wt%)	Cr	Fe	C	B	Si	Ni
G112	15-18	14.3	0.6-0.8	3.5-4.5	3.0-4.0	bal.

Some experimental activities show that fully stoichiometric rutile and titanium suboxides are rather a low-wear than a low friction material. The beneficial effects of oxygen vacancies in rutile TiO_2 has been demonstrated by Gardos [74]. The vacancies form a lubricious oxide film and thus enhance the shearing mechanism.

Storz et al. [75] studied tribological properties of thermal-sprayed Magnéli-type coatings with different stoichiometries of titanium oxides ($\text{Ti}_n\text{O}_{2n-1}$). They tested wear properties at 23 and 400 °C. Under dry sliding wear tests at 23 °C the coatings exhibited high friction coefficients at the range of 0.7-0.8. At 400 °C the friction coefficients decreased between 0.5 and 0.6 but similarly the wear rates increased for about one order of magnitude.

Manganese sulfide, MnS

Manganese sulfide, MnS, has a melting point of 1610 °C, density of 3,99 g/cm³ and has shown potential to be a solid lubricant under certain conditions. Having relatively high melting point enables it to be used in high-temperature applications where lubrication, low friction coefficients and low wear rates are necessary. Skarvelis et al. [76] studied the lubrication properties of MnS addition with hard carbide particles (TiC, WC) in composite coatings with promising results. Two types of coating powders were prepared; one with TiC and the other one with WC. Powders contained 30 wt% of TiC/WC, 12.56 wt% Mn, 7.44 wt% S and 50 wt% Fe. Coatings were manufactured on steel substrates with Plasma Transferred Arc (PTA) welding. Self-lubricating properties of MnS occur on the wear tracks as formation of manganese sulfide film. The addition of manganese sulfide affected the friction coefficients decreasing them from 0.50-0.60 to 0.25-0.28 compared to similar hard coatings without the MnS addition. Simultaneously, wear rates were two orders of magnitude lower (order of 10^{-5} mm³/m N) than without the MnS addition. The studies also showed, that to achieve low wear rates also hard particles are needed in the matrix; MnS addition cannot provide low wear on its own. The hard particles support the applied load and dampen mechanisms of wear. This result was discovered when comparing results of another investigation of Skarvelis et al. [77]. The wear rates decreased by approximately 100 times in the presence of enhancing particles. [78]

Zuomin et al. [79] studied the effects of TiC together with CaF_2 /MnS particles on sintered high speed steels at elevated temperatures. The lubricants were sintered into the metal matrix instead of cladding. The addition on MnS has some negative effects on hardness

since its hexaplanaric structure, especially in higher temperatures. Wear tests indicated that sintered steels with TiC+MnS performed better against softer materials, but with harder ceramic counterpiece the friction coefficients were still improved compared to plain sintered steel. The negative effects of MnS addition to hardness were also noticed by Bolton et al [80].

Calcium difluoride, CaF₂

At lower temperatures calcium difluoride, CaF₂, is brittle and has no lubricating properties, but with rising temperature a transition occurs from a brittle state to plastic state, and enables the lubricative properties of the material. The lamellar structure of CaF₂ shears along the basal plane of the hexagonal structure creating a transfer film [64]. Xiang et al. [81] investigated high-temperature anti-wear composite coatings on Ti6Al4V alloy with self-lubricating CaF₂ using CO₂-laser cladding. They added 20 wt% of CaF₂ into a γ -NiCrAlTi/TiC powder. It was discovered, that the coating with CaF₂ has superior wear and friction properties compared to a similar coating without the addition of the lubricant. It exhibited a friction coefficient of 0.21 at 600 °C, which was approximately 50 % lower than the coating without CaF₂. The wear rates were quite similar at low and 300 °C temperatures compared to γ -NiCrAlTi/TiC coating, but at 600 °C the addition of CaF₂ seemed to decrease the wear rates under dry sliding test. Lower wear rates at 600 °C were explained by wear mechanisms; the addition of CaF₂ altered the mechanism from abrasive and oxidative wear into the generation of transfer films.

Wang et al. [82] studied wear-resistant CaF₂/Al₂O₃ coatings laser cladded on Al₂O₃ substrates. They used Al₂O₃-30 % CaF₂ powder mixtures and lower laser power density in order to avoid the decomposition and vaporization of CaF₂ powders. The specimens were pre-heated before cladding. Compared to laser clad monolithic Al₂O₃ coating, the addition of CaF₂ greatly improved wear resistance (from 1 to 29.29) and lowered friction coefficient (from 0.60 to 0.48) under dry sliding wear test even at room temperature. Liu et al. [83] studied composite Ni-Cr-C-CaF₂ coatings laser cladded on a γ -TiAl alloys. They used a high content of 40 wt% of CaF₂ in the powder and a 5 kW CW CO₂ laser with 2.0 kW of laser power. Good quality coatings were produced although some vaporization of CaF₂ was bound to happen during the cladding process. In a further study by Liu et al. [84] with Nd:YAG laser in producing γ /Al₄C₃/TiC/CaF₂ coatings on γ -TiAl alloy, electroless plating of CaF₂ with Ni-P was used. Similar 40 wt% of CaF₂ was also used in this study. It was discovered, that the electroless plating of CaF₂ reduced friction coefficient of the coating significantly compared to non-plated powder coating. Also wear mass loss was decreased meaning a better wear resistance with CaF₂. Results mean that the electroless plating of CaF₂ affect the floating, decomposition and vaporization of CaF₂ during the cladding process towards a positive direction enhancing the wear properties of the coating.

5. OBJECTIVE OF THE THESIS

In the pursuit of more reliable, lasting and high-quality solutions in engine technology, material technology and surface engineering are the key players in the field. Engine components have to withstand high amounts of mechanical and thermal stresses with every revolution of the engine. Especially the components in the combustion chamber are under heavy service conditions and must endure in order to engine to continue working as planned. Malfunctioning of these components may result in severe damage to the engine and thus result in extra costs and downtime of the machine in question and in worst cases even endangering lives.

In the circumstances mentioned most commonly used materials are highly alloyed, for example superalloys, stainless steels and other special steels. But in many occasions the materials are still not durable enough, and for this reason these components can be clad with a thick layer of wear and hot corrosion resistant coatings. These clads increase the lifespan of components by a huge factor. There are many different cladding techniques which are used to manufacture these type of coatings. For example, different types of arc-welding, thermal spraying and laser cladding methods are used. These methods provide excellent adhesion properties between the substrate and the coating and are well-known, thus are available in the market with good practical experience. The usual disadvantages of coating processes, especially arc-welding, is the high heat input. This affects the base metal properties, increase the risk of cracking and can bend or shape the components in an unwanted way.

In this thesis a relatively new method of arc-welding is being studied called Cold Metal Transfer (CMT). This arc-welding process was brought to the market by Fronius International GmbH in 2005, and was first developed for thin section welding and brazing purposes. The heat input of the process is dramatically lower than in conventional welding processes. This has been achieved by the digital process control which was explained in more detail in the previous chapters. The coatings studied in this thesis are those enhancing wear and corrosion resistance in engine components.

The CMT-equipment in Tampere University of Technology (TUT) is rather new and only a few cladding tests have been run before the beginning of this thesis. For this reason, there were some (and still are) some new things for the research team working with the CMT. The CMT-equipment is located at TUT in a facility with other heavy equipment (lasers, lathes and some other machining apparatus). The CMT-equipment is made by Fronius and is called CMT Advanced 4000R single-wire and it is attached to ABB IRB 4600 robot. The robot controls the movement of the welding torch, and it can be programmed for different types of welding, cladding or additive manufacturing applications

(one pass, weaving motion, multipass with overlapping, etc.). The welding platform is a round plate with the ability to a rotating motion for circular welding/cladding.

A few different types of base material discs were mainly used, diameters varying from approximately 60 mm to 120 mm, thicknesses being from 20 mm to 30 mm. The materials were 42CrMo4 (quenched and tempered), which is a tempering steel. Other materials are a nickel-based superalloy and martensitic stainless steel. The coating materials are Stellite 12, a Co-base superalloy, and both together with a solid lubricant powder addition, which enhances sliding properties in low sulphur fuels burning engines.

The goal is to find the optimal cladding parameters for the Co-base filler material by searching similar studies and experiments, but mainly by making cladding tests, researching the samples and analyzing the results. The base materials can be quite difficult to clad because of their tendencies of cracking, and therefore some heat treatments are necessary before and/or after the cladding process to avoid cracking and to achieve wanted material properties and structures. CMT provides many process parameters for adjusting the coating properties.

Other challenge is that the desired coating materials are not available as solid wire. Due to manufacturing difficulties (low ductility), Stellites are available only as tubular wires and they are designed mainly for hot arc welding processes. The diameter of flux-cored wires is usually above 1.6 mm and CMT-process may not function with such great diameters. The availability of 1.2 mm diameter flux-cored wires can also be an issue as there are not many manufacturers for wires like this.

EXPERIMENTAL PART

6. MATERIALS

In this chapter the materials vital to this thesis are presented. The base materials include a nickel-base superalloy (to be known as “Nialloy”) and a martensitic stainless steel (to be known as “Cr-steel”). The coating material wire include a Stellite 21 wire, a Stellite 12 wire and a Co-base wire (to be known as “Co-alloy”). The base material pieces are presented in Figure 41; Cr-steel in the middle and Nialloy on the right hand side. The exact compositions of the base materials are not reported in this thesis due confidentiality reasons.



Figure 41. Base material discs: Cr-steel discs on the left and Nialloy on the right

6.1 Base materials

Nialloy discs were 30 mm thick discs with a diameter of 63 mm. The alloy mainly consists of nickel and chromium together with some other alloying elements. Cr-steel material was used as discs ($D=100$ mm, $t=30$ mm). The composition of Cr-steel consists mainly from chromium and iron with some other alloying elements.

6.2 Stellite 21 wire consumable

The coating tests were started with Stellite 21 tubular wire with 1.2 mm diameter. This wire was only used as a training material, as it was already in our possession and ready to be used. Stellite 21 is trademarked name for a CoCr-alloy by Kennametal Incorporation. It is a corrosion resistant solid solution strengthened type alloy with multiple applications, e.g. biocompatible hip implants, denture alloy and jet engines. The structure of

Stellite 21 consists of a CoCrMo alloy matrix with a small amount of dispersed hard carbides. These carbides both strengthen and add hardness to the alloy with the expense of ductility. The final properties of the alloy can be altered via heat treatments and process parameters. The nominal composition of Stellite 21 is presented in Table 8. Co-based matrix dominates the corrosion properties, bringing excellent cavitation, galling and metal-to-metal sliding wear resistance. Hard particle abrasive wear is not recommended for Stellite 21. Surface has tendency to work harden significantly. This alloy is hypoeutectic. [1,85]

Table 8. Nominal composition (wt%) of Stellite 21 wire consumable [85]

Material	C	Mn	Si	Fe	Cr	Mo	Ni	Co
Stellite 21	0.25	0.8	0.8	<3.0	27	5.5	2.5	bal.

As this alloy is not the primary material concerning this thesis, no further investigation will be done.

6.3 Co-alloy wire consumable

The tubular, Co-base wire used is 1.2 mm in diameter. It is quite similar to Stellite 21 but with some changes in the composition. It has good resistance to abrasion, erosion, cavitation and severe sliding wear.

6.4 Stellite 12 powder

Stellite 12 powder was used together with MoS₂ and WS₂ solid lubricants. Stellite powder and selected solid lubricant were ball milled together to enhance the mobility of the lubricant in the powder feeder. Powder is manufactured by Höganäs Belgium NV. The name of the powder is HMSP 2541 with particle size of 150-53 µm. The composition of presented in Table 9.

Table 9. Nominal composition (wt%) of HMSP 2541 powder

Material	C	Si	Fe	Cr	W	Ni	Co
HMSP 2541	1.4	1.1	1.0	28.5	8.0	1.5	bal.

This powder was selected as it exhibits similar properties than the Co-base wire and was only used with WS₂ and MoS₂ powders.

6.5 Solid lubricants

Different types of solid lubricant powders were used with the powder feeder unit. These powder and their properties are presented in Table 10.

Table 10. Properties of the solid lubricants

Powder	Composition	Particle size	Density (g/cm ³)
MoS ₂	99 % MoS ₂	average 1 μm	4.8
CaF ₂	98 % CaF ₂	-100 +44 μm	3.2
WS ₂	99.8 % WS ₂	average 1 μm	7.5
TiO ₂	99 % TiO ₂	45/22 μm	4.0

Titanium dioxide powder is manufactured by H.C. Stark GmbH. The melting temperature is 1843 °C. Wolfram disulfide powder is manufactured by Cerac and the melting point is 1250 °C. The microstructures of the powders are presented in Figure 41.

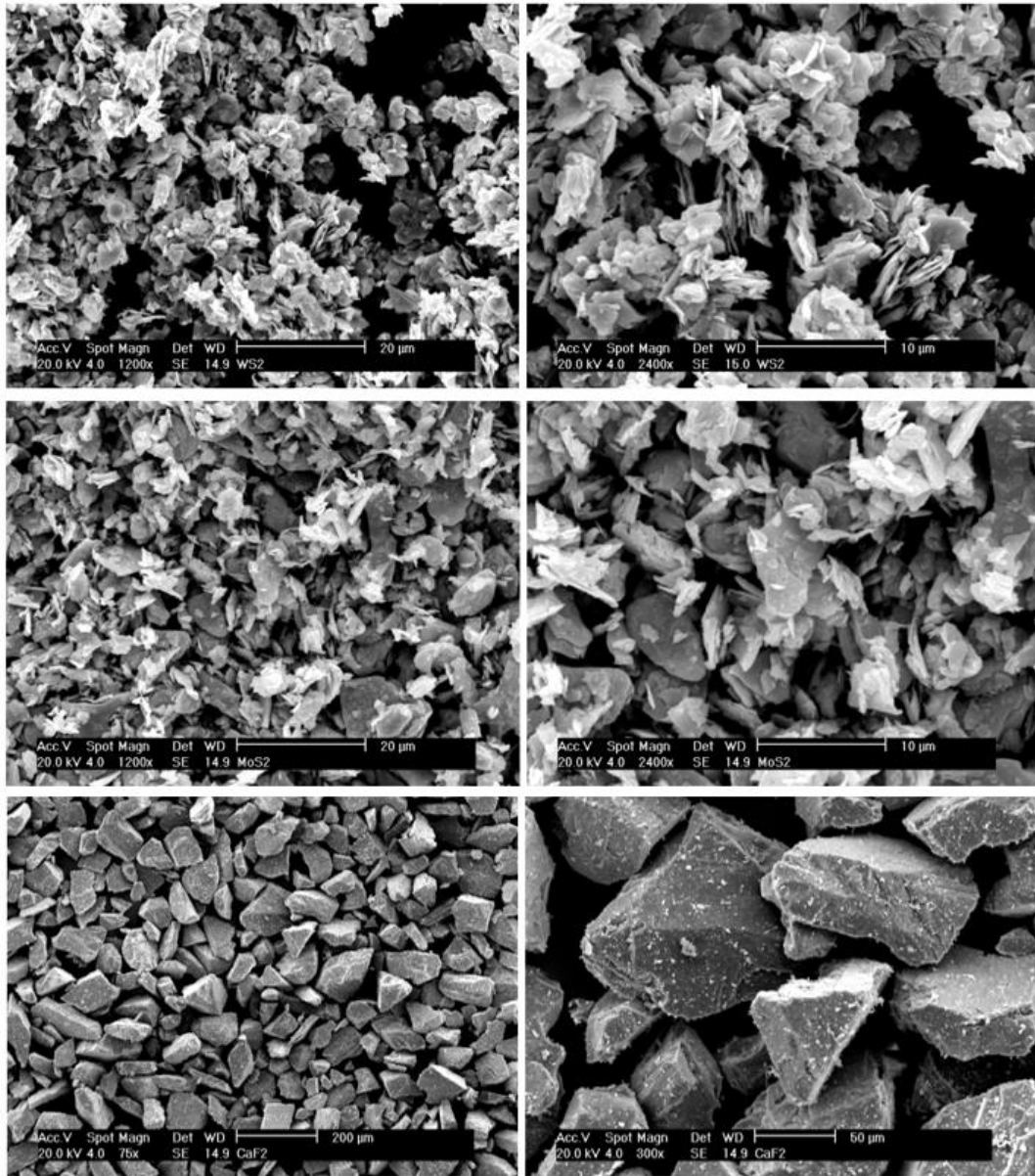


Figure 42. Solid lubricants: WS₂ (top), MoS₂ (middle), CaF₂ (bottom) [86]

7. RESEARCH METHODS AND EQUIPMENT

This chapter introduces the CMT-welding equipment as well as the research methods and equipment used. Various different research methods were practiced in order to investigate the materials. Most of these methods are destructive, meaning that the component must be broke apart in order to test certain properties.

7.1 CMT welding equipment

Welding experiments were conducted in the Laboratory of Mechanical Engineering and Industrial Systems (MEI) at Tampere University of Technology. The characterization and sample preparation was done at the facilities of Laboratory of Material Science. In this chapter the practical part of this thesis is presented along with the equipment and reasons behind the experiments.

Fronius International GmbH manufactures all of the CMT welding equipment. The welding equipment consists of a TransPuls Synergic 4000 R power-source (1), FK 4000 R cooling unit (3), VR 7000 CMT wirefeeder (5), Robacta Drive CMT welding torch (6), and a wire buffer (7). This whole is controlled with RCU 5000i remote control (2). The equipment is attached to an ABB IRB 4600-40/2.55 robot-unit with digital controller (4). This equipment is presented in Figure 43.

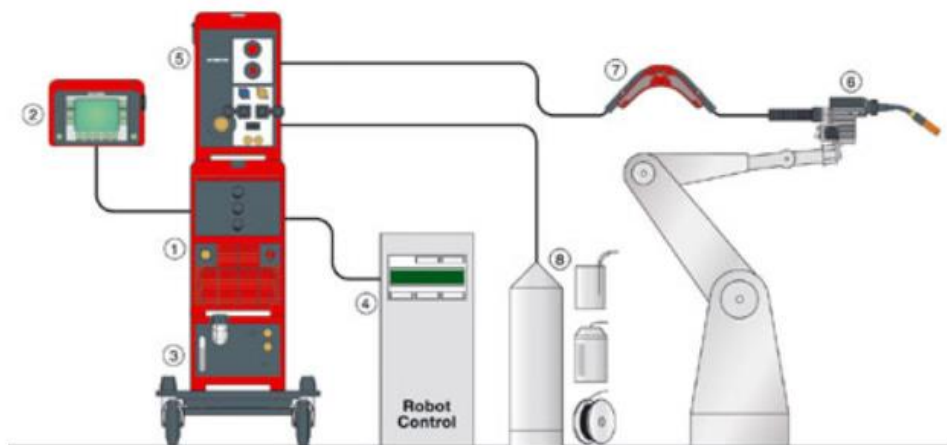


Figure 43. CMT-welding equipment [87]

The power source is fully digitized and microprocessor-controlled MIG/MAG power source for short circuit, spray and pulsed arcs. It also supports the CMT Advanced welding. It is designed for industrial use in automated and robot applications. Its welding current range is 3-400 A (MIG/MAG) with a working voltage of 7-34.0 V. Synergic operation means that the welding is made easy by just selecting material and sheet thickness and the machine controls the welding process automatically. Recommended base materials for this power source are aluminum, CrNi, special metals and steel. This unit is water-cooled by FK 4000 R attached at the bottom of the unit. [88]

VR 7000 CMT wire feeder pushes the wire from the coil into towards the welding torch via wire conductor with its small feeding motor. The wire buffer is an important part of the process, as the wire feeder only pushes the wire forward. The welding torch has its own motor for wire feeding also generating the back-and-forth motion of the wire. The wire buffer lets the wire length vary meaning that it decouples the front and rear wire-drives. Wire buffer and its functionality is presented in Figure 44.



Figure 44. Wire buffer. Arrow indicates the movement of the wire conductor as the length of the wire changes [87]

This whole equipment is controlled by the remote control, RCU 5000i. It controls the power source along with values related to welding via a digital display. It is connected to the system with a LocalNet connector. With this controller almost every aspect and finesse can be controlled even during the welding. Databases with preset welding programs for different filler materials can be uploaded into it, and these “jobs” can be altered to fit different purposes. Jobs have certain synergic lines for materials depending on the composition and other properties of the fillers. Synergic lines/curves were explained in chapter 3.3. The controller also stores data for each welding with timestamps and welding values, such as minimum and maximum currents, voltages, job number and the number of the synergic curve used.

This welding system is connected, and controlled by ABB IRB 4600-40/2.55 robot-unit. This robot-unit also includes a coordination (turn table, rotating table) table for the work piece. Many types of movement can be executed to create welds wherever they need to be done, including cylindrical shaped rod cladding etc. Rotating table also provides good possibilities for additive manufacturing with CMT. The reach of the robot is 2.55 meters with a payload capacity of 40 kg and an armload of 20 kg. Capacity of the turn table is 700 kg. The whole system at TUT was built in a way that the robot actually controls the beginning and the end of the welding, acting as a master in a way, the CMT-equipment being a slave.

7.2 Powder feeder

For cladding tests with solid lubricants an external powder feeder, Medicoat AG “Stand Alone, Duo Laser”, was used. The feeder nozzle was attached with a clamp to the welding torch and aimed towards the tip of the wire consumable. The distance from the nozzle tip to the wire tip was approximately 3-4 cm with 40-45° angle.

7.3 Planetary mill

Ball milling was used to mill Stellite 12 powder and solid lubricants to enhance the mobility of the solid lubricant particles in the powder feeder hoses. Type of the planetary mill was Fritsch Pulverisette 5. Steel balls with 11 mm diameter were used in the milling process.

7.4 Sample preparation

The metallographic specimens prepared were 30 mm diameter Polyfast specimens (Figure 46). The resin conducts electricity, which is required for scanning electron microscopy (SEM) inspections. This type of specimen is used because it can be examined with almost all of the research equipment required in the tests executed (microscopy: optical and SEM; hardness testing). Preparation includes a few steps to get the kind of specimen necessary. First, the base needs to be cut to get the cross-section of the weld bead. This usually takes many cuts to get a suitable micro section, as the specimen must fit into the 30 mm Polyfast specimen button. In Figure 45 a base material disc with sample cut away is shown. When the micro section is ready, sample preparation with Struers CitoPress-10 comes next. The micro section is inserted into the machine and PolyFast-substance is

placed on top and around of it into the tube. The machine then adds heat and pressure to mold the PolyFast resin into a hard button with the micro section in it.



Figure 45. *The base material with overlay welding*

After the specimen button is molded it needs to be ground and polished to get the cross section visible. For that a Struers manufactured Pedemax-2 grinder, polishing and lapping machine was used. It has an adjustable rotating plate capable of doing 150 or 300 rpm, to which the abrasive paper of polisher plate is set. The specimens are put on a specimen holder (1-6 pieces) which is then fixed on a holder on top of the rotating plate. Correct pressure is adjusted for the grinding using a knob in the grinder itself.

For these specimens, a basic “program” was used and it resulted in good, mirror-like surfaces. The program consists of 1 minute of grinding with P220, P600 and P1200 (ISO/FEPA) papers with 30 N load. This brings the micro section visible if there was any resin on it and makes the surface flat. After this the grinding paper is switched to a polishing cloth, in this case MD-DAC by Struers. It is made of satin woven acetate. As an abrasive DiaPro Dac 3 μm water-based diamond suspension is used. Specimen is polished with these for 3 minutes, suspension added for approx. every 30 seconds. Then the specimen is finished with even finer cloth made of porous neoprene, MD-Chem from Struers. A colloidal silica suspension, OP-U, with grain size of 0.04 μm . This final polishing is done for two minutes; first minute the lubrication with OP-U suspension and the second minute with just tap water. The results with this type of preparation has proved to be suitable and good for our specimens. [89]



Figure 46. *Typical specimen button, ground and polished*

After polishing the specimens are washed using an ultrasonic washer FinnSonic m08. This removes any dirt and impurities so that the specimen can be safely inspected with SEM and other equipment without the fear of contamination.

7.5 Microscopy

Different kind of microscopes were used for their special capabilities for inspecting the macro- and microstructures of the specimens prepared. Typically, the first one was the optical microscope, which is versatile and quick to use with magnifications from 2.5x up to 200x. Optical Microscopy (OM) was used to inspect the macroscopic properties of the coatings. The optical microscope used was Leica DM 2500M. The Scanning Electron Microscope used was Philips XL-30 with some external analyzers. SEM was used to inspect the microstructure and composition of the specimens.

7.5.1 Low-magnification images with optical microscopy (OM)

Optical microscopy is a fast way to analyze visual properties of the specimens. It is a quick way to inspect if the coating has desired properties like fusion with the base material, if it is pore-free or if there are many unmelted particles and such. With OM, Live Image Builder -function was used to compile multiple images to get the whole cross-section into one image. After acquiring images with OM they can be further analyzed to calculate things like dilution, penetration depth, deposition rate, clad angle and other properties. For this thesis a program called ImageJ was used to calculate the properties mentioned. One has to bear in mind that the image acquired with OM (or SEM) is only one cross-section of a larger whole. If the coating is not smooth and there is lot of variation, a simple cross-section is not enough to provide reliable information about the coating.

7.5.2 High-magnification images with Scanning Electron Microscopy

Scanning Electron Microscopy (SEM) was used to further analyze the specimens as it brings out different elements as different shades in the images. It is also capable of much greater magnifications (from 10-200000x) than OM to observe the specimens with a higher precision. With some add-on of the equipment it also possible to identify different elements in the specimen from a certain area. One other strength of SEM is the much greater depth of field compared to OM. With the equipment at TUT also microhardness measurements can be done.

7.6 Composition and material phases

It is important to understand the effects of the welding process to the materials involved. That is why the chemical composition and phases need to be analyzed in order to predict the behavior of the material under stress. This chapter reviews shortly the research methods used.

7.6.1 Energy-Dispersive X-Ray Spectroscopy (EDS)

Energy-Dispersive X-Ray Spectroscopy, EDS, is used to identify the characteristic x-rays of different elements as the material is exposed to an electron beam. EDS-detector, EDAX DX 4, integrated into the SEM-equipment collects these X-rays and turns them into a spectrum from which specific elements can be identified. It can be used to determine chemical composition from a smaller area, e.g. size of a few microns of interest, or to map a larger area. EDS, in this thesis, was used to identify compositional dilution of the specimens, different carbides, unmelted particles and solid lubricants. [90]

7.6.2 X-Ray Diffraction (XRD)

X-ray diffraction (XRD) is the only laboratory technique that reveals certain structural information of materials. With XRD such properties like chemical composition, crystal structure, strain and layer thickness can be obtained. The equipment at TUT is called Panalytical Empyrean Multipurpose Diffractometer. It exploits the unique d-spacings of each material to identify them, by directing monochromatic radiation towards the specimen. The incident rays interact with the material and the specimen produces constructive interference and a diffracted X-ray, which are then detected. By counting and processing these X-rays and comparing them with standard reference patterns materials can be identified. XRD-analysis can be used to many forms of materials including solids, powders to thin films and coatings. In this thesis XRD was used to observe the material phases. [91,92]

7.7 Surface roughness

Surface roughness measurements were used to estimate the quality of the surface of wear test pieces, as the wear surfaces needed to be fine enough for the wear tests to be reliable and consistent. At this point the disks were already ground to achieve a surface fine enough. Mitutoyo SJ-301 device was used to measure the roughness's. According to standard ASTM-G99 the surface roughness needs to be at least Ra0.8 μm .

7.8 Vickers hardness measurements

Material hardness is measured by its ability to withstand dents caused by another material whose hardness is known. Hardness is evaluated by the size of the indentation caused by the test; in softer materials the mark is deeper and bigger than in harder materials. In other words, hardness is materials ability to withstand plastic deformation. Hardness measurements are executed to evaluate materials properties and to predict functionality in different circumstances. Hardness effects wear, brittleness, machinability and many other vital properties of a material.

Hardness measurements of this thesis were executed with Vickers hardness test, using a Matsuzawa MMT-X7 hardness tester. Vickers test can be executed to all metallic materials and it has the widest range of hardness values. In this test, a pyramid shaped diamond tip (facet angle 136°) is pressed with a certain load F (in N) onto a surface of material, in this case the cross section of the specimens. The load is applied for 10 seconds. Dimensions d_1 and d_2 of the indentation caused by the tip are measured, and the hardness value is a result from the ratio between the load value and the area of the dent. Depth of the indentation is marked with the letter h . Indentation is presumed to be similar, square-based pyramid, as the diamond tip with the same apex angle. The test arrangement is presented in Figure 47. [93,94]

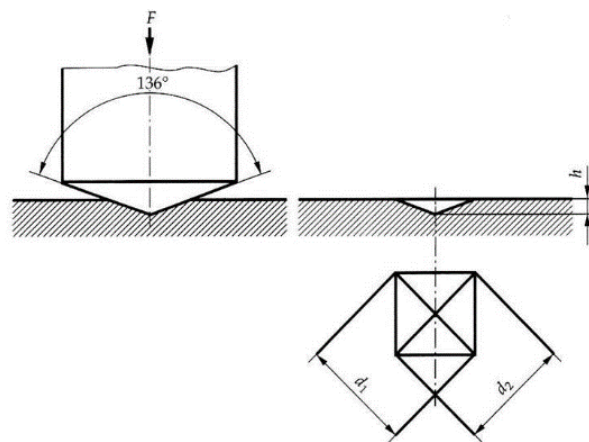


Figure 47. Principle of the Vickers hardness test [94]

The result of the test is presented as follows: xxxHVyy, for example 350HV10. If the load time differs from the defined 10-15 seconds, values are presented xxxHVyy/zz, for example 350HV10/20. [93]

- 350 is the hardness value,
- HV is the unit,
- 10 is the approximate load in kilogram-force (kgf), where $10 \text{ kgf} = 98,0665 \text{ N}$,
- 20 is load time (20 s), only stated if differs from defined (10-15s)

Standard SFS-EN ISO 6507-1 states some requirements for the circumstances and the test piece itself. The concern mainly the cleanliness and surface of the test piece. The surface investigated must be smooth and flat, free from impurities, foreign materials and especially from lubricants. The surface quality must be good enough for reliable measurements of the indentations. In sample preparation it must be taken into account that the surface hardness is not affected by measures used via hot or cold forming. [93]

All of the hardness measurements were done with a similar method and pattern which is described in Figure 48.

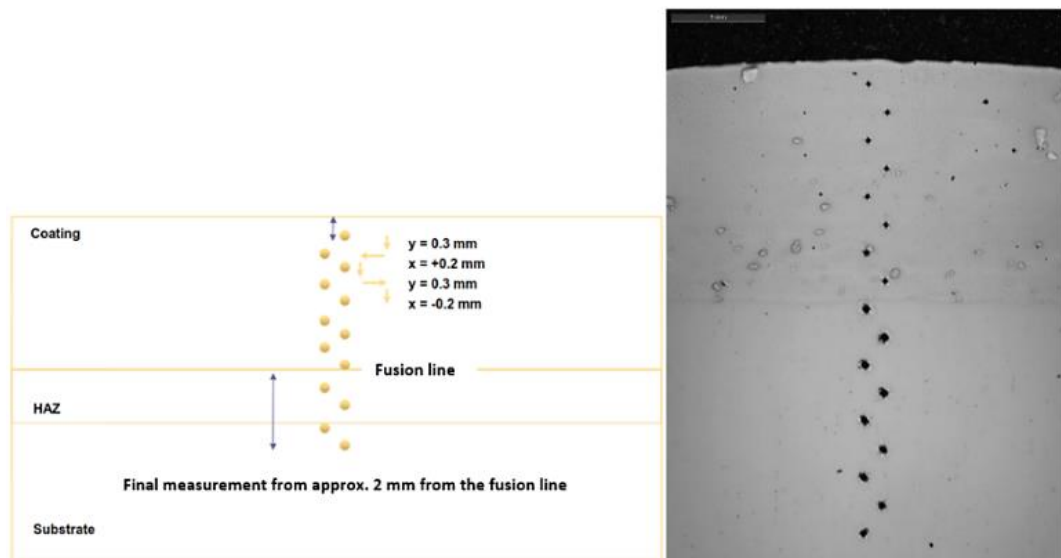


Figure 48. Hardness measurement pattern and an example OM-image

7.9 Wear tests (Pin-on-disc, ASTM-G99)

Wear tests for specimens have been run to determine their wear behavior under conditions similar to service conditions. Pin-on-disk tests also gives friction coefficient values. Wear tests were done at TUT with pin-on-disk device CETR UMT-2. The equipment in TUT enables the testing to be done also in elevated temperatures which is an important issue considering the operating environment of e.g. engine components in a diesel or a gas motor. Materials tend to behave differently under room temperature and in elevated temperatures. Below is a schematic presentation of a pin-on-disk test device, where R is the pin contact distance from the center of the disk, r_0 is the diameter of the disk, F_N the predetermined force of the test and ω is the rotational velocity of the disk. The sliding velocity $v = R\omega$. Testing time is also predetermined. The wear results are measured by the material loss in the specimens, both separately. The test schematic is presented in Figure 49. [95]

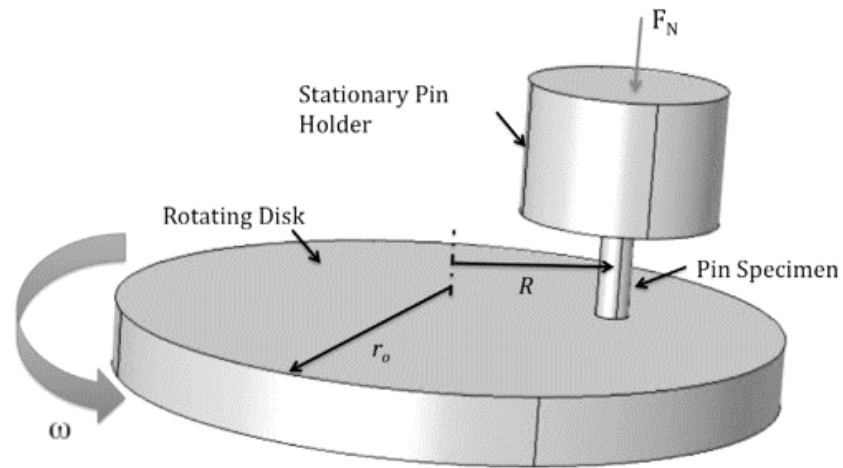


Figure 49. Schematic presentation of a typical pin-on-disk test device [95]

In this thesis, a force sensor with range of 0.5-200N with 10 mN resolution was used. The disk size is 70 mm in diameter, and the pin diameter is 6.35 mm.

8. CLADDING TESTS

The goal of this thesis was to investigate the suitability of CMT-cladding of wear and corrosion resistant coatings with Co-alloy on materials used in engine components. Another main agenda was to sort out a suitable solid lubricant that can withstand the process, in order to further reduce friction and wear in the applications mentioned. A large amount of coatings with altered process parameters on different substrates were produced during the completion of this thesis. Tests were executed in order to gain knowledge on the process and to optimize the properties of the coating. In this chapter the results of these claddings are reviewed.

8.1 Basic cladding tests

The basic tests were executed to investigate the CMT-process and the effect of the vast amount of parameters in the properties of the coating. The tests were executed with Stellite 21 wire and Co-alloy consumables trying out synergic lines and protective gases. The first tests executed with Stellite 21 were not that vital and were executed to optimize parameters before starting out with Co-alloy; that is why the tests using Co-alloy are emphasized more. During all of the tests, the angle of the torch was 90° perpendicular to the base material. The complete minutes of tests can be found in appendix A and B.

8.1.1 Stellite 21 coatings

The cladding tests began with Stellite 21 wire. The goal with these tests was to optimize parameters towards a low dilution and low heat input direction. The substrate material used was mainly a 20 mm thick disc of 42CrMo4 with a diameter of 120 mm. Some claddings were manufactured on Nialloy substrate and on Cr-steel to see the effects different base materials have on the process. Discs were cleaned with acetone prior to experiments and clamped to avoid the movement and distortion during the welding tests. All of the tests were run with CMT-process using synergy curve no. 1291 “Stellit21 1.2 mm” in database M03-0271 with Argon as the protective gas. Other parameters such as wire feed rate (WFR), travel speed and arc length correction (ALC) were changed one at a time to observe and monitor the effects of each parameter. During cladding tests, both stringer beads and weave beads were manufactured with one or multiple overlapping beads. The complete parameter proceedings can be found as appendix A.

Wire feed rate was altered between 5.0 and 8.0 m/min depending whether weaving motion was used or not. With weaving motion WFR was at the low end of this range. Transverse velocity was altered between 3.5 mm/s and 13.3 mm/s. With single bead the velocity can be higher and when using weaving motion, the value we found close to optimal was 3.5 mm/s. Although the cored wire showed a bit of sparking and crackling during the tests, cladding with both weaving and linear motion, using single and multiple passes, CMT was successful of manufacturing nearly spatter-free and defect-free coatings when inspected with the naked eye. Figure 50 presents sample ST21-022. The parameters used in manufacturing of this clad are shown in Table 11 along with other coatings which were prepared to samples. The cross-sections of the samples in the table are presented in chapter 9.1.1.

Table 11. Stellite 21 cladding process parameters

Sample		ST21-004	ST21-006	ST21-020	ST21-022
Material	Clad	Stellite 21	Stellite 21	Stellite 21	Stellite 21
	Base	42CrMo4	42CrMo4	42CrMo4	Nialloy
Number of beads		1	4	2	1
Synergic line		1291 (Stellit 21)	1291 (Stellit 21)	1291 (Stellit 21)	1291 (Stellit 21)
Voltage (V_{ave})		10.4	10.3	11.6	12.1
Current (A_{ave})		194	187	152	139
Arc power, $U \times I$ (W)		2018	1926	1763	1682
Welding energy $E = ((U \times I) / v)$ (J/mm)		202	193	504	481
Wire feed rate (m/min)		8.0	8.0	5.0	5.0
ALC (%)		-30	-30	+15	+30
DC		-5	-5	-5	-5
Protective gas		100% Ar	100% Ar	100% Ar	100% Ar
Travel speed, v (mm/s)		10.0	10.0	3.5	3.5
Weaving/stringer (width)		stringer	stringer	weaving (12 mm)	weaving (12 mm)



Figure 50. Sample ST21-022

8.1.2 Co-alloy coatings

The tests with this wire were started after parameter optimization with Stellite 21 filler material. Stick-out remained the same during all of the tests at 17 mm. First coatings, samples TH12G-001 to TH12G-002, were produced with a high heat input synergy line, “FCW Hardfacing (1357)”, and with a straightforward motion without weaving. Mison18 was used as protective gas. Tests with this synergic line produced lots of spatter and seemed to be too hot. The parameters of some tests are presented in Table 12. Figure 51 presents the first samples produced with Co-alloy.

Table 12. Co-alloy process parameters

Sample		TH12G-001	TH12G-007	TH12G-016
Material	Clad	Co-alloy	Co-alloy	Co-alloy
	Base	42CrMo4	42CrMo4	Cr-steel
Number of beads		1	3 (layered)	1
Synergic line		FCW Hardfacing (1357)	G3Si (1362)	G3Si dynamic (1640)
Voltage (V_{ave})		25.6	9.4, 9.0, 7.8	14.8
Current (A_{ave})		242	60, 59, 58	190
Arc power, $U \times I$ (W)		6195	564, 531, 452	2812
Welding energy $E = ((U \times I) / v)$ (J/mm)		466	56, 53, 38	803
Wire feed rate (m/min)		8.0	1.0	5.0
ALC (%)		-30	-6, -11, -17	-30
DC		-5	0	-5
Protective gas		Mison18	Mison18	Mison18
Travel speed (mm/s)		13.3	10, 10, 12	3.5
Weaving/stringer (width)		stringer	stringer	weaving (16 mm)

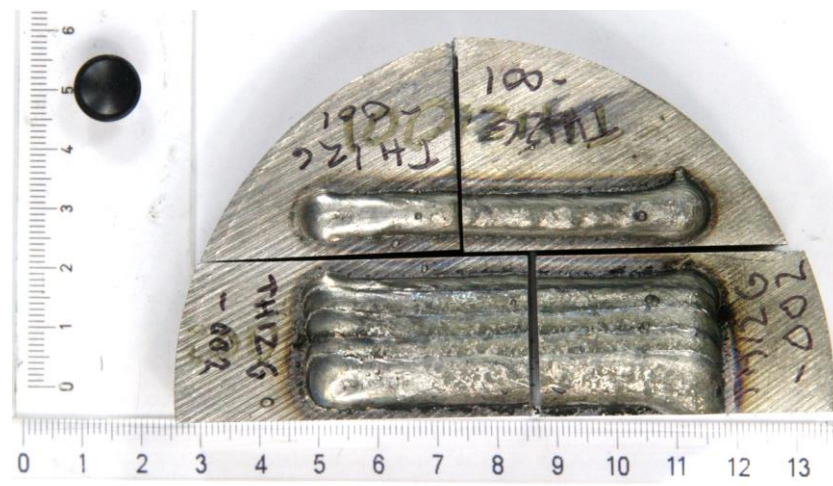


Figure 51. Sample TH12G-001(top) and TH12G-002 (latter)

After these first tests and the evaluations of properties it was decided to change the synergic line to a one with less heat input for samples TH12G-003 to TH12G-010. Some help

from a representative from Pronius was received and a new synergy line for G3Si was chosen. One reason for this selection was the fact that there was also a dynamic synergic line for this material, which was to be tested. The “dynamic” term means that the average wire motion is increased from 70 Hz to up to 140 Hz compared to the normal CMT option. During first tests also a coating with three layers on top of each other was manufactured for the purposes of testing the hardness that can be achieved with the equipment and filler material. This excludes the issues with dilution affecting the hardness and gives a reference point for the achievable hardness values for the coating. These beads are presented in Figure 52. The objective of these first tests was to optimize the parameters, and to test how the stringer beads could be overlapped. WFR was altered between 8 m/min and 9.5 m/min and travel speed between 8.5 mm/s and 16.7 mm/s. Coatings were produced both on Cr-steel and 42CrMo4 substrates and Mison18 was used as the protective gas. DC was mainly set at 0 and ALC was set to 0 % and 10 %. All of the processes seemed to produce solid and pore-free coatings with only a minimal amount of spattering.



Figure 52. Samples TH12G-006 (top) and TH12G-007 (latter)

After stringer bead tests and some microscopic and other measurements it was decided to carry on the test with weaving motion. Base material was mainly S355 steel plate (200x400 mm, thickness 15 mm), but with some samples also Cr-steel discs were used. Tests TH12G-011 to TH12G-016 were operated with G3Si1 (dynamic and normal) synergic lines with ALC -30 % and DC at -5. They were manufactured with weaving motion and the goal was to optimize the width of the bead to approximately 19 mm; this is the optimum value for one application. This was done by adjusting the weaving motion width at the range of 12 to 16 mm. Other parameters were kept constant; WFR 5.0 m/min with 3.5 mm/s travel speed. Mison18 was used as the protective gas. Samples TH12G-015 and -016 are presented in Figure 53.

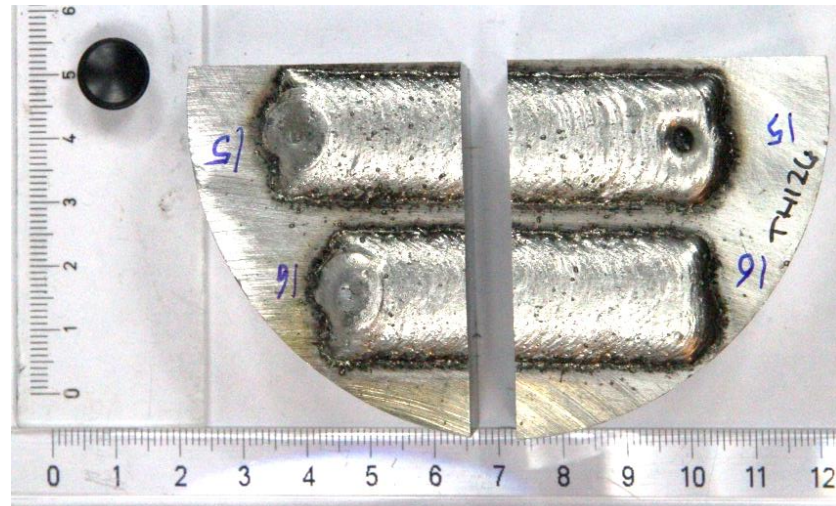


Figure 53. Samples TH12G-015 (top) and TH12G-016 (latter)

Next samples TH12G-017 to TH12G-024 were manufactured with synergy line 1291 for Stellite21, other parameters were kept almost the same; ALC was adjusted at the range of -15 % to +30 % and travel speed was lowered to 3.0 mm/s to reach a good coating quality. These coatings were manufactured on S355 steel plate. Also starting current and duration were increased a bit (120 % current for 0.4 seconds) to get rid of a hole that appeared at the start. At the end of these tests the best result (TH12G-024) was achieved with ALC 0 %, DC -5, WFR 5.0 m/min with 3.0 mm/s travel speed as the width of the weaving motion was 16 mm. Sample TH12G-024 is presented in Figure 55. Table 13 presents process parameters of further tests.



Figure 54. Sample TH12G-024

Table 13. Co-alloy process parameters

Sample		TH12G-024	TH12G-030	TH12G-034
Material	Clad	Co-alloy	Co-alloy	Co-alloy
	Base	Cr-steel	Cr-steel	Nialloy
Number of beads		1	1	1
Synergic line		Stellit21 1.2mm (1291)	Stellite6 1.2mm (1656)	Stellite21 1.2mm (1657)
Voltage (V_{ave})		14.9	13.7	15.4
Current (A_{ave})		155	166	172
Arc power, $U \times I$ (W)		2310	2274	2649
Welding energy $E = ((U \times I) / v)$ (J/mm)		770	758	883
Wire feed rate (m/min)		5.0	6.0	6.0
ALC (%)		0	0	0
DC		-5	-5	-5
Protective gas		Mison18	Mison2	Mison2
Travel speed (mm/s)		3.0	3.0	3.0
Weaving/stringer (width)		weaving (16 mm)	weaving (16 mm)	weaving (16 mm)

After examination it was ruled, that too high dilution caused the lack of hardness with the previous tests. The protective gas, Mison18, with high amount of CO₂, may also have caused this. Gas was changed to pure Argon (TH12G-025 – TH12G-027) and then to Mison2 with 98 % Ar and 2 % CO₂ for TH12G-028 to TH12-034. Base materials were Cr-steel discs, and with TH12G-033 and -034 the base was Nialloy. ALC was kept at 0 % and DC at -5. WFR was altered between 5.0 m/min and 6.0 m/min to provide enough material to produce a dense coating with all of the synergic lines. Travel speed was kept at 3.0 mm/s. Different Stellite-synergic lines were used to see the differences between them. The lines used were “1291 Stellit21”, “1657 Stellite 21”, “1656 Stellite 6” and “1653 Stellite 26”. Visually inspected, they all seemed to produce dense and decent looking coating with no holes and reasonably smooth surfaces. Average voltage values ranged from 12.0V to 15.4V and current from 149A to 176A. Figures 55 and 56 present samples TH12G-030 and TH12G-034, respectively.

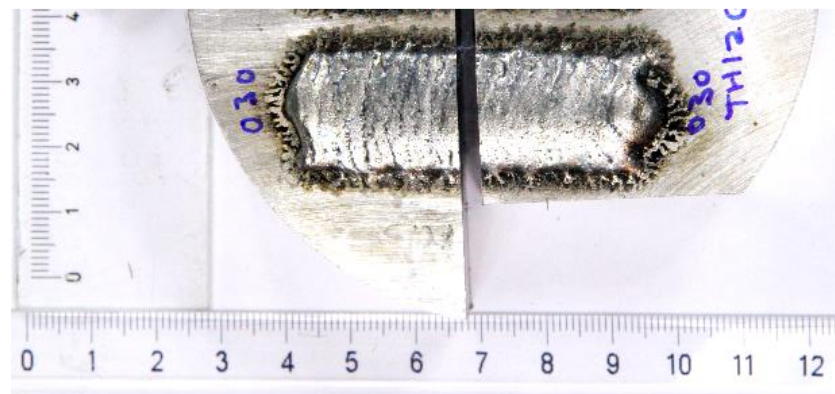
**Figure 55. Sample TH12G-030**



Figure 56. Sample TH12G-034

Fronius Xplorer was introduced at one point of the claddings. It is a program which collects data of the process at 0.1 second intervals. A clad with the parameters of TH12G-030 on Cr-steel disc with 6.5 m/min wire feed speed was manufactured and the graphs of process parameters are presented in Figure 57. The parameters are also presented in Table 14. Although the wire feed rate seems to vary vastly, the mean value calculated from this data is 6.5 m/min, which was the preset value. This exhibits how the process is adapting all the time during cladding.

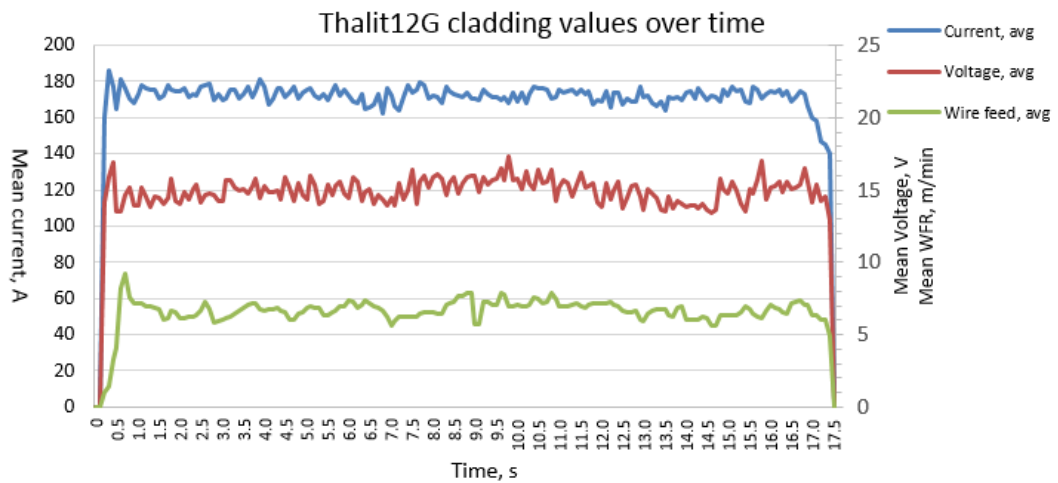


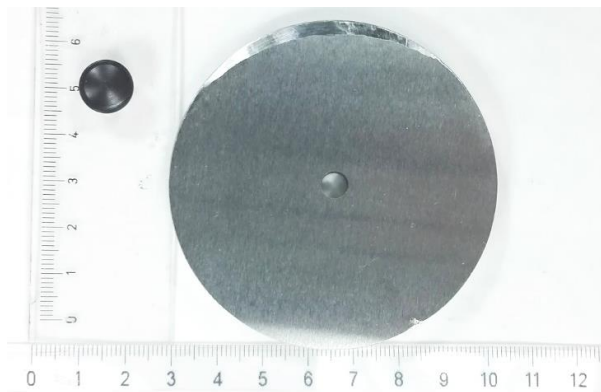
Figure 57. TH12G-045 cladding parameters

Table 14. Co-alloy process parameters

Sample	TH12G-045	
Material	Clad	Co-alloy
	Base	Cr-steel
Number of beads	1	
Synergic line	Stellite6 1.2mm (1656)	
Voltage (V_{ave})	14.7	
Current (A_{ave})	169	
Arc power, $U \times I$ (W)	2484	
Welding energy $E = ((U \times I) / v)$ (J/mm)	828	
Wire feed rate (m/min)	6.5	
ALC (%)	0	
DC	-5	
Protective gas	Mison2	
Travel speed (mm/s)	3.0	
Weaving/stringer (width)	weaving (16 mm)	

After evaluating these samples pin-on-disk wear test disks were cladded. For this purpose, synergic line “1656 Stellite 6” was chosen. Mison2 was used as the protective gas, travel speed of 3.5 mm/s, WFR 6.0 m/min, ALC 0 %, DC -5 and weaving width was decreased to from 16 mm to 12 mm. Base material was 42CrMo4 steel. A larger area needed to be coated, so 8 beads were produced with 10 mm inter-track advance and 80 mm bead length. Total amount of 5 disks were cladded with these parameters, average voltages were around 13 V and currents at around 165 A. No cracking was detected during cladding and the coatings seemed to be dense with no blow holes. After cladding the disks were immediately put between ceramic plates to cool down.

After cooling down the discs were lathed to 70 mm diameter and 10 mm thick discs to prepare them for pin-on-disk wear tests. The cladded surfaces were also fine ground to reach a fine surface roughness of Ra0.30 – 0.40. After the treatments the thickness of the clad in the discs was approximately 2-3 mm. One machined disc is presented in Figure 58.

**Figure 58.** Wear test disc

8.1.3 Stellite 12 coatings (reference)

During the tests, a coil of Stellite 12 cored-wire with was found with no proper markings about manufacturer or composition. It was decided to be used as a reference to see the differences between this and the Co-alloy used. Only one test clad was manufactured and the parameters can be seen in Table 15. There is no knowledge of the age or the manufacturer of this wire.

Table 15. *Stellite 12 process parameters*

Sample		ST12-001
Material	Clad	Stellite 12
	Base	Cr-steel
Number of beads		1
Synergic line		Stellite 21 1.2mm (1657)
Voltage (V_{ave})		12.9
Current (A_{ave})		176
Arc power, $U \times I$ (W)		2270
Welding energy $E = ((U \times I) / v)$ (J/mm)		757
Wire feed rate (m/min)		6.0
ALC (%)		0
DC		-5
Protective gas		Mison2
Travel speed (mm/s)		3.0
Weaving/stringer (width)		weaving (16 mm)

The clad looked similar to Co-alloy and the welding and melt pool seemed to act also in a similar way than Co-alloy. Sample ST12-001 is presented in Figure 59.

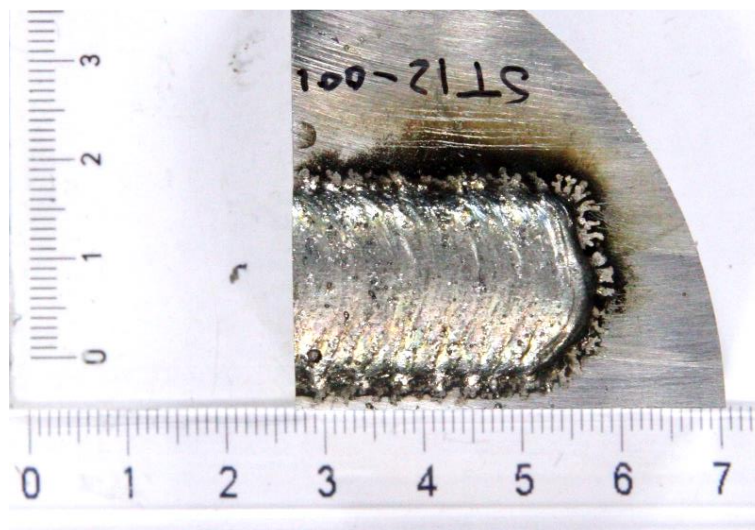


Figure 59. *Sample ST12-001*

8.2 Cladding tests with solid lubricant powders

Some tests with external powder feeder connected to the welding torch were conducted with CaF_2 , TiO_2 and WS_2 solid lubricants. The manufacturer of CaF_2 -powder is Cerac with grain size of 45-100 μm , TiO_2 -powder is manufactured by HC Stark Amperit with grain size of 45/22 μm and WS_2 manufactured by Cerac with grain size less than 1 μm . The test set-up is presented in Figure 60. Medicoat AG “Stand alone” -powder feeder was used with a powder feeding nozzle type Coax 8 (manufactured by Fraunhofer IWS, Dresden, Germany). Argon acted as the carrier gas at 6 l/min, and in addition to carrier gas, shielding gas with a flow rate of 15 l/min was used. The powder feeding nozzle can be seen on the left side.



Figure 60. CMT and powder feeder nozzle setup

The feed rate of the CaF_2 -lubricant was calculated via deposition rate of the Co-alloy-cladding (~ 3.0 kg/h) so that the goal was to have approximately 10-20 wt% of CaF_2 in the finished cladding. The feed rate was set at 7 % (8.2 g/min), and was raised to 8 % considering the amount of powder bouncing away from the melt pool. Powder stirrer was set to 30 %. Tests were run with pushing and dragging motion; meaning the movement of the welding torch was altered between tests. With CaF_2 , Co-alloy consumable was used, and with TiO_2 Stellite 12 wire was selected. The table of parameters is presented below. Table 16 lists the parameters for the cladding manufactured with dragging motion.

Table 16. Solid lubricant addition coating process parameters

Sample		TH12G-037	ST12-003
Material	Clad	Co-alloy	Stellite 12
	Base	42CrMo4	42CrMo4
Solid lubricant (feed rate)		100 % CaF ₂ (~9 g/min)	100 % TiO ₂ (~1 g/min)
Number of beads		1	1
Synergic line		Stellite6 1.2mm (1656)	Stellite21 1.2mm (1657)
Voltage (V_{ave})		13.1	12.9
Current (A_{ave})		161	169
Arc power, $U \times I$ (W)		2109	2180
Welding energy $E = ((U \times I) / v)$ (J/mm)		703	727
Wire feed rate (m/min)		6.0	6.0
ALC (%)		0	0
DC		-5	-5
Protective gas		Mison2	Mison2
Travel speed (mm/s)		3.0	3.0
Weaving/stringer (width)		weaving (12 mm)	weaving (12 mm)

Less amount of TiO₂ was used in literature so it was decided to set the feed rate to approximately 1 g/min for TiO₂. This means around 2 wt% TiO₂-content in the finished coating. The flow of powder and gas from the powder feeder seemed to have a “cooling” effect on the process and perhaps a little more power could have been used to guarantee proper adhesion. Similarly, higher amount of welding energy will cause the decomposition of the solid lubricants particles which have much lower melting point than the metallic materials used. The clads with lubricant addition can be seen in Figures 61 and 62.

**Figure 61.** Sample TH12G-037; CaF₂-addition, dragging motion.

CaF₂ seemed to rise on top of the clad and dark, brittle slag was formed on top and on the sides of the weld bead. Also a greenish color could be observed in the slag. TiO₂ formed a darker slag on top of the bead and seemed to have a stronger cooling effect on the

process. Lubricant additions also had an effect on fluidity of the melt pool and both seemed to make the contact angle smaller; the effect was stronger with TiO_2 .



Figure 62. Samples ST12-002 and -003; TiO_2 addition. ST12-003 with dragging motion (right to left), ST12-002 with pushing motion (left to right).

Other solid lubricants, MoS_2 and WS_2 , were also used, but for their fine particle size ($<1 \mu\text{m}$) another kind of approach was used to get a proper feed from our powder feeder. The lubricants were mixed with a PTA-grade Stellite 12 powder (grain size $50\text{-}150 \mu\text{m}$) using planetary mill, Fritsch Pulverisette 5. The powders were mixed as different compounds for 3 hours, with 11 mm steel balls and 4:1 ball-powder-ratio. Powder mix 1: 10wt% MoS_2 + 90wt% Stellite 12 and two mixes of WS_2 -powder: powder mix 2. with 70wt% Stellite 12 and 30wt% WS_2 , and powder mix 3. with 50wt% Stellite 12 and 50wt% WS_2 . Table 17 presents process parameters for the cladding tests.

Table 17. Solid lubricant addition cladding process parameters

Sample		TH12G-041	TH12G-042
Material	Clad	Co-alloy	Co-alloy
	Base	Cr-steel	Cr-steel
Solid lubricant (feed rate)		Powder mix 1. (14.5 g/min)	Powder mix 1. (14.5 g/min)
Number of beads		1	1
Synergic line		Stellite6 1.2mm (1656)	Stellite6 1.2mm (1656)
Voltage (V_{ave})		16.4	15.7
Current (A_{ave})		172	176
Arc power, $U \times I$ (W)		2821	2763
Welding energy $E = ((U \times I) / v)$ (J/mm)		940	921
Wire feed rate (m/min)		6.5	6.5
ALC (%)		0	0
DC		-5	-5
Protective gas		Mison2	Mison2
Travel speed (mm/s)		3.0	3.0
Weaving/stringer (width)		weaving (12 mm)	weaving (12 mm)

Tests with Powder Mix 1. seemed both to produce dense and hole-free coatings. The color difference of the two beads is significant as can be seen in Figure 63. TH12G-041 produced with pushing motion of the powder nozzle seems to have a visible dark slag layer on top the bead that TH12G-042 does not have. The processes themselves looked quite similar, only the gas flow from the powder nozzle seems to have some effects on the shape and looks of the beads.



Figure 63. Samples TH12G-041 (pushing) and TH12G-042 (dragging)

Two mixtures of Stellite 12 + WS₂ powders were milled, but only a coating with Powder mix 2. addition was successfully manufactured. Powder mix 3. with higher wt% of fine sized WS₂ did not run through the powder feeder because of the small particle size, and a coating was not manufactured. Table 18 presents the coating parameters.

Table 18. Solid lubricant addition coating parameters

Sample	TH12G-043		TH12G-044
Material	Clad	Co-alloy	Co-alloy
	Base	Cr-steel	Cr-steel
Solid lubricant (feed rate)	Powder mix 2. (15.2 g/min)		Powder mix 2. (15.2 g/min)
Number of beads	1		1
Synergic line	Stellite6 1.2mm (1656)		Stellite6 1.2mm (1656)
Voltage (V_{ave})	17.2		17.1
Current (A_{ave})	172		173
Arc power, $U \times I$ (W)	2958		2958
Welding energy $E = ((U \times I) / v)$ (J/mm)	986		986
Wire feed rate (m/min)	6.5		6.5
ALC (%)	0		0
DC	-5		-5
Protective gas	Mison2		Mison2
Travel speed (mm/s)	3.0		3.0
Weaving/stringer (width)	weaving (12 mm)		weaving (12 mm)

Similarly, as with powder mix 1, the coatings seem dense and defect free. Also the color differences are comparable, as the bead produced with the pushing motion of the powder feeder is significantly darker than the one produced with dragging motion, presumably because of a slag layer (Figure 64). A high speed video was also recorded of TH12G-044 which shows that the powder feeder nozzle is headed correctly and the powder particles hit both the melt pool and the arc.

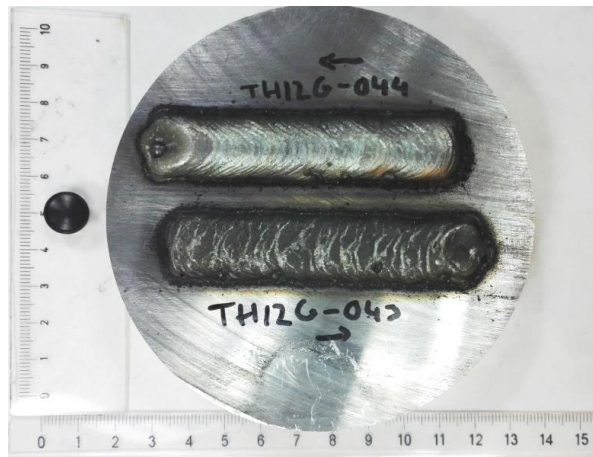


Figure 64. Samples TH12G-043 (pushing) and TH12G-044 (dragging)

8.3 Remarks during basic cladding tests

It was noticed that especially the Co-alloy wire is “leaking” material into the wire conductor thus impairing the movement of the wire and resulting in defect in the cladding process and the coatings themselves. In worst case scenario the powder can block the movement of the wire entirely and cause the stoppage of the welding process. This leakage also affects the composition of the powder inside the wire and therefore to the composition and material properties of the clad itself, including properties like hardness and wear resistance. During the pin-on-disk cladding, that lasted a few minutes, the wire conductor, especially the part from the wire buffer to the welding torch, needed to be removed and cleaned with pressurized air between each disk to maintain proper movement of the wire. This issue might be influenced with drive roll wheels designed for tubular wires and the adjustment of the drive roll pressure. These things may cause distortion of the wire shape and open up the seam, together with the back-and-fro movement of the wire, probably caused the leaking of the wire. When this leaked powder material was collected from the wire conductor and analyzed with SEM, it was discovered to include particles of chrome, boron, silicon and calcium. With solid wires this problem does not exist to our knowledge.

To find the optimal parameters and synergic lines can be time consuming, but with experience this thing will not be an issue any longer. Usually, even with incorrect parameters, a coating was able to be manufactured.

9. RESULTS, DISCUSSION AND FURTHER ACTIONS

A large amount of test coatings were manufactured during the completion of this thesis. The results of these tests were presented in the previous chapter, 8. Cladding Tests. In this chapter the results and the reasons behind them are analyzed. Also further actions are considered.

9.1 Characterization

In basic cladding tests different parameters, synergic lines and protective gases were tried to optimize the process characteristics for Stellite 21 and Co-alloy consumables with different substrate materials. Agenda of these tests was to find out the effect of different parameters to the macroscopic and microscopic properties of the coatings.

9.1.1 Stellite 21

As mentioned, this filler wire was only used to manufacture a decent coating to find the parameters to begin with Co-alloy. Single stringer beads appeared to be quite good, with a limited amount of dilution. As multiple stringer beads were overlapped to produce a wider coating, it was found that the parameters were too cold and there was no fusion bond. Single stringer bead can be seen in figure 65. and 4 bead coating with overlapping is presented in Figure 66. The height of the bead in Figure 65 is 3.04 mm and the width is 3.67 mm.

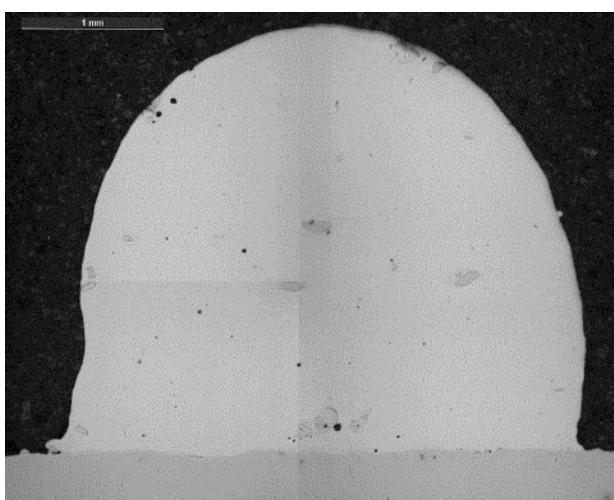


Figure 65. Specimen ST21-004. Single stringer bead.

When inspecting Figure 66, specimen ST21-006, it can clearly be seen that the process has not enough heat for a proper fusion and the dilution is practically 0 %. There are many defects between the beads and the overlapping probably causes the lack of fusion, as the beads only fuse with each other and not the base material. This is caused by both the lack of welding energy and the perpendicular angle of the welding torch. The angle can cause the arc to jump into the previous bead instead into the base material. In this figure the first bead is on the right side of the image showing a better adhesion into the base material.

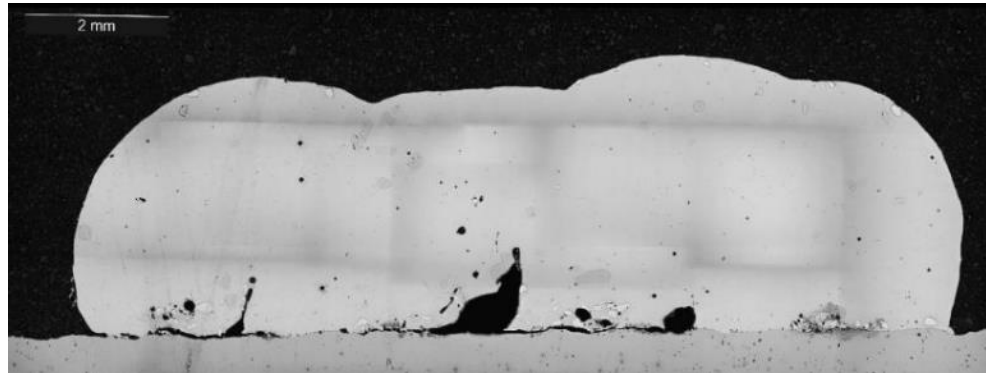


Figure 66. Specimen ST21-006. 4 stringer beads overlapped.

After first tests it was decided to experiment with weaving motion. After a few parameter optimization test a weaving bead was manufactured on Nialloy. It seemed to be low-diluted and still dense with the naked eye, but the OM-images revealed that the dilution was not sufficient for a proper adhesion. There is also a lot of unmelted particles near the fusion at the bottom of the weld bead. This is presented in Figure 67. The height of the bead is 2.55 mm and the width is 13.83 mm.

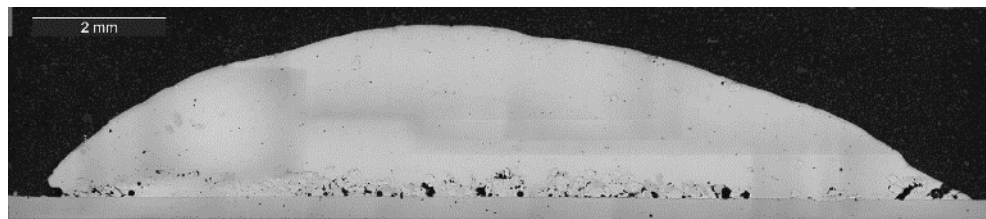


Figure 67. Specimen ST21-014. Single bead with weaving.

Also two-bead cladding with weaving motion was manufactured with 10 mm inter-track advance, but after OM-inspection lack of fusion at the edges was discovered and also some holes and unmelted particles near the fusion line. Otherwise the coating is good with a low amount of dilution. This specimen is presented in Figure 68.

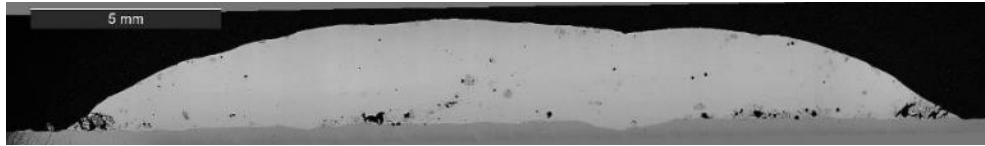


Figure 68. Specimen ST21-020. Two beads with weaving.

After two-bead testing we returned to single-bead weaving on Nialloy and added a bit of power by increasing ALC to +30 %. This resulted in a very good coating with proper amount of dilution. The bead can be seen in fig. 69. The etched specimen is shown in Figure 69 at the latter image, where HAZ is visible as a darker area beneath the clad. The depth of the HAZ is only 0.89 mm, which is an excellent value for coating produced with a welding process. The dilution is even and there are hardly any defects or unmelted particles. The width of the bead is 14.67 mm and the height is 2.2 mm with 6.5 % dilution and a deposition rate of 2.32 kg/h.

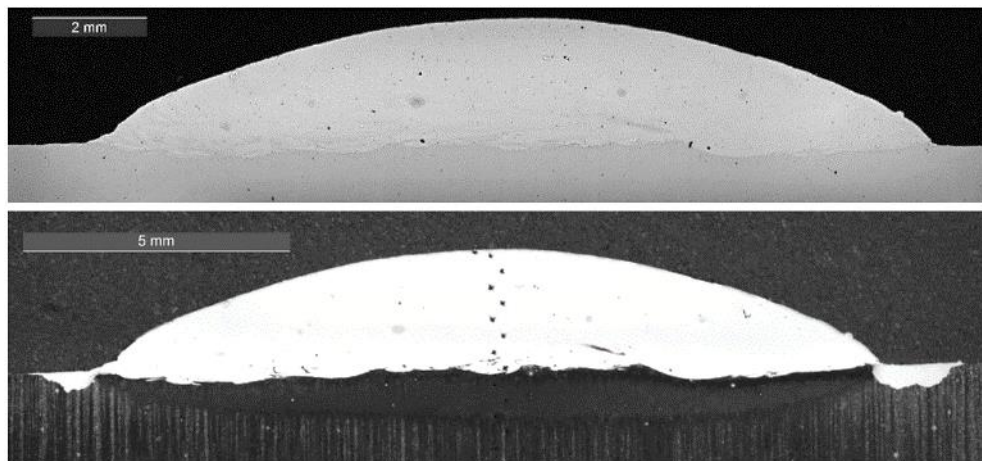


Figure 69. Specimen ST21-022. Single bead with weaving motion. The specimen in the latter image is etched to reveal the HAZ.

After this test, it was decided that the parameter optimization had been successful and it was time to concentrate on the more essential material, Co-alloy.

9.1.2 Co-alloy

At the beginning of Co-alloy cladding tests it was important to find some boundary values for the welding energy to optimize dilution of the clad. It was decided to start with a synergic line with high energy. For this purpose, an “overall” synergic line for cored wires, 1357 “FCW Hardfacing”, was chosen. When investigated it was clear that the synergic line was way too hot and the dilution was >30 %. The hardness measurements presented later on confirmed the negative effect of dilution on the microhardness. Specimen TH12G-001 is presented in Figure 70. The clad is otherwise good with no visible defects

and only a small amount of unmelted particles near the fusion line. The height of the clad is 2.6 mm, width 7.1 mm and dilution 37 %. The deposition rate was 5.0 kg/h.

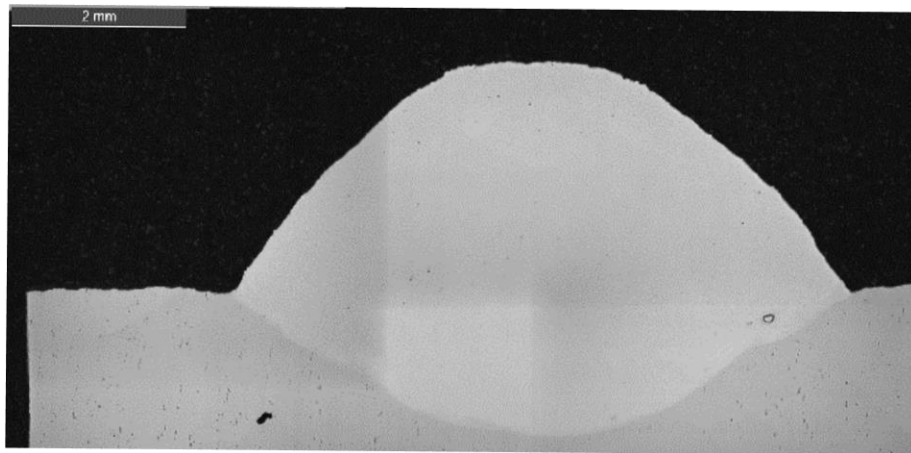


Figure 70. Specimen TH12G-001. Single stringer bead.

Similar results were observed with specimens TH12G-003 to -005, with slightly lower dilution rate and a bit more unmelted particles. The cross-section of the 3-layer cladding with extremely low welding energy is presented in Figure 71. Even though the welding energy was low, the bead is attached properly and some amount of dilution happened. As mentioned, this test was done to exclude the effect of dilution on hardness. This was successful and measured microhardness readings were over 500 HV₁.



Figure 71. Specimen TH12G-007, 3 layers on top of each other.

Otherwise the G3Si (1362) and G3Si1 Dynamic (1640) synergic lines proved to have too high welding energy and were not appropriate for overlay welding of this particular wire. Some tests were run (TH12G-008 – TH12G-015) with these or similar (G3Si1 (1622)) synergic lines, but even with ALC -30 % the welding energy was too high. Figure 72

presents specimen TH12G-016. The height of the clad is 2.6 mm, width 19.3 mm and dilution 16 % with 3.9 kg/h deposition rate. The level of penetration was still too high, as hardness measurements presented later, will exhibit.

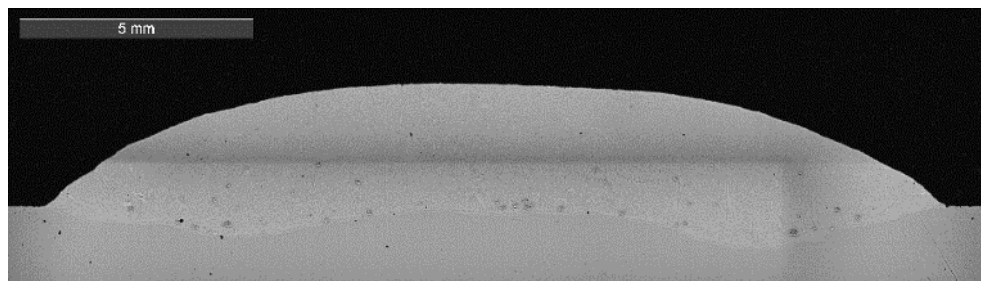


Figure 72. Specimen TH12G-016. Single bead with weaving.

Specimen TH12G-016 was also etched with Kalling's No. 2 etchant to reveal the HAZ. The OM-image of the etched specimen is shown in Figure 73. The depth of the HAZ is 2.72 mm measured from the original surface of the base material. The hardness measurement marks are also visible in this image. The etch was clearly too strong as the clad is corroded together with the substrate.

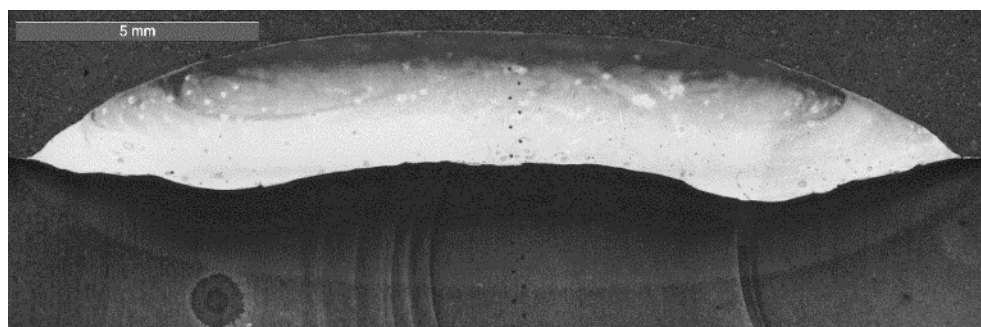


Figure 73. Specimen TH12G-016, etched.

At this point it was decided to change the synergic line back the “Stellit 21 (1291)” which had been reasonably good with the Stellite 21 cored wire. The next coatings were prepared with this “1291” synergic line and with Mison18 protective gas. Although the process seemed cooler with the selected program, the properties of the coating were still inadequate in terms of hardness. Figure 74 presents specimen TH12G-024. Even though the welding energy is significantly lower than in e.g. TH12G-016, the dilution was still at 21 %. This may have been caused by the reduction in travel speed and/or the change in ALC-value. TH12G-016 was manufactured with “dynamic” synergic line, which also might have an effect on the properties.

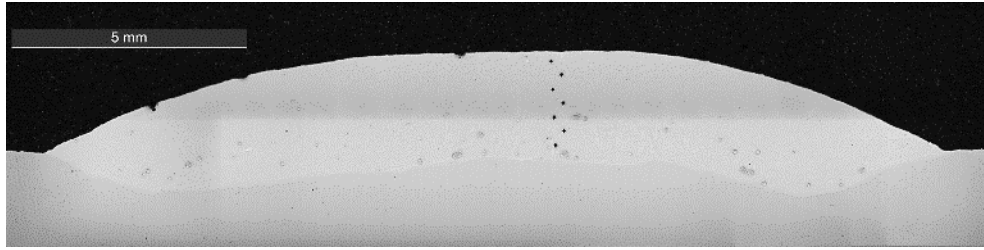


Figure 74. Specimen TH12G-024. Single bead with weaving.

After analyzing these samples, the protective gas was taken under evaluation and then changed to pure argon, and on to Mison2 (Argon with 2 % CO₂). CO₂ typically increases the penetration, which was the problem in the manufactured clads. With Mison2, the dilution seemed to be more under control and more easily adjusted with parameter optimization. At this point other synergic lines for Stellites were tried to see the effects. It was noticed, that the best results were obtained with Stellite 6 (1656) and Stellite 21 (1657) synergic lines, which are really close to each other in terms of heat input. Specimen TH12G-030 is shown (Figure 75). The height of the bead is 2.3 mm, width 19.3 mm with 1.7 % dilution and 3.0 kg/h deposition rate. Even though the dilution is close to zero, the coating is still adhered to the base material properly. Quite a lot of unmelted particles are visible, otherwise the coating is dense with some minor defects.

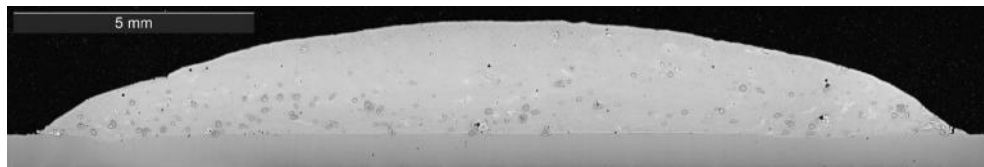


Figure 75. Specimen TH12G-030. Single bead with weaving.

Different base materials were also tested; both Cr-steel and Nialloy to see the effects of base to the process. The effects were not significant, and clads with consistent quality were able to be produced. Figure 76 presents specimen TH12G-034. It is practically similar to TH12G-030 although the base material is different. With slightly increased welding energy the dilution rate is 4 % with deposition rate of 3.3 kg/h. The height of the clad is 2.5 mm and the width is 19.2 mm. The latter image presents the same specimen when etched. HAZ is very narrow; only 1.19 mm. HAZ is visible as the gray, separate area beneath the clad.

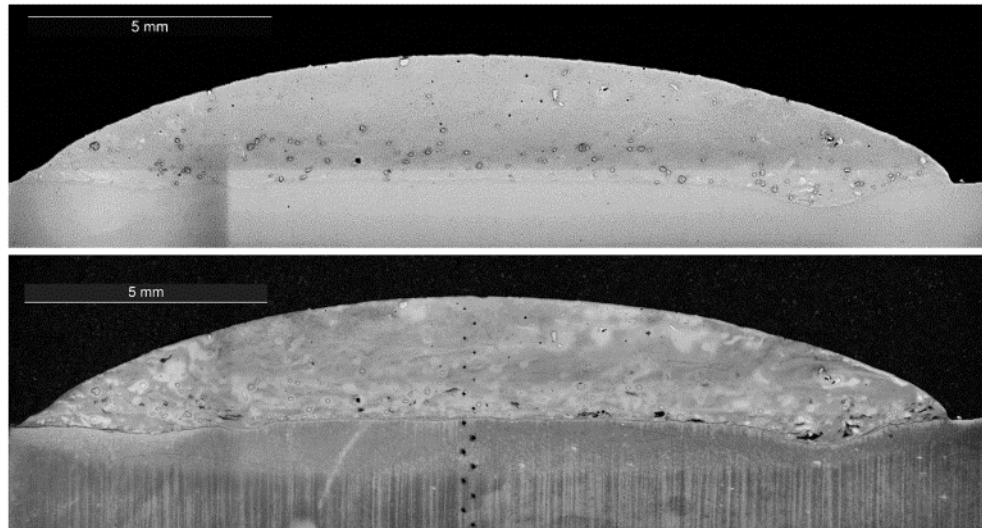


Figure 76. Specimen TH12G-034. Single bead with weaving. Specimen in the latter image is etched to reveal the HAZ.

Further analysis revealed that now the hardness level of 450-550 HV was obtained and the basic cladding tests were finished with the goals achieved. SEM-image (Figure 77) reveals that the unmelted particles are mostly chromium and tungsten. The white particles are 100 wt% tungsten and the dark are 100 wt% chromium. An EDS-analysis was taken from the black spot marked with number 1.

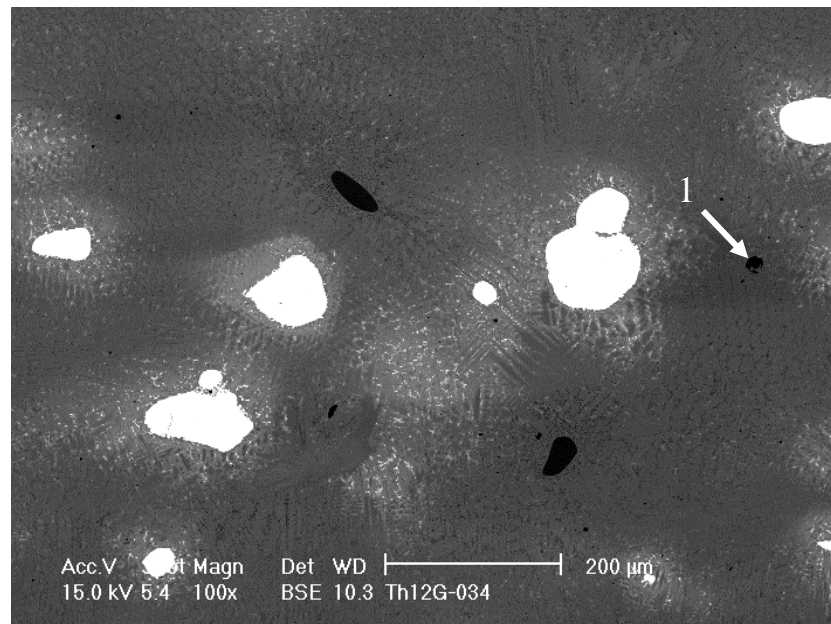


Figure 77. TH12G-034, SEM-image

The results of the EDS-analysis can be found in Table 19. The results indicate that there are some substances related to the manufacturing of the wire and/or the weldability of the

material inside the wire or at the shell of the wire which are not listed in the material certificate. The amounts of these elements are low.

Table 19. Results of EDS-analysis, TH12G-034

Element (wt%)	Al	Si	Cr	Mn	Ti	Co	F	O	Ca	K	Na	Mg	S
Point 1.	24.0	7.2	12.5	0.3	1.4	4.4	7.7	19.1	3.0	11.2	7.6	1.2	0.6

EDS-analysis was also taken from smaller areas to inspect composition in different structural areas. The spots are marked with numbers in Figure 78 and the compositions are listed in Table 20.

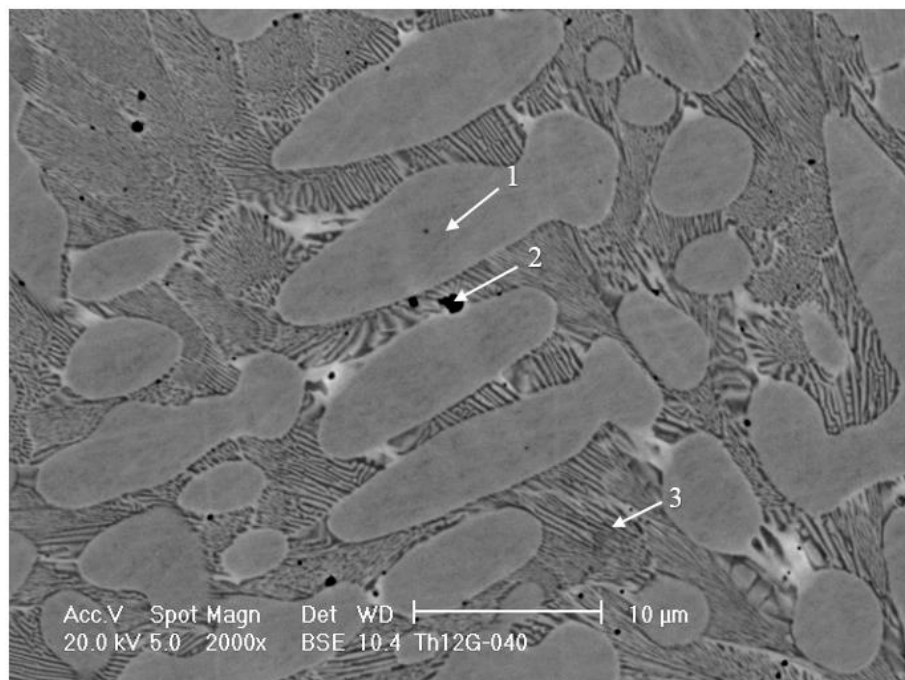


Figure 78. TH12G-040, SEM-image. EDS-point analysis from the numbered points

The EDS-analysis points were chosen from the dendrite, from the interdendritic zone and one from a black particle/area between the dendrites. The composition of the areas was quite different, as the following Table 20 presents.

Table 20. Results of the EDS-analysis, TH12G-040

Element (wt%)	Al	Si	Cr	Mn	Fe	Co	W	O	Ca
Point 1	0.3	1.2	21.6	0.7	8.2	64.1	3.9	-	-
Point 2.	12.1	0.9	29.6	0.9	5.3	40.0	4.0	6.8	0.3
Point 3.	0.2	1.4	33.5	1.0	7.2	52.0	4.7	-	-

The black area seems to be a bit similar than the black dot in ST12-001 (Figure 84 and Table 24) with high amount of aluminum and other substances not mentioned in the material certificate. The tungsten content within all areas is a bit low, as some amount of it remains unmelted even after the process. The chromium content seems to be higher in the interdendritic zone, as the cobalt content is higher in the dendrites. Although carbon is a difficult element for EDS and its composition cannot be accurately measured with it, the results show that carbon tends to locate in the interdendritic zone; the carbon spikes are higher there than in the dendritic zones. It forms carbides with chromium and tungsten.

EDS was also used to identify different zones and some bigger particles in the matrix. It was also used to reveal iron concentration in clads. Figure 79 presents an EDS analysis through the whole depth of the cladding. The points of analysis were chosen on the hardness measurement marks with an area of $150 \times 30 \mu\text{m}$. The thickness of the clad is $2500 \mu\text{m}$. The iron concentration is below 10 wt% which is good value and indicates low dilution.

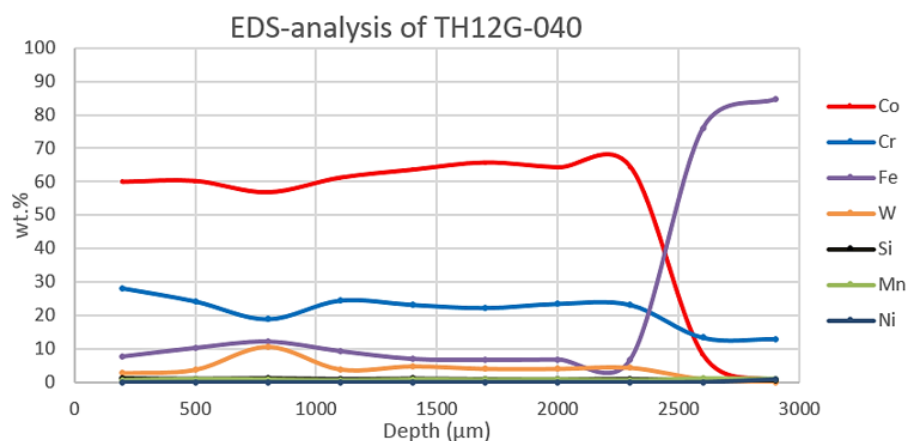


Figure 79. Composition (wt%) of clad TH12G-040

An XRD-analysis was also run to identify material phases in the clad. The diagram of the results is presented in Figure 80. The peaks that could be identified were cubic Co, hexagonal Co and orthorhombic chromium carbide, Cr_7C_3 .

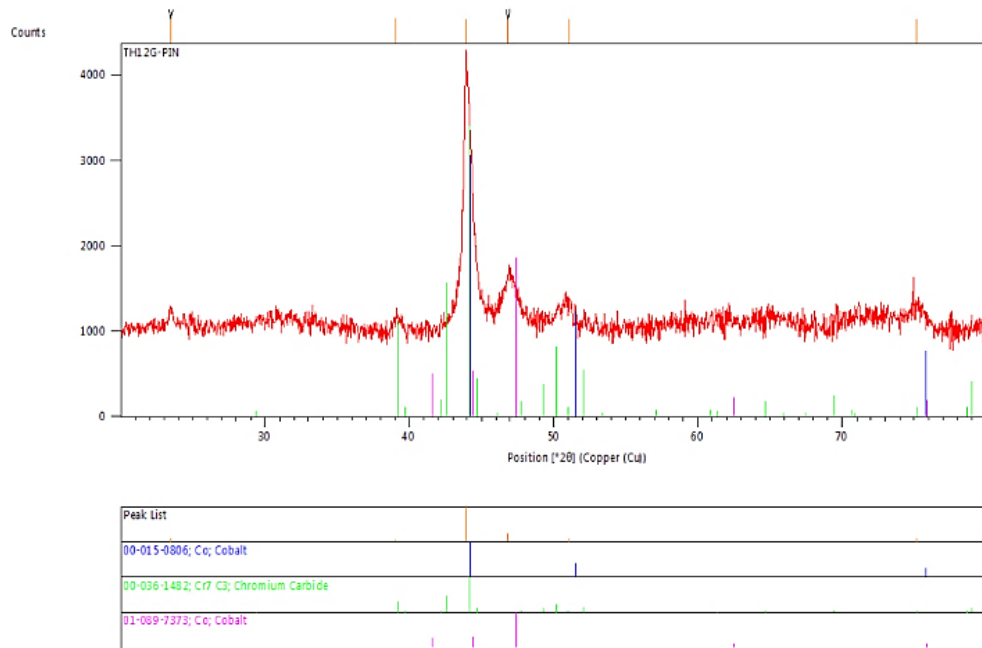


Figure 80. XRD-analysis of TH12G-PIN

9.1.3 Stellite 12 (reference)

The reference wire was tested with “Stellite 6 (1656)” synergic line. The result seemed to be very close to that with Co-alloy. The most noticeable difference when inspected with OM is that the unmelted particles are more evenly spread across the clad and not so strongly localized near the fusion line. The welding energy of the process also could have been a bit higher to guarantee proper adhesion, as there are some defects in the boundary between the clad and the base material. Height of the bead is 2.77 mm and width is 18.9 mm. This specimen is presented in Figure 81.

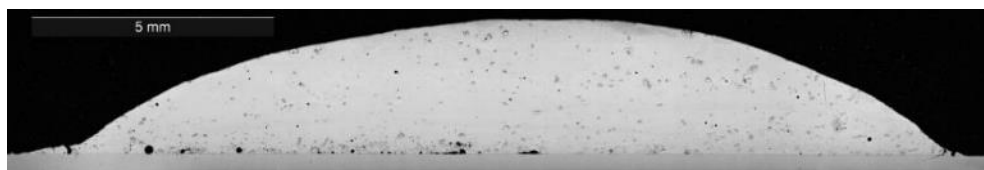


Figure 81. Specimen ST12-001. Single bead with weaving.

The SEM-images and EDS-analysis showed that this wire had some differences to Co-alloy. In Stellite 12 wire, the chromium exists as chromium carbide (CrC)-particles, as in Co-alloy the particles are pure chromium. Also in the melted area the concentration of W and Cr are higher than in Co-alloy. Three particles were analyzed using EDS; these areas of analysis are numbered from 1 to 3 in Figure 80. Also an area with both dendrite and interdendritic zone was analyzed. This area is presented in Figure 81 with white rectangular.

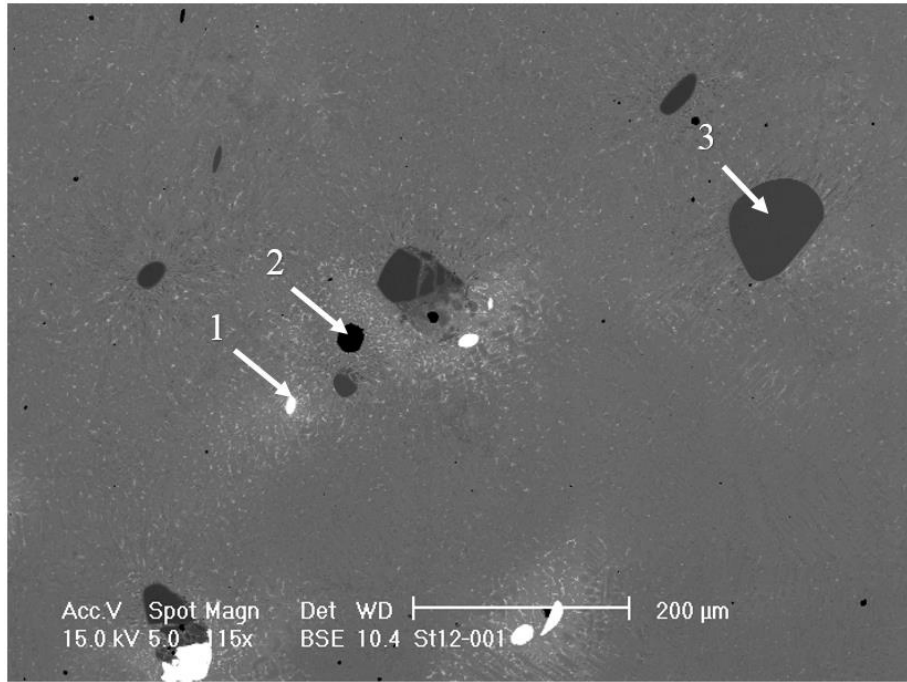


Figure 82. ST12-001, SEM-image

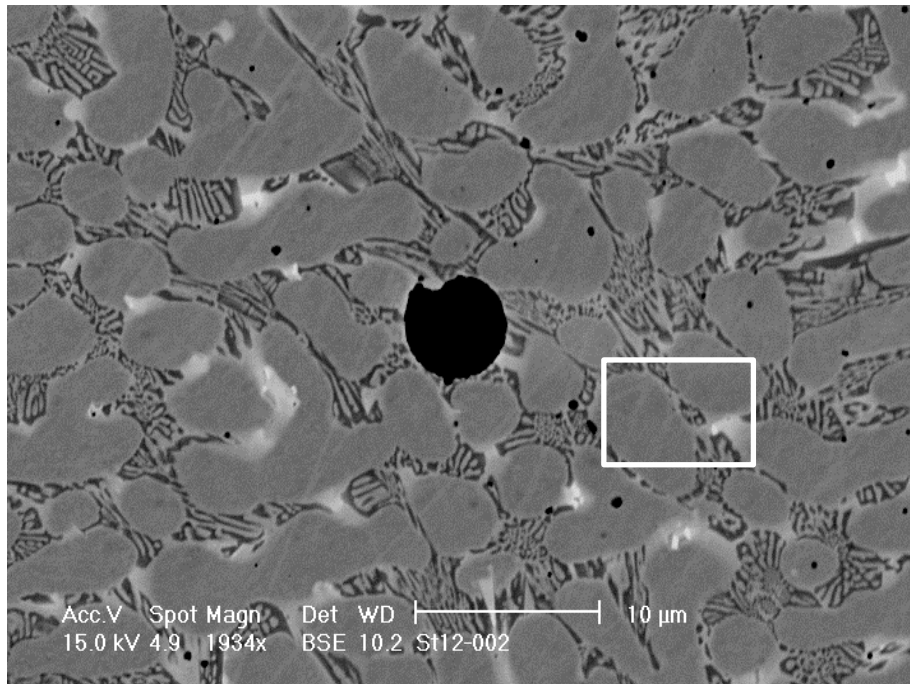


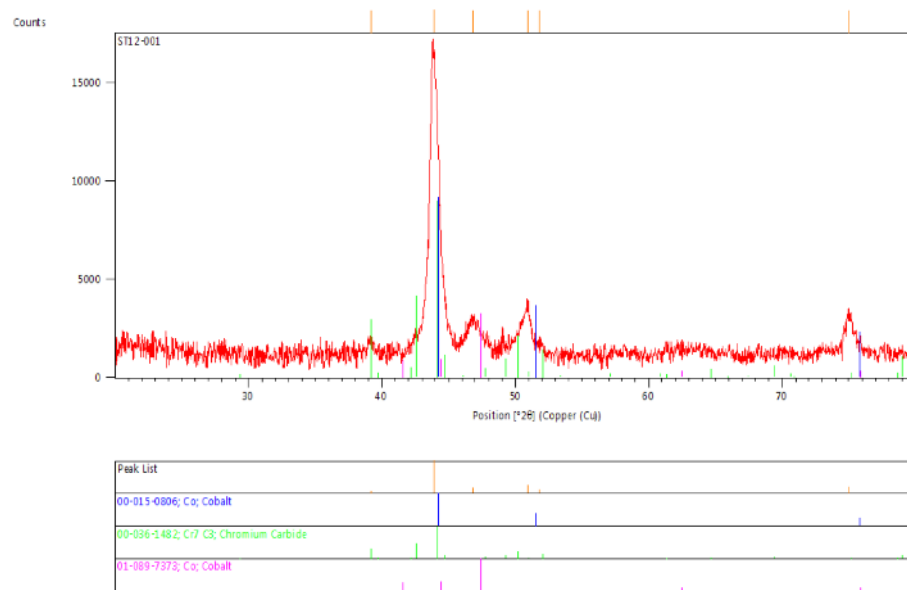
Figure 83. ST12-002, SEM-image

The results of the EDS-analysis are presented in Table 21.

Table 21. Results of EDS-analysis, ST12-001 and ST12-002

Element (wt%)	Al	Si	Cr	Mn	Ti	Co	W	O	Ca	K	C	Fe
Point 1.	-	-	-	-	-	-	100	-	-	-	-	-
Point 2.	18.1	11.3	11.6	30.7	7.8	3.4	-	12.4	1.2	3.7	-	-
Point 3.	-	-	88.1	-	-	-	-	-	-	-	11.9	-
Area	-	1.1	27.8	1.5	-	54.3	11.2	-	-	-	-	4.1

The XRD-analysis (Figure 84) shows higher peaks of Co and Cr_7C_3 than Co-alloy cladding. Otherwise than that the identified phases are the same; cubic Co, hexagonal Co and orthorhombic chromium carbide, Cr_7C_3 .

**Figure 84. XRD-analysis of ST12-001**

9.1.4 Solid lubricant coatings

First test with the CMT + powder feeder was done with Co-alloy wire with CaF_2 addition. The OM-image, Figure 85, shows no signs of any extra particles in the clad, only some greenish color on top of the bead with the naked eye. Other than that, the clad looks similar with some unmelted particles and a few defects. The holes are probably caused by the carrier gas flow from the powder feeder, which makes the process cooler and destabilizes it. In this chapter, the direction of the motion, dragging or pushing, means the angle of the powder feeder nozzle. This angle does not seem to have much of an effect on the structure of the bead. The angle of the welding torch has been the same 90° during all tests.

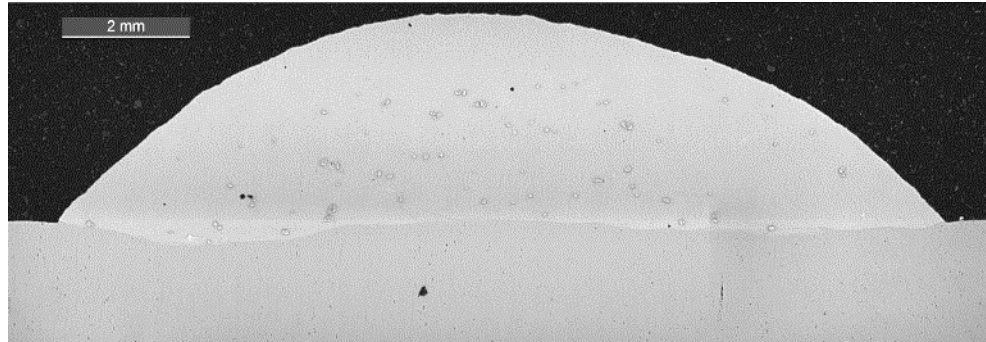


Figure 85. TH12G-037. Single bead, dragging motion, CaF_2 -addition

As the clad was analyzed with SEM+EDS, a layer was found on the surface of the clad. The results of EDS-analysis are presented in Table 22. The areas of analysis are marked with numbers in Figure 86.

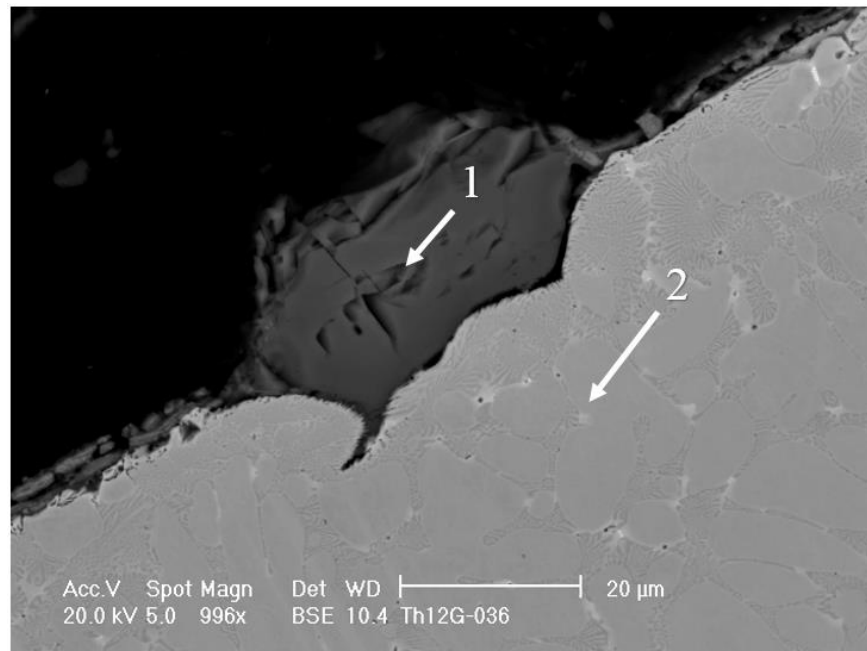


Figure 86. TH12G-036, SEM-image

The results of the analysis suggest that the CaF_2 -lubricant has not wetted properly and has rose on the surface of the clad. Only a few particles were found inside the clad with some indication of Ca or F. This result applies both on TH12G-036 and -037.

Table 22. Result of EDS-analysis, TH12G-036

Element (wt%)	Si	Cr	Mn	Fe	Co	W	F	Ca
Point 1.	-	-	-	-	-	-	38.3	6.17
Point 2.	0.8	18.0	0.7	14.1	62.3	4.1	-	-

For TiO₂-lubricant, Stellite 12 wire consumable was used. The test setup was similar with some changes in the feed rate of the powder. As Figure 87 shows, there are a bit more holes in the fusion layer area which indicates lack of energy in the cladding process, although welding energies were basically similar with both solid lubricant tests. Similarly, as the previous, there is no indications of TiO₂-particles of any kind in the OM-images.

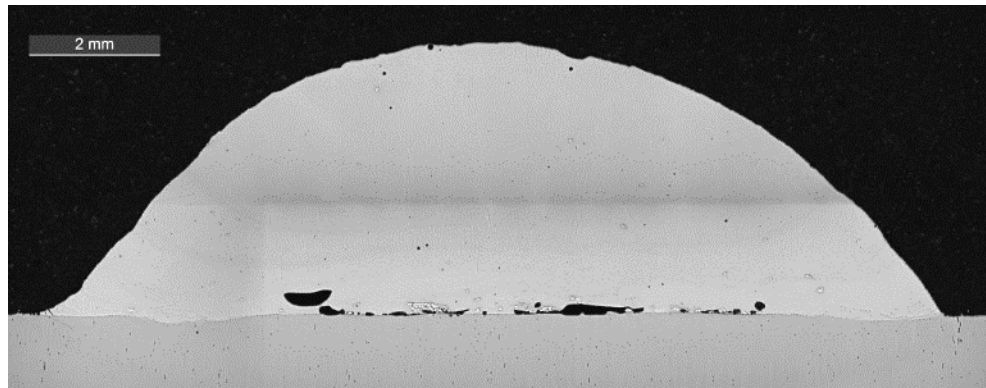


Figure 87. ST12-003. Single bead, dragging motion, TiO₂-addition

A closer inspection with SEM and EDS revealed that there are no signs of TiO₂ inside the clad. As the surface was inspected with higher magnification, a layer was found. This layer is presented in Figure 88. This layer was analyzed with SEM+EDS. The results of the analyze are presented in Table 23. The results show that the TiO₂-lubricant has not diluted into the matrix but has rose on the top of the clad.

Table 23. Results of EDS-analysis, ST12-003

Element (wt%)	Al	Ti	Cr	Mn	W	O
Surface layer	1.2	50.0	18.1	5.0	1.4	24.3

XRD-analysis of TH12G-037 and ST12-003 shows no signs of any other phases than the ones in pure wire without any solid lubricant additions: cubic Co, hexagonal Co and orthorhombic chromium carbide, Cr₇C₃.

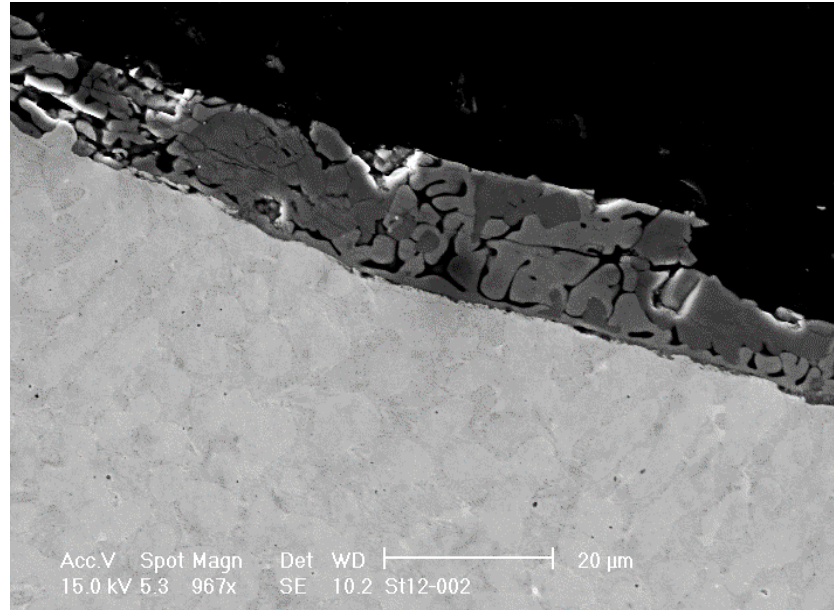


Figure 88. ST12-003, SEM-image

To improve the flow of the lubricant particles in the powder feeder hoses, and also to add some weight to improve the wettability of the particles, Stellite 12 powder and solid lubricant particles were ball-milled. Figure 89 presents a clad produced with powder mix 1, which contained 90 wt% Stellite 12 and 10 wt% MoS_2 . Slight undercut can be observed at the edges of the clad. This can be a sign of either too high travel speed or too low arc voltage [96], as the rapid solidification draws the melted base material into the weld and not allowed to be wetted properly. Torch angle adjustment could also fix this problem. Most likely this is caused by the extra material addition as a powder which causes the lack of voltage. Otherwise the clad is dense with only a few minor porosities near the fusion border.

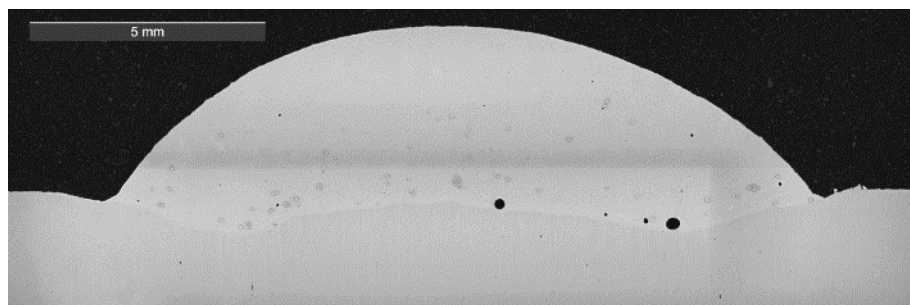


Figure 89. TH12G-042. Single bead, dragging motion, MoS_2 -addition

SEM-image shows tiny black dots ($< 1 \mu\text{m}$) in the interdentritic regions. These kind of dots are not visible in pure Co-alloy-clad, as seen in Figure 90 of TH12G-042. EDS-point analysis indicates a strong Mo and/or S peak at these regions, but as the area of measurement is bigger than these particles/dots, the analyzation proved to be a bit troublesome.

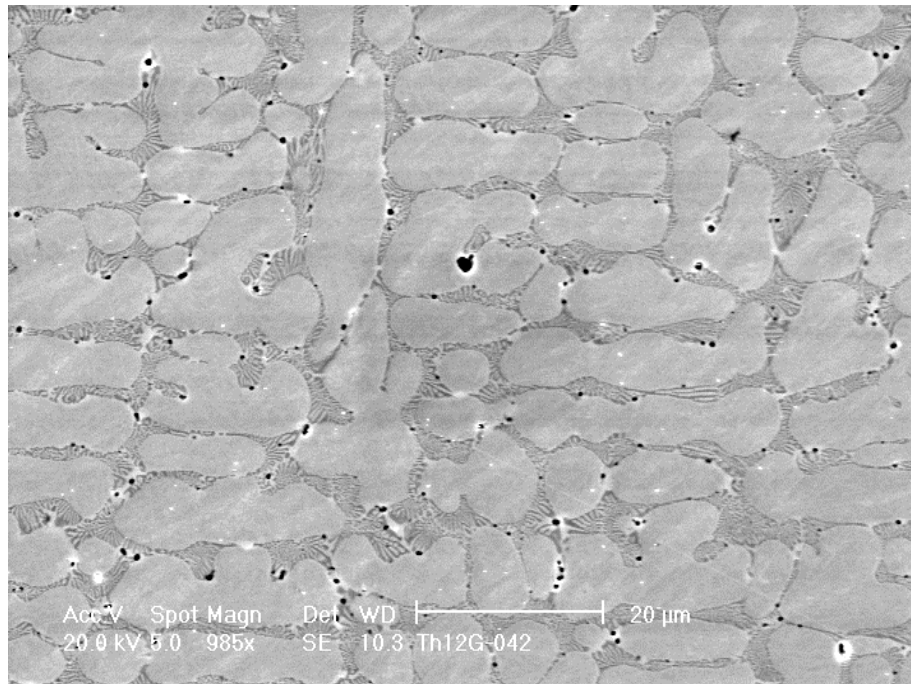


Figure 90. TH12G-042, SEM-image

The black dots were analyzed and for that an image with greater magnification was taken. In this image (Figure 91) the areas of interest are marked with corresponding numbers for EDS-analysis. Table 24 also presents composition of an area analyzed from approximately 20 μm from the surface of the clad.

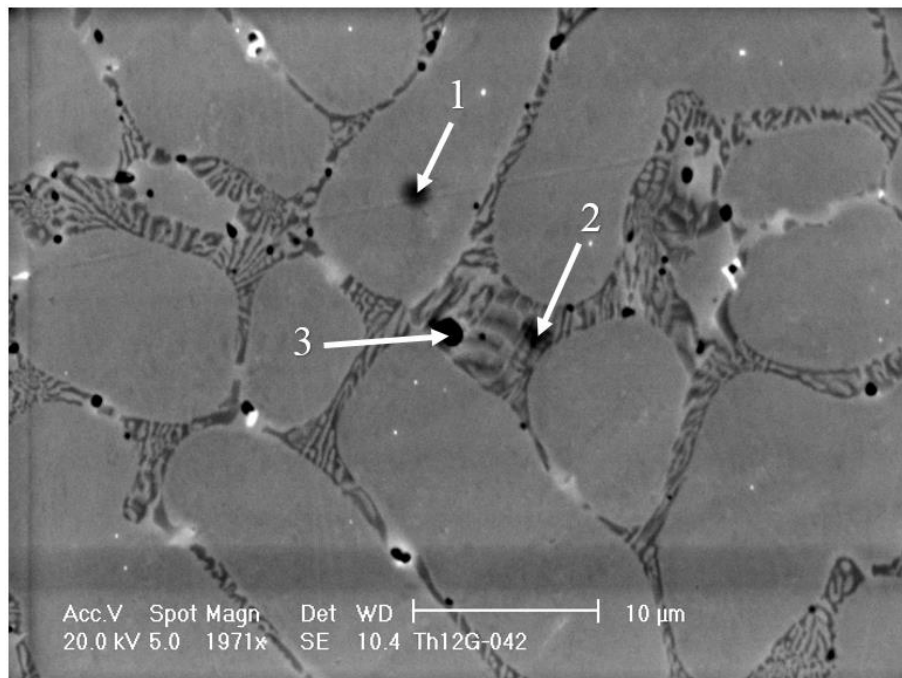


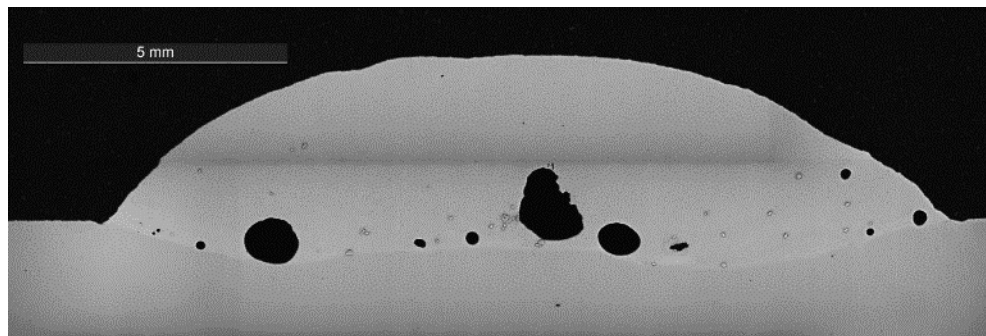
Figure 91. TH12G-042, SEM-image

Table 24. Results of EDS-analysis, TH12G-042

Element (wt%)	Al	Si	Cr	Mn	Fe	Co	W	O	Ca	Mo	S
Point 1.	-	1.4	18.8	0.8	18.6	56.9	3.5	-	-	-	-
Point 2.	0.4	1.8	39.1	0.9	13.6	38.5	5.8	-	-	-	-
Point 3.	7.3	-	29.7	6.5	9.0	24.5	2.7	5.8	0.6	3.9	8.8
Area near the surface	-	1.7	22.9	0.8	17.4	51.9	5.3	-	-	-	-

The analysis show that the lubricant/Stellite 12 powder mix has diluted into the matrix of the clad. It can be presumed that a portion of the black dots consist of the solid lubricant. The iron content of this coating is a bit higher due to higher amount of dilution caused by the higher welding energy.

The clad produced with powder mix 2 addition with dragging motion has some big porosities at the bottom of the clad. This specimen TH12G-044 is presented in Figure 92. Very minor undercutting effect is also visible, but not as clear as with TH12G-042. These porosities appeared to be smaller with the pulling motion of the powder feeder nozzle, at least at the cross sections observed. This has usually been vice versa with the solid lubricant specimens.

**Figure 92. TH12G-044. Single bead, dragging motion, WS₂-addition**

SEM-images were also taken to inspect any signs of WS₂ in the matrix. As Figure 93 indicates, there are some black dots similarly as in TH12G-042 with MoS₂. The spots of EDS-analysis are marked with numbers in the figure.

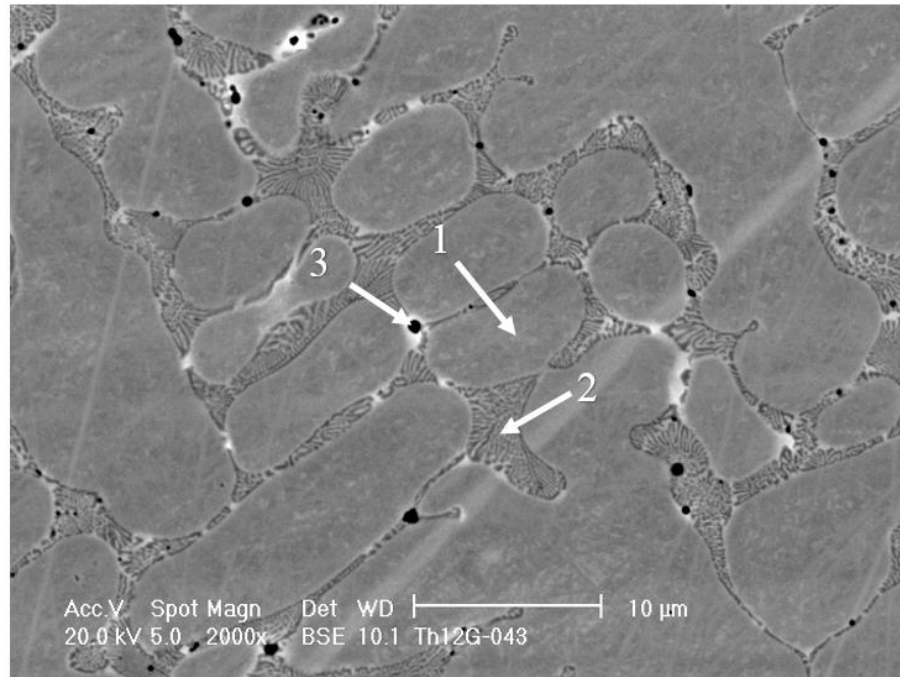


Figure 93. TH12G-043, SEM-image

As these areas/spots were analyzed with EDS, there were clear signs of WS_2 in the black particles. The overall content of WS_2 remains quite low in the coating, but it was managed to insert some of the lubricant inside the clad. The results are listed in Table 25.

Table 25. Results of EDS-analysis, TH12G-043

Element (wt%)	F	Si	Cr	Mn	Fe	Co	W	S
Point 1.	-	1.4	19.0	0.7	24.7	50.9	3.3	-
Point 2.	-	2.3	35.6	0.8	18.9	35.8	6.6	-
Point 3.	2.7	1.8	31.0	6.0	13.9	26.9	7.7	9.9

Similarly, as before, the interdendritic zone seems to be richer in chromium than the dendrite, as the cobalt content is higher within the dendrites. The black dot (point 3) has more tungsten and sulphur that indicate the presence of a solid lubricant.

9.2 Hardness measurements

Hardness of selected coatings were tested as it is one of the most important factors affecting the wear. Co-alloy coating should have hardness values in the range of 450-550 HV_1 and that was also the goal for our CMT-cladded coatings. The main factors affecting hardness are dilution and the melting of all particles inside the cored wire. If some particles, e.g. W or Cr, do not melt, it decreases the hardness as these are the main carbide-formers. The hardness curves are presented in different graphs because of the different

thicknesses of the coatings, different base materials and different scales. This way they are more readable.

9.2.1 Stellite 21

Hardness measurement of ST21-022 shows that the hardness is consistent throughout the coating layer and at an optimal level when it comes to Stellite 21 typical hardness levels. The base material in this specimen is Nialloy. The hardness curve is presented in Figure 94. The HAZ is also quite narrow, approximately 1.5 mm.

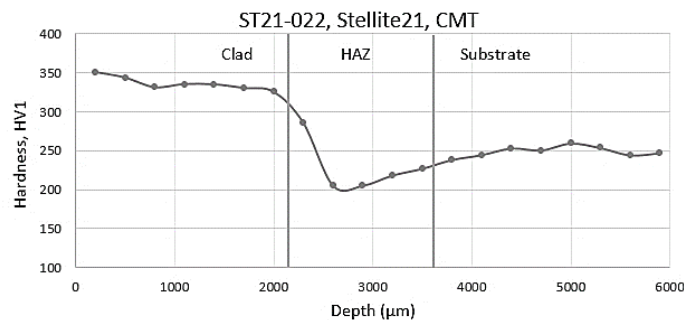


Figure 94. Vickers hardness graph, ST21-022, base Nialloy

This result confirmed us about the ability of CMT in producing low-dilution coatings with limited heat input, as the result is so consistent, and encouraged us to move on to Co-alloy consumable.

9.2.2 Co-alloy

The first hardness measurements were to the first specimen manufactured with Co-alloy. The synergic line was ruled to have too high heat input based on the high level of dilution, that the result of hardness measurement confirms. The hardness of the coatings should be approximately between 450-550 HV1, but the high iron content decreases the value to 350 HV1. Hardness curve is presented in Figure 95. This base material was used only to try out different lines and only the hardness of the coating is relevant at this point.

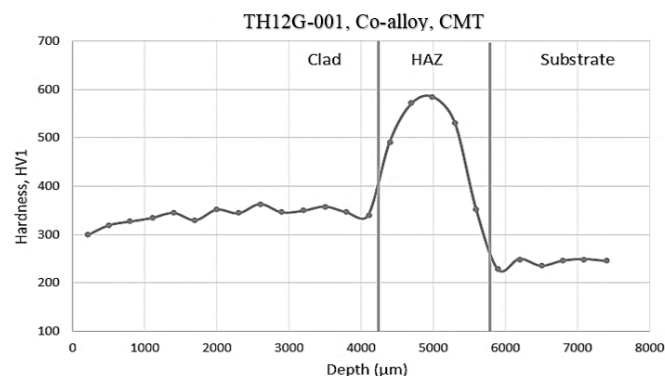


Figure 95. Hardness curve of TH12G-001, base 42CrMo4

At this point the 3-layered low-diluted cladding, TH12G-007, was also tested for hardness. Some random test points throughout the cladding were chosen, and the results clearly show that hardness levels from 500 to 550 HV1 can be achieved with this material. Only the parameters, mainly the dilution rate, must be optimized to reach certain levels. After this, TH12G-009 was taken under the scope (Figure 96). A slight increase in the hardness of the coating is clearly visible compared to the previous specimen as the heat input is remarkable lower. This specimen was produced with a “dynamic” synergic line. Some hardening of the base material can be detected in the HAZ.

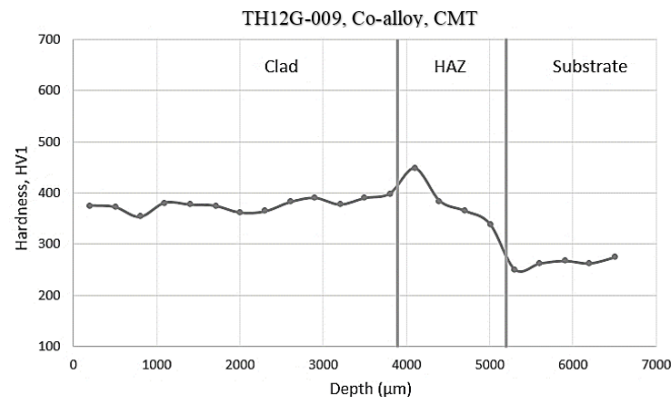


Figure 96. Hardness curve of TH12G-009, base Cr-steel

The hardness of coatings increased with every step that was taken into the direction of less heat input and less penetration. The wire feed rate and ALC were decreased significantly compared to the previous specimen, which means less dilution and thus an increase in hardness. TH12G-016 was also a step closer to the target, as shown in Figure 97.

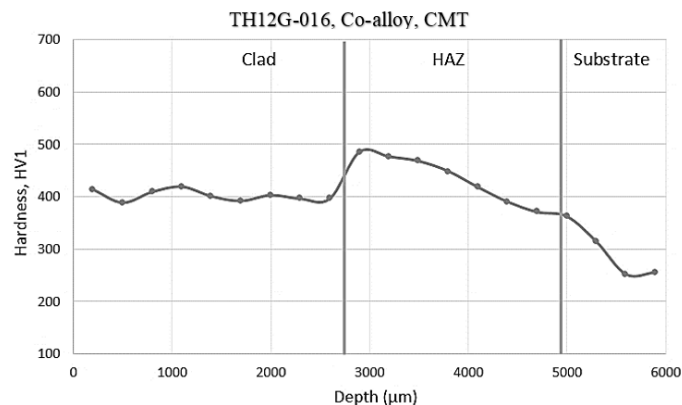


Figure 97. Hardness curve of TH12G-016, base Cr-steel

The reduction of welding energy and changing the protective gas to a one with less CO₂ led to desired results. The hardness of the clad was somewhat consistent and above 450 HV1 throughout the cladding. The result of the hardness measurement of the optimized process is presented in Figure 98. The border between the clad and the base material is

very clear which indicates low dilution. In the cross-section presented in Figure 76. (TH12G-034), it is also seen that the coating is properly attached to be base material.

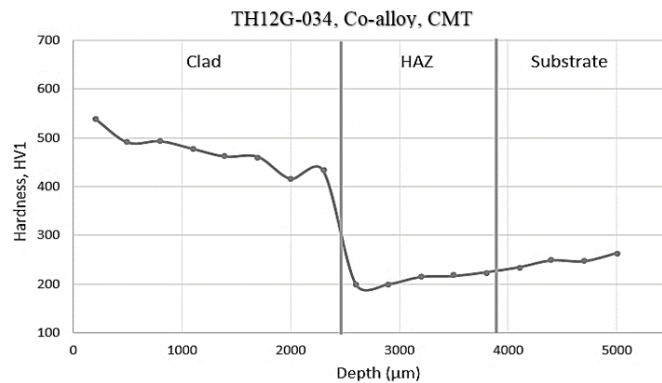


Figure 98. Hardness curve of TH12G-034, base Nialloy

This result confirmed that the process parameters were now very close to optimal and further tests could be performed.

9.2.3 Stellite 12

Reference-wire was also tested to see any differences in the hardness values. Figure 99 shows the hardness curve of ST12-001 and TH12G-030 in the same graph. The curves are almost identical despite the small differences. The difference in the depth area of 2000-3000 μm can be explained with the different thicknesses of the cladding resulted from a different synergic lines used. The thickness of the coating in ST12-001 is about 2.7 mm, and thickness of coating in TH12G-030 is about 2.4 mm. The dotted vertical line indicates the thickness of TH12G-030, the solid vertical ST12-001. The base material is the same with both and the welding energy also basically the same. This brings out also the individualistic nature of the synergic lines; the parameters are exactly the same but the thicknesses have a significant difference.

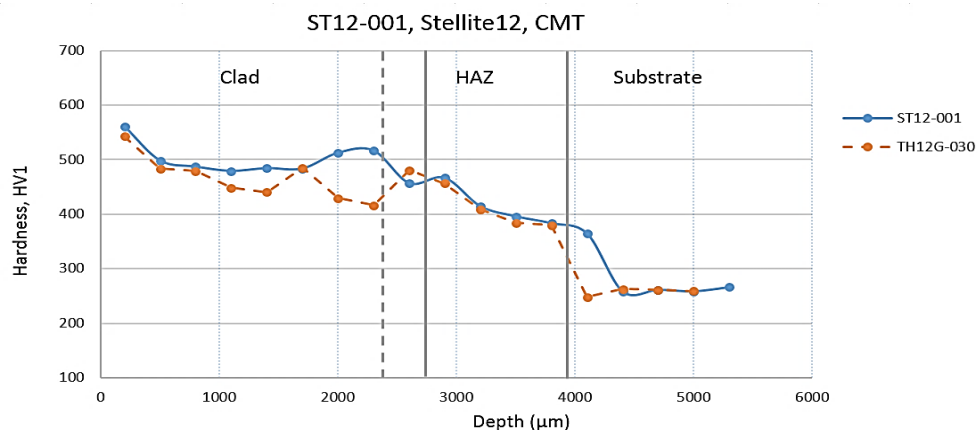


Figure 99. Hardness curve of ST12-001 and TH12G-030, base Cr-steel

9.3 Summary

This chapter summarizes the results from the previous chapters. In Table 26 some properties of the best quality coatings are listed.

Table 26. Summary of results

Specimen	Welding Energy E (J/mm)	Clad thickness (mm)	Dilution rate (%)	Deposition rate (kg/h)	Clad hardness, HV1 (average)	Material phases	Amount of un-melted particles
ST21-024	492	2.22	2.3	2.10	362.9	-	low
ST12-001	757	2.73	> 1.0	3.31	497.4	Co, Cr ₃ C ₇	medium
TH12G-030	758	2.32	1.7	2.99	472.5	-	high
TH12G-040	586	2.47	6.1	3.11	448.5	Co, Cr ₃ C ₇	med-high
TH12G-042	921	3.52	19.4	3.13*	401.5	-	low-med
TH12G-043	986	3.69	17.66	3.23*	391.7	-	low

*the amount of Stellite 12 in powder form has not been taken in consideration when calculating this

Figure 101 presents results of hardness measurements with all the different filler materials on the same base material, Cr-steel. The dotted line represents the borders of clad/HAZ of TH12G-030 and ST21-024, and solid lines those of ST12-001. Different lines are used because of the differences in clad thicknesses. The width of HAZ is basically the same with all of the three materials, which indicate optimized process parameters in terms of dilution and heat input. This graph also brings out the differences between Stellite 21 and Stellite 12. The increased amount of C and W in Stellite 12 brings hardness into the alloy.

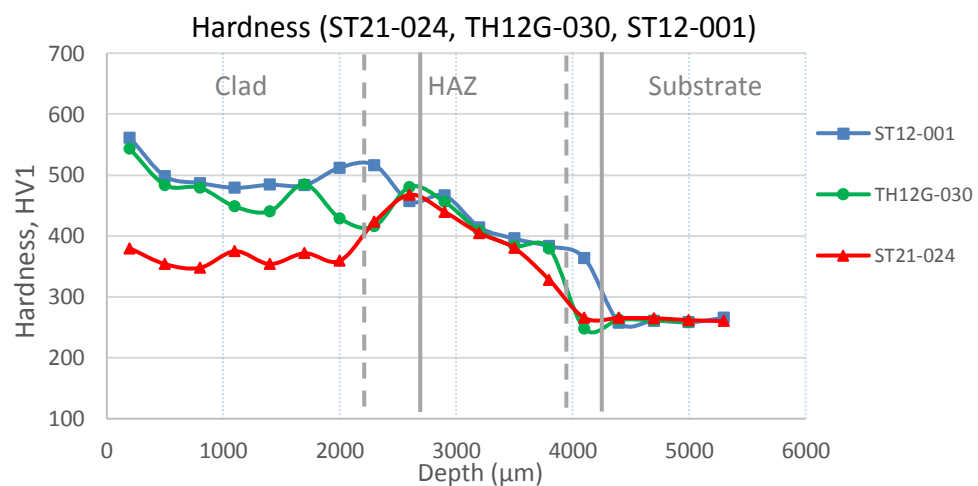


Figure 100. Hardness curves of different filler materials on the same base material

9.4 Surface roughness

The wear test discs were measured for their surface roughness properties. All of the five discs were ground at Juha Tuomainen Oy to reach fine and flat surfaces. The measured surface roughness' were in the area of $Ra0.30 - 0.40 \mu\text{m}$ for all discs. Three measurements were done to each discs measuring from the center outwards at different parts of the discs.

9.5 Wear tests

Four different wear tests were run at two different temperatures:

1. Co-alloy clad disc (CMT) vs. Co-alloy clad –pin (CMT), RT
2. Co-alloy clad disc (CMT) vs. Nialloy –pin, RT
3. Co-alloy clad disc (CMT) vs. CrNi –pin, RT
4. Co-alloy clad disc (CMT) vs. Co-alloy clad –pin (CMT), 300 °C

Co-alloy clad –pins were manufactured from a weave bead by wire cutting. The Nialloy and CrNi –pins had been wire cut of a component. All of the pins' wear surfaces were ground to reach a surface roughness finer than $Ra0.25 \mu\text{m}$ and to make sure they are parallel to the discs. Figure 102 shows the meaning of each parameter that was used in these tests. Originally more tests were planned in 300 °C, but unfortunately an important part of the wear test device went into poor state during Test 4, and rest of the tests had to be cancelled.

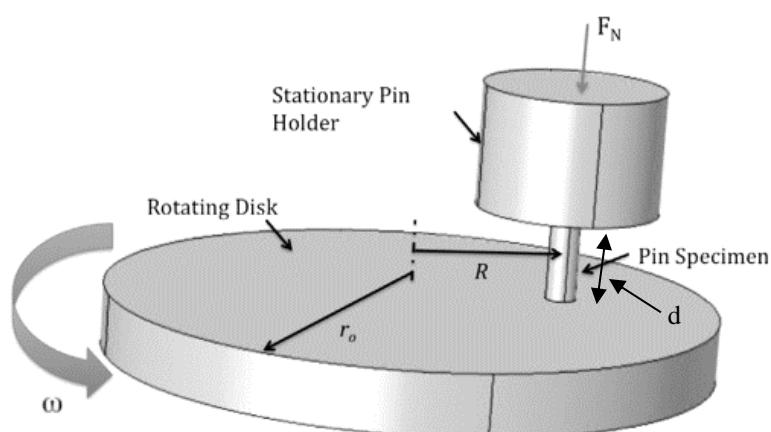


Figure 101. Schematic presentation of a typical pin-on-disk test device [95]

The wear test parameters are presented in Table 27. Nialloy –pins were shorter than the other pins and the d is thus smaller. Otherwise, the parameters of each test were kept the same.

Table 27. Wear test parameters

Wear test	F_z, N	r, mm	R, rpm	$v, mm/min$	t, h	$T, ^\circ C$	C	d, mm
1.	150	28	13.64	2400	6	RT	dry	14.3
2.	150	28	13.64	2400	6	RT	dry	9.0
3.	150	28	13.64	2400	6	RT	dry	14.3
4.	150	20	19.10	2400	0.2	300	dry	16.1

Before each test, the wear surfaces of both the disc and the pin were cleaned with ethanol. The weighing was done with a TEOPAL scale (accuracy 0.001 g) at the wear laboratory of TUT. Table 28 presents the results of the weighing before and after the tests. The test pieces were weighed 5 times and the average was calculated before and after the tests. After the tests, there was no signs of cracking or separation of the clad, neither in the pin nor in the disc, in any of the tests.

Table 28. Weight of the wear pieces

	Weight (g)			
	Test 1.	Test 2.	Test 3.	Test 4.
Disc (before)	309.630	307.438	308.162	309.547
Disc (after)	309.545	307.311	308.037	309.534
Difference	-85 mg	-127 mg	-125 mg	-13 mg
Pin (before)	7.958	4.592	7.918	7.933
Pin (after)	7.908	4.570	7.899	7.932
Difference	-50 mg	-22 mg	-19 mg	-1 mg
TOTAL	-135 mg	-149 mg	-144 mg	-14 mg

Hardnesses were measured prior and after the wear tests from the wear surfaces. Four measurements were done on different areas of the surfaces and average was calculated. Measurements were taken on different parts of the wear track randomly. Results of these measurements are listed in Table 29. As can be seen, all materials have work-hardened during the tests, some significantly and some a bit less.

Table 29. Hardness of wear surfaces prior and after the wear tests

	Hardness (HV ₁)							
	Test 1		Test 2		Test 3		Test 4	
	Pin	Disc	Pin	Disc	Pin	Disc	Pin	Disc
Before	450.9	643.1	439.8	643.1	396.6	643.1	450.9	643.1
After	711.8	738.1	536.8	659.1	581.1	666.1	734.8	715.4
Difference	260.9	95.0	97.0	16.1	184.5	23.0	283.9	72.3

The work-hardening occurring in Tests 1 and 4 is significant compared to the other. In both of these test the material paired are the same, although the discs are already harder than the pins as they have been lathed and ground before these tests. This work-hardening phenomenon happens via the transformation of fcc structure to hcp structure meaning less interaction between stacking faults because of the low SFE. Another remark is that all of the discs exhibited low (<6 wt%) amount of iron meaning that dilution is under control.

9.5.1 Co-alloy disc (CMT) vs. Co-alloy pin (CMT), RT

Figure 103 presents the friction coefficient value of Test 1 over time. A logarithmic trend-line has been fitted into the graph. The average COF-value in the 6-hour test is 0.329. The transfer distance in z-axis (vertical) from the beginning until the end of the test is 0.293 mm. During the first hour of testing, the average COF is approximately 0.30 and after this period it raises to between 0.32-0.34.

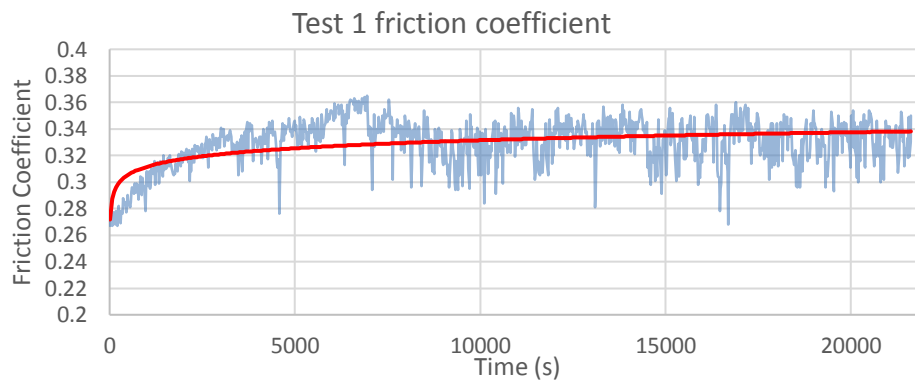


Figure 102. Coefficient of friction over time, Test 1

Figure 114 presents the Co-alloy clad disc. The inner wear track is the result of Test 4 and the outer track is the result from Test 1. As the test times were so far apart, the wear tracks are not comparable with each other.

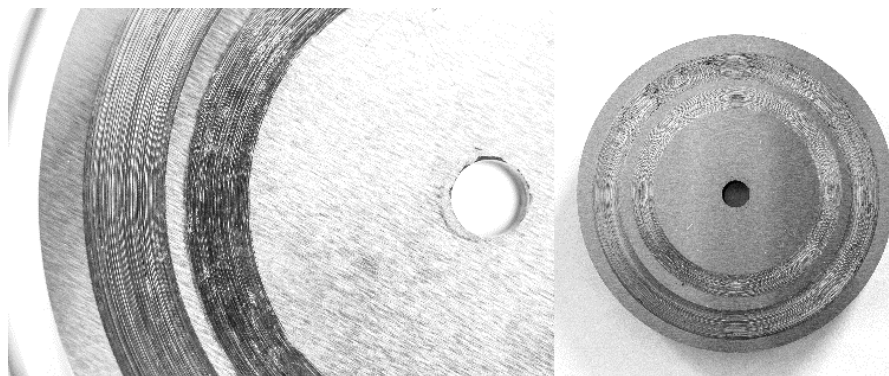


Figure 103. Co-alloy clad disc, Test 1 (outer track) and Test 4 (inner track)

A closer inspection with SEM+EDS (Figure 105) on Test 1 disc reveals that an oxide layer has formed on top of the tungsten particles in the wear track (the spots marked with number 1 in fig. 105). Both the disc and the pin exhibit this behavior in RT. Particle 2. was identified as 100 wt% Cr and particle 3. as 100 wt% W. The amount of iron was also inspected from the pin and the disc; the biggest reading was at 5.6 wt%, so it can be assumed that the dilution is at a good level. The area of EDS-analysis is marked as a rectangle in the SEM-image. The results of this analysis are presented in Table 30. Point analysis of the oxide-covered tungsten particle in the wear track are presented also in Table 30.

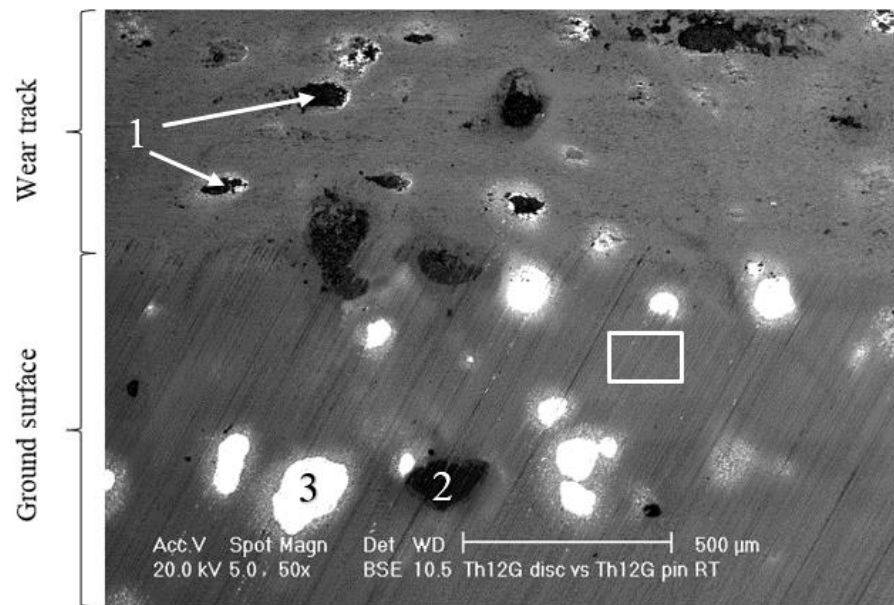


Figure 104. SEM-image of disc, Test 1

A greater magnification image (Figure 106) reveals the grooves on the wear track of the disc. The amount of wear debris collected from the disc indicates an abrasive wear mechanism as ruling, but also erosive wear and oxidative wear are visible as the EDS-analysis shows. There are no clear signs of plastic deformation or adhering. The wear debris has not stuck into the wear track but come off it during the test.

Table 30. Results of EDS-analysis of Co-alloy clad disc after Test 1

Element (wt%)	Si	Cr	Mn	Fe	Co	W	O
Area	0.7	22.7	0.6	5.0	67.2	2.8	-
Point 1 (top)	0.9	20.8	0.6	4.5	58.6	5.5	9.2

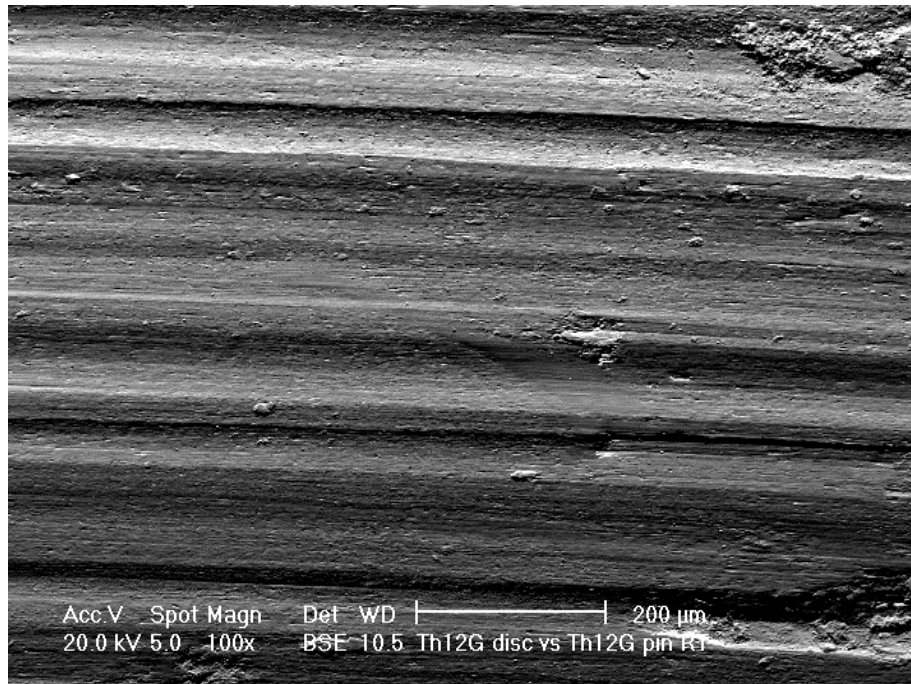


Figure 105. SEM-image of the wear track of Test 1

Figure 107 presents the Co-alloy clad pin after Test 1. The wear track seems similar than the one in the disc, which is expectable as the materials are the same. Some deeper grooves are visible but no signs of plastic deformation are visible. The wear mechanism can be assumed to be similar than in the disc.

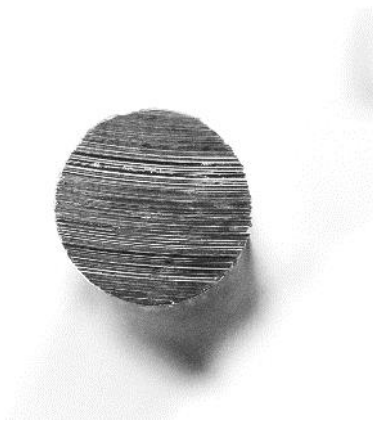


Figure 106. Co-alloy clad pin, Test 1

There are some differences in the wear track when inspecting the SEM-image of the pin (Figure 108). The dark oxide layers seem to be elongating from top of the tungsten particles. This kind of behavior was not found in the disc. The presence of the oxide layer was verified with an EDS-analysis.

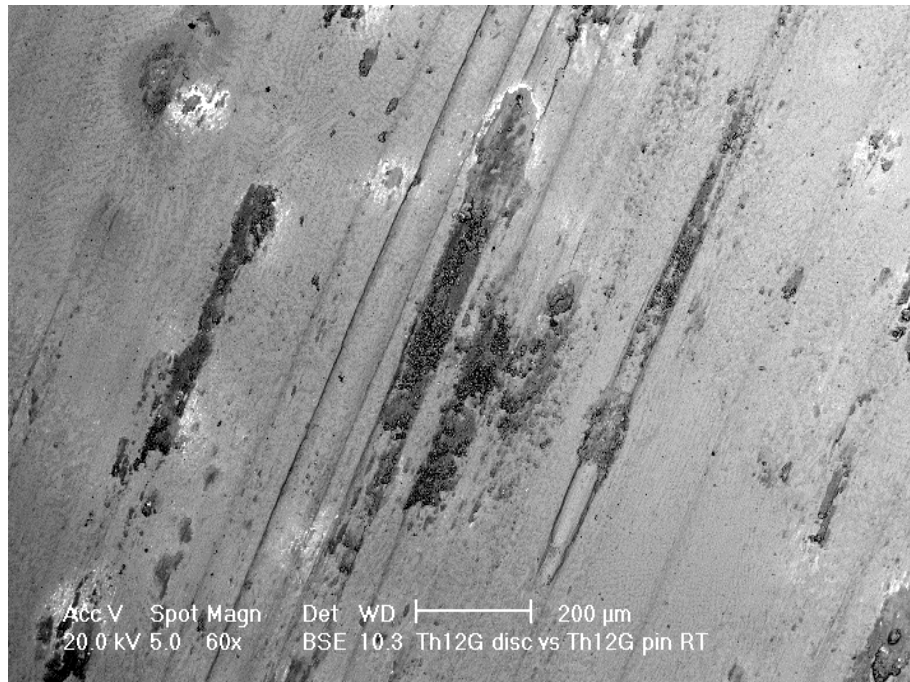


Figure 107. SEM-image of the wear surface of the pin in after Test 1

9.5.2 Co-alloy disc (CMT) vs. Nialloy pin, RT

Figure 109 presents the friction coefficient value of Test 2 over time. A logarithmic trend-line has been fitted into the graph. The average COF-value in the 6-hour test is 0.280. The transfer distance in z-axis (vertical) from the beginning until the end of the test is 0.153 mm.

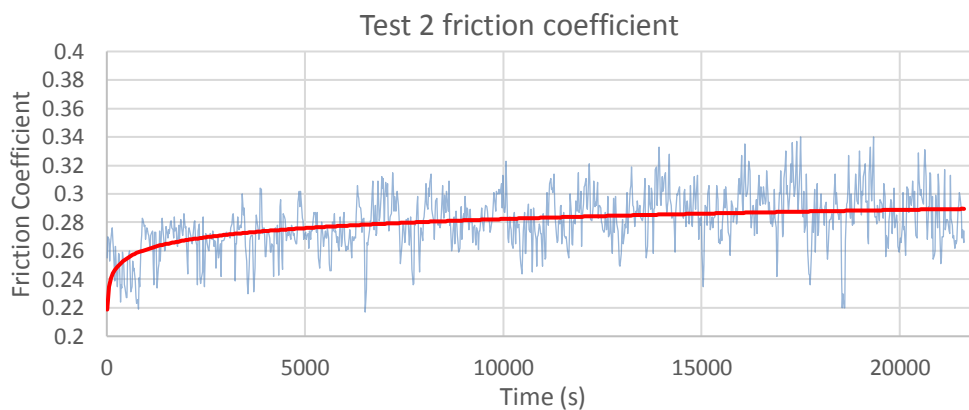


Figure 108. Coefficient of friction over time, Test 2

Image of the disc and the wear track are presented on Figure 110.

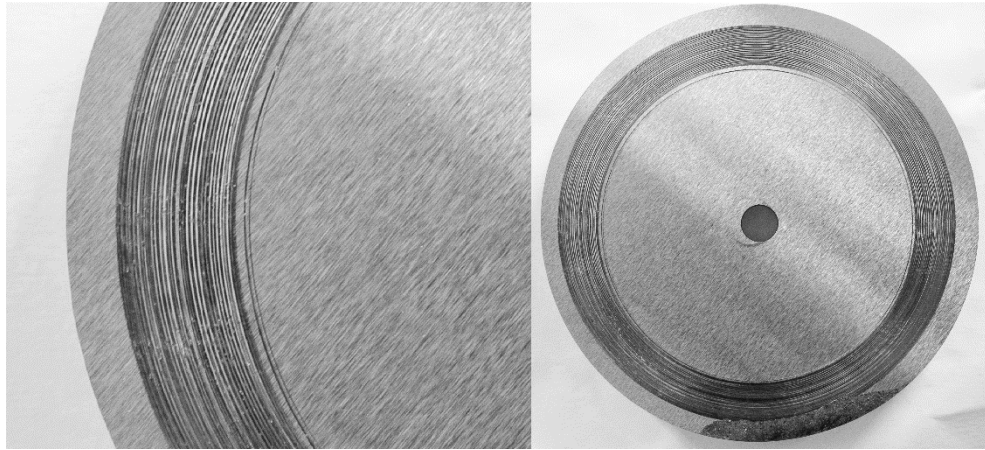


Figure 109. Co-alloy clad disc, Test 2

Analysis of the disc and wear track revealed that Ni-alloy from the pin has been stuck into the unmelted W-particles of the disc. In addition, oxides were present on these particles. SEM-image of the wear track is presented in Figure 111. The white rectangular indicates the area where Figure 112 has been captured from.

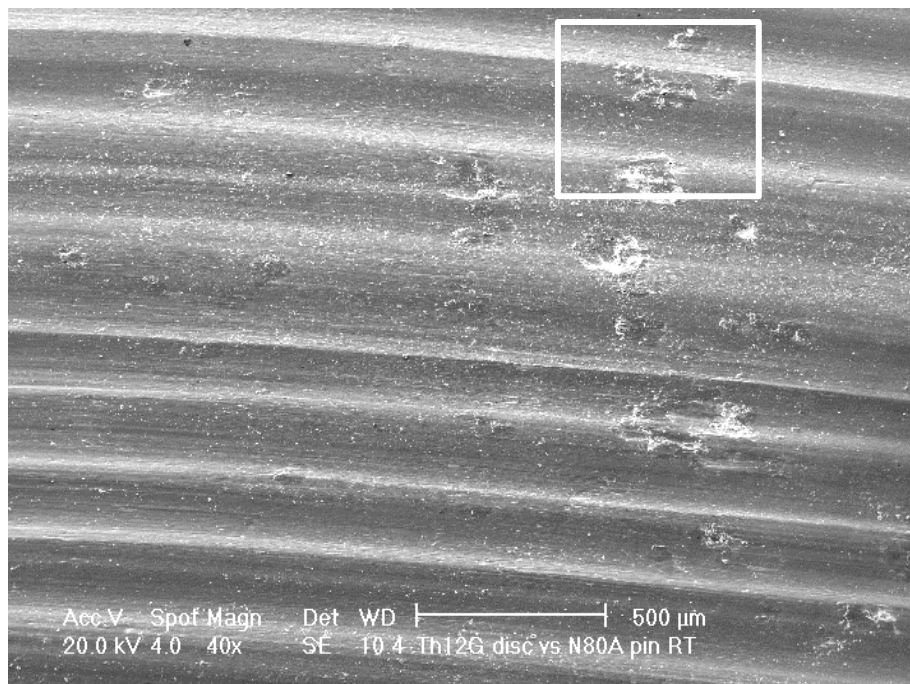


Figure 110. SEM-image of wear track of Co-alloy clad disc after Test 2

A SEM-image with greater magnification is presented in Figure 112. EDS-analysis verifies the presence of Ni-alloy, especially on top the tungsten particles. The results of the EDS-analysis are presented in Table 31.

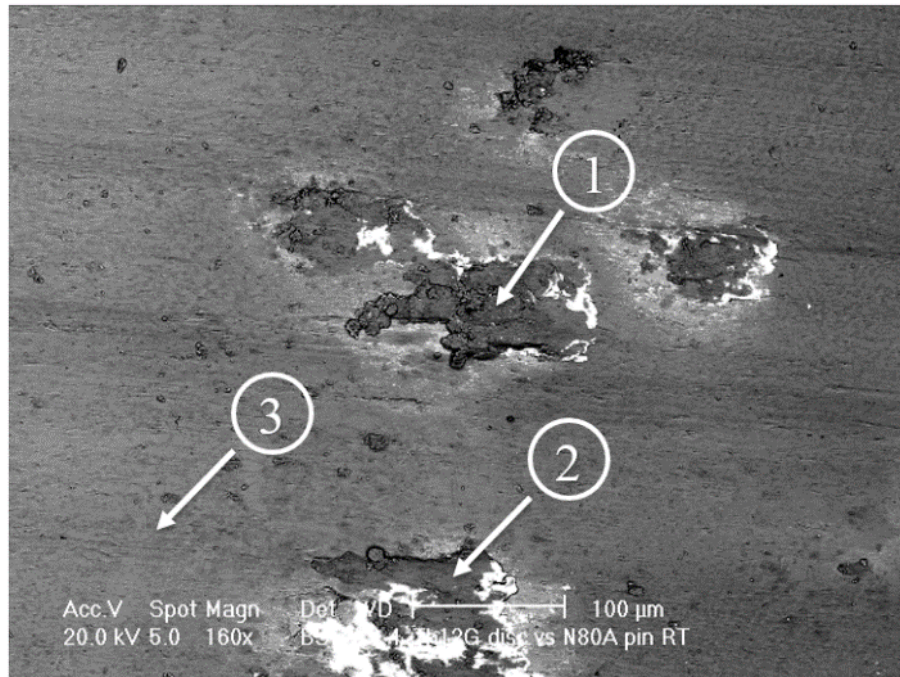


Figure 111. SEM-image of wear track of Co-alloy clad disc after Test 2

Table 31. Results of EDS-analysis on Co-alloy clad disc after Test 2

Element (wt%)	Si	Cr	Mn	Fe	Co	W	O	Ti	Ni
Point 1.	0.9	21.2	0.5	4.3	51.7	4.2	8.5	0.4	8.4
Point 2.	0.6	21.5	0.5	4.5	54.3	4.9	5.6	0.3	7.7
Point 3.	0.6	23.6	0.6	5.4	65.2	4.6	0.1	-	1.4

The wear pin shows very strong signs of Stellite presence adhered from the wear disc. As Nialloy has a different, more ductile behavior, the Co-alloy cladding from the disc has stuck into the pin. This explains the big difference between the mass losses of different tests, as mass from the disc has transferred into the wear surface of the pin. The wear surface of the pin has gone through strong plastic deformation. The scars are not as clear and smooth as they were in Test 1, as presented in Figure 113.

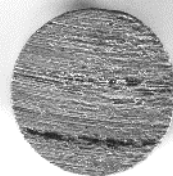
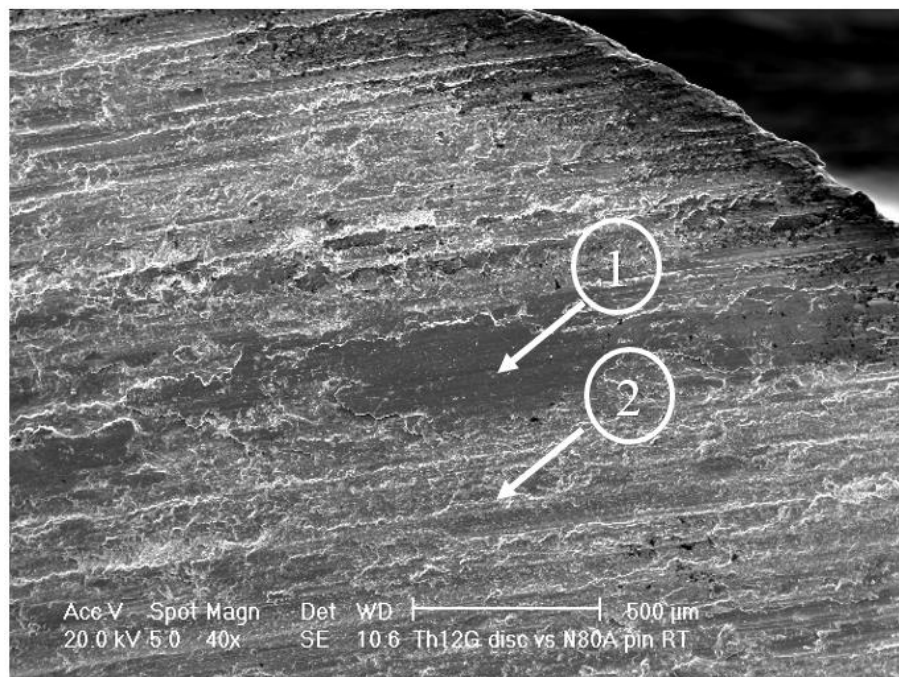


Figure 112. Nialloy -pin, Test 2

Table 32. Results of EDS-analysis on Nialloy wear surface after Test 2

Element (wt%)	Si	Cr	Mn	Fe	Co	W	O	Ti	Ni	Al
Point 1.	1.4	22.6	0.4	4.0	50.0	2.5	7.0	0.4	11.6	-
Point 2.	0.7	22.9	0.4	3.9	48.1	2.8	7.6	0.6	12.8	0.2
Area	0.5	20.8	0.2	2.4	27.6	2.7	4.2	1.4	39.3	0.9

Visible in Figure 114, there is clearly a layer of adhered Co-alloy clad in the Nialloy-pin. This was confirmed with EDS-analysis; the points of analysis have been marked with numbers. As the pin wear surface has such a great amount of Co-alloy, it can be assumed that the wear pair has more or less changed from Nialloy vs Co-alloy to Co-alloy vs Co-alloy at some point. However, the friction coefficient is remarkably lower throughout the whole test. The EDS-analysis points are marked with numbers and the results are presented in Table 32. An area analysis was also conducted and the results are presented in the same table.

**Figure 113.** Wear surface of the Nialloy -pin after Test 2

9.5.3 Co-alloy disc (CMT) vs. CrNi pin, RT

Figure 115 presents the friction coefficient value of Test 3 over time. A logarithmic trend-line has been fitted into the graph. The average COF-value in the 6-hour test is 0.284. The movement in z-axis (vertical) from the beginning until the end of the test is 0.210 mm.

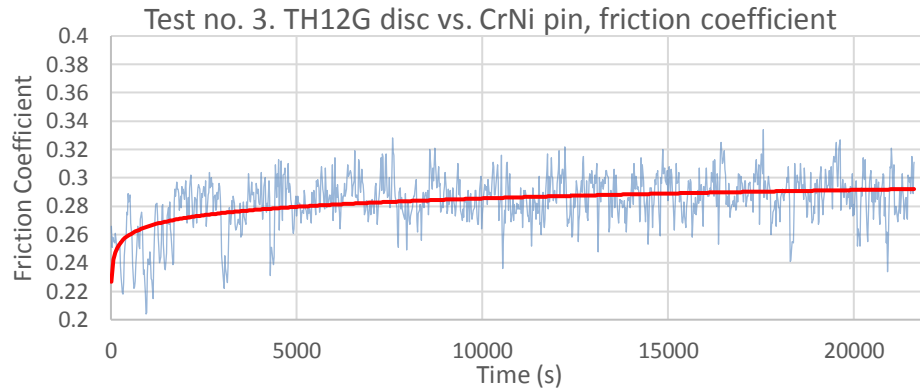


Figure 114. Coefficient of friction over time, Test 3

Image of the wear track of TH12G-disc after Test 3 is presented in Figure 116. EDS-analysis from the ground surface resulted in iron content of 4.8 wt%.

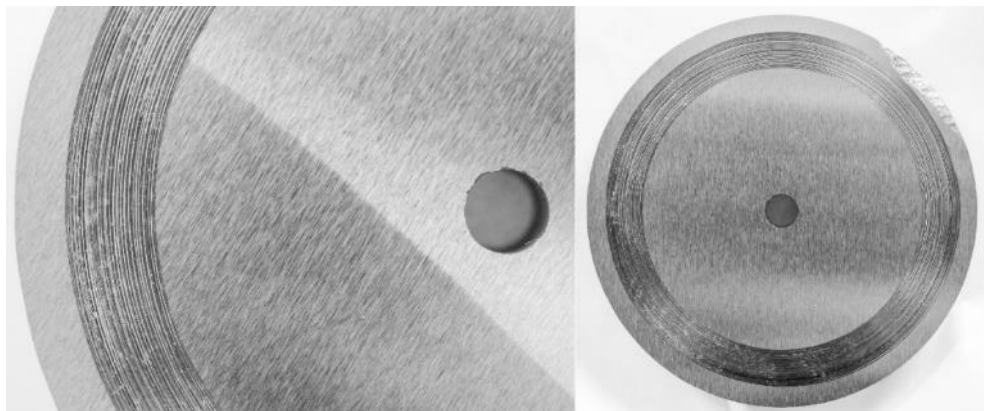


Figure 115. TH12G-disc, after Test 3

SEM-images indicates that oxide and Stellite has adhered on top of the unmelted tungsten particles marked with white arrows in the left image of Figure 117. This has happened when material from the disc has adhered on to the pin, and then from the pin onto the tungsten particles. The black arrow shows a white, 100 wt% tungsten particle off the wear track. Point analysis spots have been marked to image on the right. The results of the EDS-analysis are presented in Table 33.

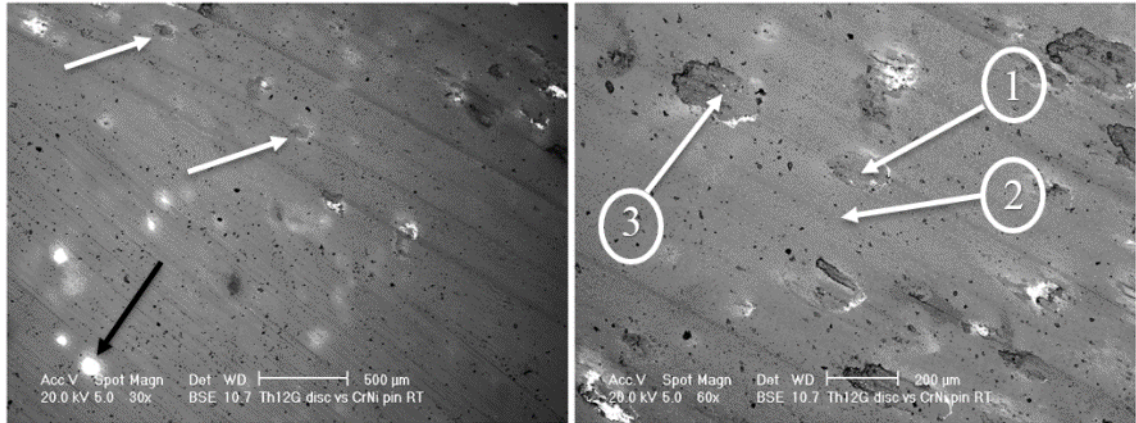


Figure 116. SEM-images of TH12G-disc after Test 3

Table 33. Results of EDS-analysis on TH12G-disc after Test 3.

Element (wt%)	Si	Cr	Mn	Fe	Co	W	O
Point 1.	0.8	24.4	0.6	4.8	61.2	4.3	4.0
Point 2.	0.8	28.7	0.5	5.0	60.6	4.5	-
Point 3.	1.0	23.8	0.4	4.6	61.7	4.3	3.1

Image of the CrNi after Test 3 is presented in Figure 118. The wear surface of the pin has not been parallel with the disc, as the corner of the pin has not worn. Marks of adhered TH12G are visible in the image.



Figure 117. CrNi-pin after Test 3

An area analysis, marked with a rectangular in Figure 119, of the pin confirms the adhering of the Stellite onto the pin, so that wear couple has transformed from CrNi vs Co-alloy into Co-alloy vs Co-alloy at some point of the test. Similar behavior is observed as in Test 2 and mass loss results also support this. Material worn from the disc has adhered into pin and thus the mass loss is not as great as in Test 1. The results of EDS-analysis are shown in Table 34.

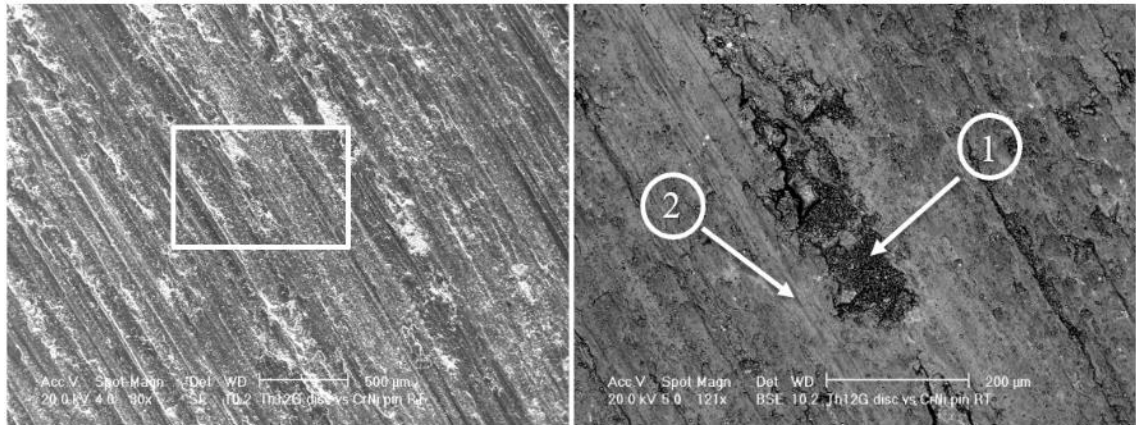


Figure 118. SEM-images of CrNi-pin after Test 3

Table 34. Results of EDS-analysis on CrNi-pin after Test 3

Element (wt%)	Si	Cr	Mn	Fe	Co	W	O	Ni
Point 1.	0.9	24.7	0.4	3.7	47.9	6.2	9.4	6.9
Point 2.	0.7	28.8	0.5	3.7	46.4	3.8	5.5	10.7
Area	1.1	41.1	0.3	2.2	26.0	-	5.8	23.6

9.5.4 Co-alloy disc (CMT) vs. Co-alloy pin (CMT), 300 °C

The test at high temperature was able to run for only a short amount of time. The results of this short wear test are presented in Figure 120. The average COF is 0.253, which is significantly lower than the COF in RT (0.281) in the same period with the same materials. It seems that the coating has a different kind of behavior in higher temperature. A logarithmic trendline has been fitted into the graph and forecasted after the test seized. The forecast may not be reliable, as the wear behavior of the material might change after a certain period. In the test at RT, the COF seems to level after 1-2 hours of testing.

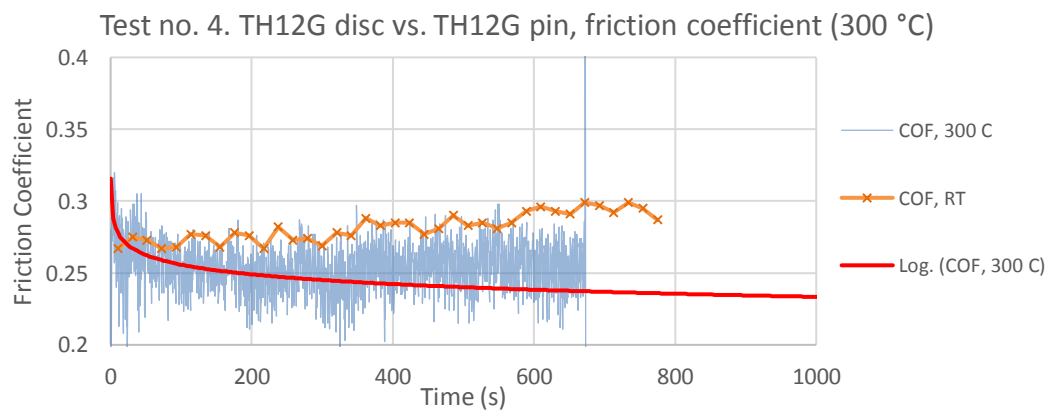


Figure 119. Coefficient of friction over time, Test 4

At elevated temperature, the clad seems to have a different behavior at the wear tests, at least if conclusions can be drawn from the results gained from the beginning of the test. The wear track shows signs of plastic deformation (Fig. 121 and 122) and perhaps even signs of adhered metal from the pin. Unfortunately, longer test period would be needed to thoroughly compare these results to the results from tests at RT. The oxidation layers on top of tungsten could not be found.

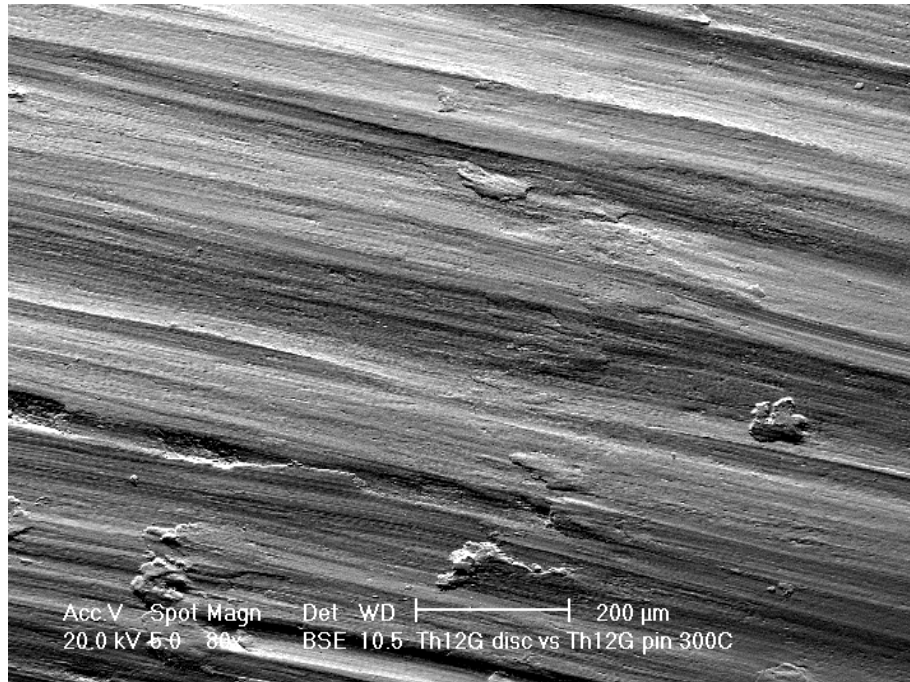


Figure 120. SEM-image of wear track, Test 4

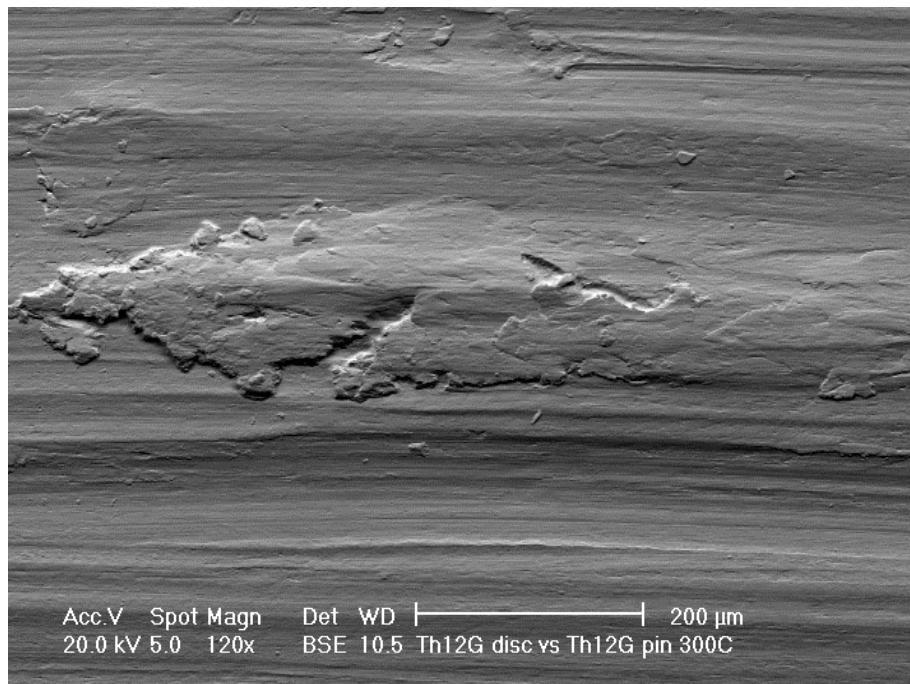


Figure 121. SEM-image of wear track, Test 4

The wear track of Test 4 was presented in Figure 104. The TH12G-pin is presented in Figure 123.

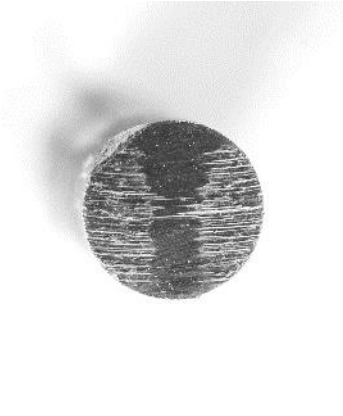


Figure 122. SEM-image of the TH12G-pin after Test 4

Figure 124 presents the movement of the pins in vertical axis over time. At the beginning of the tests, the slopes are a bit steeper, meaning higher volumetric wear losses in all test pairs. After about 0.5 hour, the slopes begin to even and the rates normalize and follow near linear paths. The linear paths are almost parallel with Test 2 and Test 3, while Test 1 follows a slightly steeper line. The COF-values support these results, as in Test 1, the COF was significantly higher than in Test 2 and 3.

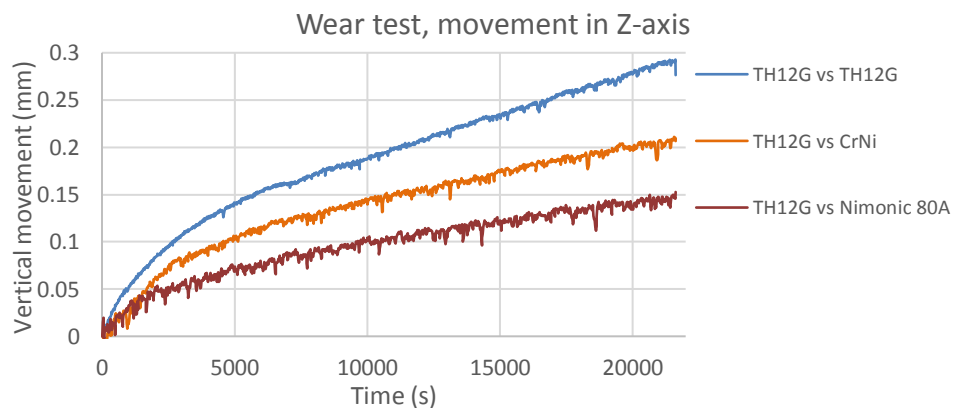


Figure 123. Transfer of the wear pins in Z-axis

Table 35 presents a short summary of the wear test results. Relative wear rate has been calculated by the mass loss of each pin and disc, the pair in Test 1 being the reference with value 1.0. Work-hardening rate has been calculated via the change of surface hardness of the wear surfaces.

Table 35. Summary of the sliding wear test results

		Test 1.	Test 2.	Test 3.	Test 4.*
COF		0.329	0.280	0.284	0.253
Relative wear rate	<i>Pin</i>	1.0	0.44	0.38	-
	<i>Disc</i>	1.0	1.49	1.47	-
Work-hardening	<i>Pin</i>	+58 %	+22 %	+47 %	+63 %
	<i>Disc</i>	+15 %	+2.5 %	+3.6 %	+11 %
Transfer in Z-axis	<i>Pin</i>	0.29 mm	0.15 mm	0.21 mm	-

*test time was remarkably shorter; not comparable results

9.6 Further Actions

Parameter optimization and cladding of actual engine components with multiple overlapping beads is one agenda after this thesis. Sliding wear tests on solid lubricant impregnated clads need to be done, in order to find out if the particles found inside the clad have any effect on wear and friction of the materials. If they have a positive effect on the wear characteristics, the result may result in other ways to impregnate the lubricants into the clad. Also, the present size of tungsten and chromium particles inside the Co-alloy wire needs to be decreased in order to melt them, to further improve the quality of the coatings.

To investigate the true behavior of the coatings in the actual application inside the engine, sliding wear tests need to be run at higher temperatures, as wear behavior might be completely different in e.g. 300 °C than in RT. XRD-analysis of the wear components would verify the phase transformation from fcc to hcp structure.

High-speed videos of cored wire cladding would show the behavior of the droplet, as it might differ greatly from solid wires. Some videos have been recorded during our studies, but the quality is still insufficient for a proper analysis.

10. CONCLUSIONS

The goal of this thesis was to investigate if CMT-cladding is suitable in producing low-dilution coating on materials used in diesel engines. The suitability of a cored filler wire with CMT-process has not been studied to my knowledge, and therefore this study meets a certain demand. Optical microscopy (OM), scanning electron microscopy (SEM), hardness measurements, X-Ray Diffraction (XRD) and Energy-Dispersive X-Ray Spectroscopy (EDS) were exploited in investigating the clad specimens. Sliding wear tests with pin-on-disk (POD) equipment were run on different material pairs. Another area of interest was to bring high temperature solid lubricant particles into the clad to reduce wear in the components. In this study, the lubricant particles were sprayed with a powder feeder into the melt pool during cladding.

It was discovered that CMT is able to produce a low-diluted coating (<5 %) with a proper hardness (450-500 HV₁). The fusion bond is strong and HAZ remains very narrow. The base materials remained distortion-free so as the clads, even with no preheating. The quality of the coatings was comparable to those manufactured with more expensive methods like laser-cladding or PTA. The dilution can be controlled with different process parameters and synergic lines. CMT attenuates problems occurring with traditional arc-welding/cladding methods, such as high amount of spattering and high heat input. To manufacture more homogenous clad, the size of the tungsten and chromium particles inside the wire needs to be reduced. Currently, they remain unmelted. Higher heat input melts these particles, but similarly the dilution rate would rise and the hardness is decreased with more iron content in the clad.

The problem that was encountered was the leaking of the cored wire into the wire conductors. This issue may cause problems like difficulties of the wire movement or even stoppage of the whole process. After longer cladding sessions the wire conductors needed to be removed and cleaned with pressurized air to ensure the proper movement of the wire. Quite a lot of black powder came out of the conductor when cleaned. To solve this problem, different type of drive rolls and decrease of drive roll pressure might help. Drive rolls designed for cored wires do exist, but in this thesis normal rolls were used. Normal drive rolls might cause distortion in the shape of the wire and open up the seam a bit making it leak.

Sliding wear tests were run to determine the wear behavior of the clads produced with CMT. The work-hardening ability of Stellite was clearly visible, as hardnesses of wear surfaces increased up to 58 % (TH12G –pin) at RT and 63 % at 300 °C. This happens via the structural changes from fcc to hcp structure of cobalt. Some oxidizing of the unmelted

tungsten particles was observed during the wear tests. Sliding wear tests in higher temperatures also need to be run to predict the behavior of the material in the actual application inside the engines. The tests at RT are insufficient by themselves.

The impregnation of solid lubricants into the clads was successful when utilizing high-energy ball milling powder preparation, but the results of their effect on wear remain for future studies.

REFERENCES

- [1] B.G. Mellor, R.J.K. Wood, N.M. Jennett, M.G. Gee, P.H. Shipway, D.W. Wheeler, et al., *Surface Coatings for Protection Against Wear*, Woodhead Publishing and Maney Publishing, Cambridge, England, 2006.
- [2] A. Tahaei, F.G. Vazquez, M. Merlin, A. Arizmendi-morquecho, F. Arturo, R. Valdes, et al., "Metallurgical Characterization of a Weld Bead Coating Applied by the PTA Process on the D2 Tool Steel", Vol. 21, 2016, pp. 209–219.
- [3] T.P. Hasselberg, "A Feasibility Study of "Cold Metal Transfer"–Gas Metal Arc Welding", 2009.
- [4] D.B. Holliday, Volume 6: Welding, Brazing, and Soldering, in: *ASM Handbook*, ASM International, 1993.
- [5] S.S. Glickstein, E. Friedman, R.P. Martukanitz, Volume 6A: Welding Fundamentals and Processes, in: *ASM Handbook*, ASM International, 2011.
- [6] J. Lukkari, *Opetushallitus, Hitsaustekniikka*, 4., Edita Prima Oy, Helsinki, 2002.
- [7] A. Scotti, V. Ponomarev, W. Lucas, "A scientific application oriented classification for metal transfer modes in GMA welding", *Journal of Materials Processing Technology*. Vol. 212, 2012, pp. 1406–1413.
- [8] F. Armao, L. Byall, D. Kotecki, D. Miller, *Gas Metal Arc Welding Guide*, 2014.
- [9] K. Weman, *Welding Processes Handbook*, Second Edi, Woodhead Publishing Limited, Stockholm, 2012.
- [10] Oy AGA Ab, T. Kuusisto, *Käytännön ohjeita MIG/MAG-hitsaukseen*, 2014.
- [11] N. Pépe, S. Egerland, P.A. Colegrove, D. Yapp, A. Leonhartsberger, A. Scotti, "Measuring the Process Efficiency of Controlled Gas Metal Arc Welding Processes", *Science and Technology of Welding & Joining*. Vol. 16, 2011, pp. 412–417.
- [12] Oy AGA Ab, *AGA Shielding Gases Handbook (Finnish)*, 2013.
- [13] P.F. Mendez, N. Barnes, K. Bell, S.D. Borle, S.S. Gajapathi, S.D. Guest, et al., "Welding processes for wear resistant overlays", *Journal of Manufacturing Processes*. Vol. 16, 2014, pp. 4–25.
- [14] Department of Trade and Industry, *Wear Resistant Surfaces in Engineering - a guide to their production, properties and selection*, Her Majesty's Stationery Office, Crown copyright, London, 1986.
- [15] M.M. Quazi, M.A. Fazal, A.S.M.A. Haseeb, F. Yusof, H.H. Masjuki, A. Arslan, "A Review to the Laser Cladding of Self-Lubricating Composite Coatings", *Lasers in Manufacturing and Materials Processing*. 2016, pp. 1–33.

- [16] J. Nurminen, "LasERPinnOitus Laitteistot , menetelmä , pinnoitteet ja käyttökohteet",n.d.
- [17] M. Zhong, W. Liu, "Laser surface cladding: the state of the art and challenges", *Proceedings of the Institution of Mechanical Engineers, Part C: Journal of Mechanical Engineering Science*. Vol. 224, 2010, pp. 1041–1060.
- [18] A. Barroi, J. Hermsdorf, U. Prank, S. Kaielerle, "Lasers in Manufacturing Conference 2013 A novel approach for high deposition rate cladding with minimal dilution with an arc - laser process combination",Vol. 41, 2013, pp. 249–254.
- [19] J. Tuominen, Engineering Coatings by Laser Cladding – The Study of Wear and Corrosion Properties, Ph.D Dessertation, 2009.
- [20] J. Tuominen, J. Näkki, H. Pajukoski, T. Nyssönen, T. Ristonen, T. Peltola, et al., "High Performance Wear and Corrosion Resistant Coatings by Novel Cladding Techniques", *Surface Modification Technologies XXVIII*. n.d., pp. 13.
- [21] GERMAN DEVELOPMENT SERVICE, "Gas Tungsten Arc Welding – GTAW – (40 Hours Course)", 2000.
- [22] E. Stephan, Z. Johannes, B. Roland, N. Roland, P. Gerhard, R. Bernd, "Advanced Gas Tungsten Arc Weld Surfacing Current Status and Application", *Soldagem & Inspeção*. Vol. 20, 2015, pp. 300–314.
- [23] B.K. Henon, *Advances in Automatic Hot Wire GTAW (TIG) Welding*, 2010.
- [24] R. Shanmugam, N. Murugan, "Effect of gas tungsten arc welding process variables on dilution and bead geometry of Stellite 6 hardfaced valve seat rings", *Surface Engineering*. Vol. 22, 2006, pp. 375–383.
- [25] A. Kyröläinen, J. Lukkari, *Ruostumattomat teräkset ja niiden hitsaus, 2., Metalliteollisuuden Keskusliitto, MET, Jyväskylä, 1999.*
- [26] L. Fouilland, M. El Mansori, A. Massa, "Friction-induced work hardening of cobalt-base hardfacing deposits for hot forging tools", *Journal of Materials Processing Technology*. Vol. 209, 2009, pp. 3366–3373.
- [27] L. Fouilland, M. El Mansori, M. Gerland, "Role of welding process energy on the microstructural variations in a cobalt base superalloy hardfacing", *Surface and Coatings Technology*. Vol. 201, 2007, pp. 6445–6451.
- [28] A. Motallebzadeh, E. Atar, H. Cimenoglu, "Sliding wear characteristics of molybdenum containing Stellite 12 coating at elevated temperatures", *Tribology International*. Vol. 91, 2015, pp. 40–47.
- [29] G. Lorenzin, G. Rutili, "The innovative use of low heat input in welding : experiences on “ cladding ” and brazing using the CMT process",Vol. 7116, 2016.
- [30] Fronius, "Cold Metal Transfer", 2014, pp. 16.
- [31] Y. Huang, "Control of Metal Transfer at Given Arc Variables", 2011.

- [32] Fronius, "Fronius RCU 5000 Operating Manual", n.d.
- [33] J. Pesonen, CMT-TEKNOLOGIA ROBOTTI- HITSUKSESSA, Savonia School of Applied Science, 2015.
- [34] P. Kah, R. Suoranta, J. Martikainen, "Advanced gas metal arc welding processes", *The International Journal of Advanced Manufacturing Technology*. Vol. 67, 2012, pp. 655–674.
- [35] B. Cong, J. Ding, S. Williams, "Effect of arc mode in cold metal transfer process on porosity of additively manufactured Al-6.3%Cu alloy", *International Journal of Advanced Manufacturing Technology*. Vol. 76, 2014, pp. 1593–1606.
- [36] Fronius International GmbH, "CMT Process - Training documentation", 2013.
- [37] Toolec Inc., Fronius CMT Cold Metal Transfer, web page. (Accessed 10/2016) Available: <http://www.toolec.com.ph/products/high-technology-welding-welding/fronius-cmt-cold-metal-transfer>.
- [38] O.T. Ola, F.E. Doern, "A study of cold metal transfer clads in nickel-base INCONEL 718 superalloy", *Materials and Design*. Vol. 57, 2014, pp. 51–59.
- [39] C.G. Pickin, S.W. Williams, M. Lunt, "Characterisation of the cold metal transfer (CMT) process and its application for low dilution cladding", *Journal of Materials Processing Technology*. Vol. 211, 2011, pp. 496–502.
- [40] G.P. Rajeev, M. Kamaraj, S.R. Bakshi, "Al-Si-Mn Alloy Coating on Aluminum Substrate Using Cold Metal Transfer (CMT) Welding Technique", Vol. 66, 2014, pp. 1061–1067.
- [41] M. ROZMUS-GÓRNIKOWSKA, Ł. Cieniek, M. Blicharski, J. KUSIŃSKI, "MICROSTRUCTURE AND MICROSEGREGATION OF AN INCONEL 625 WELD OVERLAY PRODUCED ON STEEL PIPES BY THE COLD METAL TRANSFER TECHNIQUE", *Archives of Metallurgy and Materials*. Vol. 59, 2014.
- [42] H. Zhang, S. Hu, Z. Wang, Y. Liang, "The effect of welding speed on microstructures of cold metal transfer deposited AZ31 magnesium alloy clad", *JMADE*. Vol. 86, 2015, pp. 894–901.
- [43] Y. Liang, S. Hu, J. Shen, H. Zhang, P. Wang, "Geometrical and microstructural characteristics of the TIG-CMT hybrid welding in 6061 aluminum alloy cladding", *Journal of Materials Processing Technology*. Vol. 239, 2017, pp. 18–30.
- [44] J.C. Dutra, R.H.G. e Silva, C. Marques, A.B. Viviani, "A new approach for MIG/MAG cladding with Inconel 625", *Welding in the World*. 2016.
- [45] P. Praveen, P.K.D.V. Yarlagadda, M.J. Kang, "Advancements in pulse gas metal arc welding", *Journal of Materials Processing Technology*. Vol. 164–165, 2005, pp. 1113–1119.
- [46] R. Lewis, Wear of diesel engine inlet valves and seats, University of Sheffield,

2000.

- [47] P. Forsberg, P. Hollman, S. Jacobson, "Wear mechanism study of exhaust valve system in modern heavy duty combustion engines", *Wear*. Vol. 271, 2011, pp. 2477–2484.
- [48] Institute of Marine Engineers, Diesel Engine Combustion Chamber Materials For Heavy Fuel Operation, the Institute of Marine Engineers by Marine Management (Holdings) Ltd, London, UK, 1990.
- [49] S.K. Schaefer, J.M. Larson, L.F. Jenkins, Y. Wang, Evolution of heavy duty engine valves - materials and design, in: ASM International, Materials Park, OH (United States), Dearborn, MI (United States), 1997, pp. 129–139.
- [50] J. Tuominen, M. Honkanen, M. Uusitalo, S. Ahmaniemi, P. Vuoristo, T. Mäntylä, "Hot Corrosion Resistant Laser Coatings in Diesel Engine", *Solutions*. 2007, pp. 1099–1104.
- [51] N. Eliaz, G. Shemesh, R.M. Latanision, "Hot corrosion in gas turbine components", *Engineering Failure Analysis*. Vol. 9, 2002, pp. 31–43.
- [52] D. Morehouse, J. Porter, J. Hiltz, M. Brauss, Diesel engine valve failures, Virginia Beach, Virginia, USA, 2002.
- [53] M.N. Task, B. Gleeson, F.S. Pettit, G.H. Meier, "The effect of microstructure on the type II hot corrosion of Ni-base MCrAlY alloys", *Oxidation of Metals*. Vol. 80, 2013, pp. 125–146.
- [54] K. Aeberli, Experience with Sulzer Common-Rail Engines, 25th Motorship Marine Propulsion Conference, Hamburg, Germany, 2003.
- [55] H. Fellmann, T. Gross, T. Ludwig, Typical wear mechanism of 2-stroke exhaust valves, in: Proceedings of the Marine Propulsion Conference, Amsterdam, Netherlands, 2004.
- [56] D. Kaufman, "Understanding Valve Design and Alloys", *Engine Builder Magazine*. n.d.
- [57] S. Kapoor, High-Temperature Hardness and Wear Resistance of Stellite Alloys, Carleton University, Ottawa, Ontario, 2012.
- [58] N. Gilbert, "Stellite Alloys - Chemical Composition , Mechanical Properties and Common Applications Introduction to Stellite Alloys Typical Chemical Properties of Stellite Alloys", 2013, pp. 1–3.
- [59] S. Kapoor, R. Liu, X.J. Wu, M.X. Yao, "Temperature-Dependence of Hardness and Wear Resistance of Stellite Alloys", *World Academy of Science, Engineering and Technology*. Vol. 67, 2012, pp. 964–973.
- [60] I.A. Inman, S.R. Rose, P.K. Datta, "Studies of high temperature sliding wear of metallic dissimilar interfaces II: Incoloy MA956 versus Stellite 6", *Tribology International*. Vol. 39, 2006, pp. 1361–1375.

- [61] Y. Birol, "High temperature sliding wear behaviour of Inconel 617 and Stellite 6 alloys", *Wear*. Vol. 269, 2010, pp. 664–671.
- [62] K. Miyoshi, "Solid Lubricants and Coatings for Extreme Environments: State-of-the-Art Survey", 2007, pp. 1–23.
- [63] Tribology-ABC, Solid Lubricants / Dry Lubrication, web page. (Accessed 06/2016) Available: <http://www.tribology-abc.com/abc/solidlub.htm>.
- [64] A. Erdemir, "Chapter 22: Solid Lubricants and Self-Lubricating Films", 2001.
- [65] J. Xu, W. Liu, M. Zhong, "Microstructure and dry sliding wear behavior of MoS₂/TiC/Ni composite coatings prepared by laser cladding", *Surface and Coatings Technology*. Vol. 200, 2006, pp. 4227–4232.
- [66] T.W. Scharf, S. V. Prasad, "Solid lubricants: A review", *Journal of Materials Science*. Vol. 48, 2013, pp. 511–531.
- [67] M.S. Yang, X.B. Liu, J.W. Fan, X.M. He, S.H. Shi, G.Y. Fu, et al., "Microstructure and wear behaviors of laser clad NiCr/Cr₃C₂-WS₂ high temperature self-lubricating wear-resistant composite coating", *Applied Surface Science*. Vol. 258, 2012, pp. 3757–3762.
- [68] Y. Kimura, T. Wakabayashi, K. Okada, T. Wada, H. Nishikawa, "Boron nitride as a lubricant additive", *Wear*. Vol. 232, 1999, pp. 199–206.
- [69] H. Yan, a. H. Wang, X.L. Zhang, Z.W. Huang, W.Y. Wang, J.P. Xie, "Nd:YAG laser cladding Ni base alloy/nano-h-BN self-lubricating composite coatings", *Materials Science and Technology*. Vol. 26, 2010, pp. 461–468.
- [70] S. Zhang, J. Zhou, B. Guo, H. Zhou, Y. Pu, J. Chen, "Friction and wear behavior of laser cladding Ni/hBN self-lubricating composite coating", *Materials Science and Engineering A*. Vol. 491, 2008, pp. 47–54.
- [71] S. Zhang, J. Zhou, B. Guo, H. Zhou, Y. Pu, J. Chen, "Friction and Wear Behavior of Laser Cladding NiAl / hBN Self-Lubricating Composite Coating", *Materials Science and Engineering A*. Vol. 1, 2008, pp. 47–54.
- [72] Y. Lei, R. Sun, Y. Tang, W. Niu, "Microstructure and phase transformations in laser clad CrxSy/Ni coating on H13 steel", *Optics and Lasers in Engineering*. Vol. 66, 2015, pp. 181–186.
- [73] M.J. Chao, E.J. Liang, "Effect of TiO₂-doping on the microstructure and the wear properties of laser-clad nickel-based coatings", *Surface and Coatings Technology*. Vol. 179, 2004, pp. 265–271.
- [74] M.N. Gardos, "Magnéli phases of anion-deficient rutile as lubricious oxides. Part I. Tribological behavior of single-crystal and polycrystalline rutile (Ti_nO_{2n-1})", *Tribology Letters* 8. Vol. 8, 2000, pp. 65–78.
- [75] O. Storz, H. Gasthuber, M. Woydt, "Tribological properties of thermal-sprayed Magnéli-type coatings with different stoichiometries", *Surface and Coatings*

Technology. Vol. 140, 2001, pp. 76–81.

- [76] P. Skarvelis, G.D. Papadimitriou, M. Perraki, "Self Lubricating Composite Coatings Containing TiC–MnS or WC–MnS Compounds Prepared by the Plasma Transferred Arc (PTA) Technique", *Journal of Tribology*. Vol. 132, 2010, pp. 031302–031302.
- [77] P. Skarvelis, G.D. Papadimitriou, "Plasma transferred arc composite coatings with self lubricating properties, based on Fe and Ti sulfides: Microstructure and tribological behavior", *Surface and Coatings Technology*. Vol. 203, 2009, pp. 1384–1394.
- [78] A. Liersch, H. Danninger, R. Ratzi, "THE INFLUENCE OF ADMIXED INORGANIC ADDITIVES ON PROPERTIES AND MACHINABILITY OF SINTERED PLAIN IRON AND STEELS", Vol. 4, 2004, pp. 192–203.
- [79] L. Zuomin, T.H.C. Childs, "The influence of TiC, CaF₂ and MnS additives on friction and lubrication of sintered high speed steels at elevated temperature", Vol. 193, 1996, pp. 31–37.
- [80] J.D. Bolton, a J. Gant, "Fracture in ceramic-reinforced metal matrix composites based on high-speed steel", *Journal of Materials Science*. Vol. 33, 1998, pp. 939–953.
- [81] Z.F. Xiang, X.B. Liu, J. Ren, J. Luo, S.H. Shi, Y. Chen, et al., "Investigation of laser cladding high temperature anti-wear composite coatings on Ti6Al4V alloy with the addition of self-lubricant CaF₂", *Applied Surface Science*. Vol. 313, 2014, pp. 243–250.
- [82] H.M. Wang, Y.L. Yu, S.Q. Li, "Microstructure and tribological properties of laser clad CaF₂/Al₂O₃ self-lubrication wear-resistant ceramic matrix composite coatings", *Scripta Materialia*. Vol. 47, 2002, pp. 57–61.
- [83] W.G. Liu, X.B. Liu, Z.G. Zhang, J. Guo, "Development and characterization of composite Ni-Cr-C-CaF₂ laser cladding on gamma-TiAl intermetallic alloy", *Journal of Alloys and Compounds*. Vol. 470, 2009, pp. 25–28.
- [84] X.B. Liu, S.H. Shi, J. Guo, G.Y. Fu, M. Di Wang, "Microstructure and wear behavior of ??/Al₄C₃/TiC/CaF₂ composite coating on ??-TiAl intermetallic alloy prepared by Nd:YAG laser cladding", *Applied Surface Science*. Vol. 255, 2009, pp. 5662–5668.
- [85] Kennametal Stellite, "Stellite 21 Alloy Datasheet", 2013.
- [86] M. Rupponen, KAKSIVAIHEINEN LASERPINOITUS (Preplaced Laser Cladding), Tampere University of Technology, 2008.
- [87] Fronius, CMT- Some like it cold, web page. (Accessed 07/2016) Available: http://www.fronius.com/cps/rde/xchg/SID-3FA6C90E-12B3CA32/fronius_international/hs.xsl/79_11528_ENG_HTML.htm#.V5XnWnqtr-U.

- [88] Fronius, TransPuls Synergic 4000 R, web page. (Accessed 07/2016) Available: http://www.fronius.com/cps/rde/xchg/SID-702D443A-5CDB1E5A/fronius_international/hs.xsl/79_6265_ENG_HTML.htm#.V5Xnk3qr-U.
- [89] Struers, "MD-System The unique consumables for materialographic grinding and polishing", n.d.
- [90] National Science Foundation, Geochemical Instrumentation and Analysis - Energy-Dispersive X-Ray Spectroscopy (EDS), web page. (Accessed 11/2016) Available: http://serc.carleton.edu/research_education/geochemsheets/eds.html.
- [91] PANalytical, X-ray diffraction, web page. (Accessed 11/2016) Available: <http://www.panalytical.com/Xray-diffraction.htm>.
- [92] National Science Foundation, Geochemical Instrumentation and Analysis - X-ray Powder Diffraction (XRD), web page. (Accessed 11/2016) Available: http://serc.carleton.edu/research_education/geochemsheets/techniques/XRD.html.
- [93] FINFOCUS INSTRUMENTS OY, Kovuusmittaus Vickers (SFS-EN ISO 6507-1), Helsinki, n.d.
- [94] M. Alizadeh, Hardness Test, web page. (Accessed 07/2016) Available: http://me.aut.ac.ir/staff/solidmechanics/alizadeh/Hardness_Test.htm.
- [95] F.E. Kennedy, Y. Lu, I. Baker, "Contact temperatures and their influence on wear during pin-on-disk tribotesting", *Tribology International*. Vol. 82, 2015, pp. 534–542.
- [96] ESAB, ESAB - MIG Handbook - Undercutting, web page. (Accessed 12/2016) Available: http://www.esabna.com/euweb/mig_handbook/592mig10_5.htm.

APPENDIX A. MINUTES OF CLADDING TESTS, STELLITE 21

Sample	Material	Base Material	Method	Bead	Wirefeed	A/C	DC Voltage (V)	DC Current (A)	Stick-out	Protective Gas	Gas Flow	Synergic line	Beads	Bead length	Inter-track distance	Travel speed	Wear shape	Wear Type	Wear length	Wear width	
ST21-001	ST21	304L (150x150mm, 113mm)	CMT	Stringer	8.0mm/min	-30%	-5	10.3V	134A	Ar	15l/min	CMT (1291) Stellite 211.2mm DB M03-Q271	1	100	2 mm	13.3mm/s	0		2	12	
ST21-002	ST21	304L (150x150mm, 113mm)	CMT	Stringer	8.0mm/min	-30%	-5	10.3V	137A	Ar	15l/min	CMT (1291) Stellite 211.2mm DB M03-Q271	4	100	2 mm	13.3mm/s	0		2	12	
								9.9V	137A												
								9.6V	134A												
ST21-003	ST21	420Mcd (0.120, 150mm)	CMT	Stringer	8.0mm/min	-30%	-5	10.4	137A	Ar	15l/min	CMT (1291) Stellite 211.2mm DB M03-Q271	1	60	2.5 mm	13.3mm/s	0		2	12	
ST21-005	ST21	420Mcd (0.120, 150mm)	CMT	Stringer	8.0mm/min	-30%	-5	10.9	132	Ar	15l/min	CMT (1291) Stellite 211.2mm DB M03-Q271	4	60	2.5 mm	10.0mm/s	0		2	12	
								10.3	135												
								10.2	133												
								9.9	131												
ST21-006	ST21	420Mcd (0.120, 150mm)	CMT	Stringer	8.0mm/min	-30%	-5	10.3	137	Ar	15l/min	CMT (1291) Stellite 211.2mm DB M03-Q271	4	60	3.0 mm	10.0mm/s	0		2	12	
								10.3	137												
								10.3	137												
								10.2	137												
ST21-007	ST21	420Mcd (0.120, 150mm)	CMT	Stringer	8.0mm/min	-30%	-5	10.2	136	Ar	15l/min	CMT (1291) Stellite 211.2mm DB M03-Q271	4	60	3.0 mm	12.0mm/s	0		2	12	
								9.9	130												
								9.9	136												
								10.3	133												
PWM 10.5.2016 (001-007)																					
ST21-008	ST21	420Mcd (0.120, 150mm)	CMT	Weaving	5.0mm/min	-30%	-5	9.3V	139A	Ar	15l/min	CMT (1291) Stellite 211.2mm DB M03-Q271	1	60	3.5mm/s	1		2	12		
ST21-009	ST21	420Mcd (0.120, 150mm)	CMT	Stringer	8.0mm/min	-30%	-5	10.9V	131A	Ar	15l/min	CMT (1291) Stellite 211.2mm DB M03-Q271	1	60	7.0mm/s	0		2	12		
ST21-010	ST21	420Mcd (0.120, 150mm)	CMT	Stringer	8.0mm/min	-30%	-5	9.9V	130A	Ar	15l/min	CMT (1291) Stellite 211.2mm DB M03-Q271	1	60	3.5mm/s	1		2	12		
PWM 13.5.2016 (008-011)																					
ST21-012	ST21	420Mcd (0.120, 150mm)	CMT	Weaving	5.0mm/min	-30%	-5	9.6	131	Ar	15l/min	CMT (1291) Stellite 211.2mm DB M03-Q271	3	60	10 mm	3.5mm/s	1		2	12	
								9.2	139												
								9.3	139												
ST21-013	ST21	Nimonic 80A (0.63, 130mm)	CMT	Weaving	5.0mm/min	-30%	-5	9.3	138	Ar	15l/min	CMT (1291) Stellite 211.2mm DB M03-Q271	1	40	3.5mm/s	1		2	12		
ST21-014	ST21	X20Cr13 (0.100, 130mm)	CMT	Weaving	5.0mm/min	-30%	-5	9.6	161	Ar	15l/min	CMT (1291) Stellite 211.2mm DB M03-Q271	1	60	10 mm	3.5mm/s	1		2	12	
ST21-015	ST21	X20Cr13 (0.100, 130mm)	CMT	Weaving	5.0mm/min	-30%	-5	9.4	161	Ar	15l/min	CMT (1291) Stellite 211.2mm DB M03-Q271	2	60	10 mm	3.5mm/s	1		2	12	
								9.6	160												
PWM 16.5.2016 (012-015)																					
ST21-016	ST21	420Mcd (0.120, 150mm)	CMT	Weaving	5.0mm/min	-30%	-5	9.1	160	Ar	15l/min	CMT (1291) Stellite 211.2mm DB M03-Q271	1	80	10 mm	3.5mm/s	1		2	12	
ST21-017	ST21	420Mcd (0.120, 150mm)	CMT	Weaving	5.0mm/min	0%	-5	11.1	137	Ar	15l/min	CMT (1291) Stellite 211.2mm DB M03-Q271	1	40	10 mm	3.5mm/s	1		2	12	
ST21-018	ST21	420Mcd (0.120, 150mm)	CMT	Weaving	5.0mm/min	30%	-5	11.5	141	Ar	15l/min	CMT (1291) Stellite 211.2mm DB M03-Q271	1	80	10 mm	3.5mm/s	1		2	12	
ST21-019	ST21	420Mcd (0.120, 150mm)	CMT	Weaving	5.0mm/min	0%	-5	11.4	160	Ar	15l/min	CMT (1291) Stellite 211.2mm DB M03-Q271	2	80	10 mm	3.5mm/s	1		2	12	
								11.3	159												
ST21-020	ST21	420Mcd (0.120, 150mm)	CMT	Weaving	5.0mm/min	15%	-5	11.6	152	Ar	15l/min	CMT (1291) Stellite 211.2mm DB M03-Q271	2	80	10 mm	3.5mm/s	1		2	12	
								11.5	152												
ST21-021	ST21	Nimonic 80A (0.63, 130mm)	CMT	Weaving	5.0mm/min	0%	-5	11.1	137	Ar	15l/min	CMT (1291) Stellite 211.2mm DB M03-Q271	1	40	10 mm	3.5mm/s	1		2	12	
ST21-022	ST21	X20Cr13 (0.100, 130mm)	CMT	Weaving	5.0mm/min	0%	-5	11.1	139	Ar	15l/min	CMT (1291) Stellite 211.2mm DB M03-Q271	1	40	10 mm	3.5mm/s	1		2	12	
ST21-023	ST21	X20Cr13 (0.100, 130mm)	CMT	Weaving	5.0mm/min	0%	-5	11.1	160	Ar	15l/min	CMT (1291) Stellite 211.2mm DB M03-Q271	1	60	10 mm	3.5mm/s	1		2	12	
ST21-024	ST21	X20Cr13 (0.100, 130mm)	CMT	Weaving	5.0mm/min	30%	-5	12.4	139	Ar	15l/min	CMT (1291) Stellite 211.2mm DB M03-Q271	1	60	10 mm	3.5mm/s	1		2	12	
ST21-025	ST21	X20Cr13 (0.100, 130mm)	CMT	Weaving	5.0mm/min	0%	-5	11	159	Ar	15l/min	CMT (1291) Stellite 211.2mm DB M03-Q271	1	60	10 mm	3.5mm/s	1		2	16	

a) Minutes of ST21-001 to ST21-025

APPENDIX B. MINUTES OF CLADDING TESTS, CO-ALLOY

Sample	Material	Base Material	Method	Bead	Wire feed	ATC	DC Voltage (AV)	Current (AV)	Stick-out	Protective Gas	Gas flow	Spraying line	Beads	Bead length	Inter-track advance	Travel speed	Weave shape	Weave type	Weave length	Weave width
TH12G-001	Co-alloy	42CrMo4 (D130, 120mm)	CMT	Stringer	8.0m/min	-30%	236	242	17mm	Mison18	15l/min	FCW Handing (1357) (D8 0842)	1	70		13.3mm/s	0			
TH12G-002	Co-alloy	42CrMo4 (D130, 120mm)	CMT	Stringer	8.0m/min	-30%	256	239	17mm	Mison18	15l/min	FCW Handing (1357) (D8 0842)	5	70	3.5	13.3mm/s	0			
TH12G-003	Co-alloy	42CrMo4 (D130, 120mm)	CMT	Stringer	8.0m/min	-30%	256	237	17mm	Mison18	15l/min	G3S1 (1562) (D8 0842)	1	70		13.3mm/s	0			
TH12G-004	Co-alloy	42CrMo4 (D130, 120mm)	CMT	Stringer	8.5m/min	0%	20.9	212	17mm	Mison18	15l/min	G3S1 (1362) (D8 0842)	1	70		13.3mm/s	0			
TH12G-005	Co-alloy	42CrMo4 (D130, 120mm)	CMT	Stringer	1.0m/min	0%	9.5	61	17mm	Mison18	15l/min	G3S1 steel dynamic (1540) (D8 01-1387)	1	70		8.5mm/s	0			
TH12G-006	Co-alloy	42CrMo4 (D130, 120mm)	CMT	Stringer	1.0m/min	4%	9.4	60	17mm	Mison18	15l/min	G3S1 steel dynamic (1540) (D8 01-1387)	1	70		10mm/s	0			
TH12G-007	Co-alloy	42CrMo4 (D130, 120mm)	CMT	Stringer	1.0m/min	-17%	9	58	17mm	Mison18	15l/min	G3S1 steel dynamic (1540) (D8 01-1387)	1	70		12mm/s	0			
TH12G-008	Co-alloy	O-steel (D100, 130mm)	CMT	Stringer	9.5m/min	0%	213	214	17mm	Mison18	15l/min	G3S1 steel dynamic (1540) (D8 01-1387)	5	70	4	12mm/s	0			
TH12G-009	Co-alloy	O-steel (D100, 130mm)	CMT	Stringer	9.5m/min	0%	215	215	17mm	Mison18	15l/min	G3S1 steel dynamic (1540) (D8 01-1387)	3	70	4	16.7mm/s	0			
TH12G-010	Co-alloy	O-steel (D100, 130mm)	CMT	Stringer	9.5m/min	10%	20.6	215	17mm	Mison18	15l/min	G3S1 steel dynamic (1540) (D8 01-1387)	10	70	4	16.7mm/s	0			
TH12G-011	Co-alloy	S355 (D001-400, 115mm)	CMT	Weaving	5.0m/min	-30%	15.2	151	17mm	Mison18	15l/min	G3S1 steel dynamic (1540) (D8 01-1387)	1	70		3.5mm/s	1		2	12
TH12G-012	Co-alloy	S355 (D001-400, 115mm)	CMT	Weaving	5.0m/min	-30%	15.4	150	17mm	Mison18	15l/min	G3S1 steel dynamic (1540) (D8 01-1387)	1	70		3.5mm/s	1		2	14
TH12G-013	Co-alloy	S355 (D001-400, 115mm)	CMT	Weaving	5.0m/min	-30%	18.2	166	17mm	Mison18	15l/min	G3S1 (1562) (D8 01-1387)	1	70		3.5mm/s	1		2	14
TH12G-014	Co-alloy	O-steel (D100, 130mm)	CMT	Weaving	5.0m/min	-30%	17.2	168	17mm	Mison18	15l/min	G3S1 (1562) (D8 01-1387)	1	70		3.5mm/s	1		2	16
TH12G-015	Co-alloy	O-steel (D100, 130mm)	CMT	Weaving	5.0m/min	-30%	17.4	168	17mm	Mison18	15l/min	G3S1 (1562) (D8 01-1387)	1	70		3.5mm/s	1		2	16
TH12G-016	Co-alloy	S355 (D001-400, 115mm)	CMT	Weaving	5.0m/min	0%	15	155	17mm	Mison18	15l/min	G3S1 steel dynamic (1540) (D8 01-1387)	1	60		3.5mm/s	1		2	16
TH12G-017	Co-alloy	S355 (D001-400, 115mm)	CMT	Weaving	5.0m/min	30%	15	155	17mm	Mison18	15l/min	G3S1 steel dynamic (1540) (D8 01-1387)	1	70		3.5mm/s	1		2	16
TH12G-018	Co-alloy	S355 (D001-400, 115mm)	CMT	Weaving	5.0m/min	0%	15.1	144	17mm	Mison18	15l/min	G3S1 steel dynamic (1540) (D8 01-1387)	1	70		3.5mm/s	1		2	16
TH12G-019	Co-alloy	S355 (D001-400, 115mm)	CMT	Weaving	5.0m/min	0%	15.1	144	17mm	Mison18	15l/min	G3S1 steel dynamic (1540) (D8 01-1387)	1	70		3.0mm/s	1		2	16
TH12G-020	Co-alloy	S355 (D001-400, 115mm)	CMT	Weaving	5.0m/min	0%	15.3	156	17mm	Mison18	15l/min	G3S1 steel dynamic (1540) (D8 01-1387)	1	70		3.0mm/s	1		2	16
TH12G-021	Co-alloy	S355 (D001-400, 115mm)	CMT	Weaving	5.0m/min	15%	16.4	143	17mm	Mison18	15l/min	G3S1 steel dynamic (1540) (D8 01-1387)	1	70		3.0mm/s	1		2	16
TH12G-022	Co-alloy	S355 (D001-400, 115mm)	CMT	Weaving	5.0m/min	-15%	13.8	159	17mm	Mison18	15l/min	G3S1 steel dynamic (1540) (D8 01-1387)	1	70		3.0mm/s	1		2	16
TH12G-023	Co-alloy	O-steel (D100, 130mm)	CMT	Weaving	5.0m/min	0%	14.9	155	17mm	Mison18	15l/min	G3S1 steel dynamic (1540) (D8 01-1387)	1	70		3.0mm/s	1		2	16
TH12G-024	Co-alloy	O-steel (D100, 130mm)	CMT	Weaving	5.0m/min	0%	18.1	229	17mm	Mison18	15l/min	G3S1 steel dynamic (1540) (D8 01-1387)	1	70		3.0mm/s	1		2	16

a) Minutes of TH12G-001 to TH12G-024

TH12G-025	Co-alloy	Cr-steel (D100, 130mm) buidukas	CMT	Weaving	5.0m/min	0%	-5	12.2	149	17mm	Ar	15l/min	CMT(1291) Shellite 21.1 2mm DB M03-Q271	2	70			3.0mm/s	1	1	2	16
TH12G-026	Co-alloy	Cr-steel (D100, 130mm) buidukas	CMT	Weaving	5.0m/min	0%	-5	12	149	17mm	Ar	15l/min	CMT(1291) Shellite 21.1 2mm DB M03-Q271	1	50			3.0mm/s	1	1	2	16
TH12G-027	Co-alloy	Cr-steel (D100, 130mm)	CMT	Weaving	6.0m/min	0%	-5	12.6	171	17mm	Ar	15l/min	CMT(1291) Shellite 21.1 2mm DB M03-Q271	1	60			3.0mm/s	1	1	2	16
TH12G-028	Co-alloy	Cr-steel (D100, 130mm)	CMT	Weaving	6.0m/min	0%	-5	14	176	17mm	Mison2	15l/min	CMT(1657) Shellite 21.1 2mm DB 1006	1	60			3.0mm/s	1	1	2	16
TH12G-029	Co-alloy	Cr-steel (D100, 130mm)	CMT	Weaving	6.0m/min	0%	-5	12.7	186	17mm	Mison2	15l/min	CMT(1657) Shellite 21.1 2mm DB 1006	1	50			3.0mm/s	1	1	2	16
TH12G-030	Co-alloy	Cr-steel (D100, 130mm)	CMT	Weaving	6.0m/min	0%	-5	12.2	148	17mm	Mison2	15l/min	CMT(1656) Shellite 6.1 2mm DB 1006	1	60			3.0mm/s	1	1	2	16
TH12G-031	Co-alloy	Cr-steel (D100, 130mm)	CMT	Weaving	6.0m/min	0%	-5	12.2	148	17mm	Mison2	15l/min	CMT(1656) Shellite 6.1 2mm DB 1006	1	60			3.0mm/s	1	1	2	16
TH12G-032	Co-alloy	Cr-steel (D100, 130mm)	CMT	Weaving	6.0m/min	0%	-5	12.9	151	17mm	Mison2	15l/min	CMT(1653) Shellite 261 2mm DB 1006	1	60			3.0mm/s	1	1	2	16
TH12G-033	Co-alloy	Ni alloy (D63, 130mm)	CMT	Weaving	6.0m/min	0%	-5	14.8	154	17mm	Mison2	15l/min	CMT(1656) Shellite 6.1 2mm DB 1006	1	40			3.0mm/s	1	1	2	16
TH12G-034	Co-alloy	Ni alloy (D63, 130mm)	CMT	Weaving	6.0m/min	0%	-5	15.4	172	17mm	Mison2	15l/min	CMT(1657) Shellite 21.1 2mm DB 1006	1	40			3.0mm/s	1	1	2	16
PM 12.9.2016 (025-034)																						
TH12G-035	Co-alloy	42CrMo4 (D120, 120mm)	CMT	Weaving	6.0m/min	0%	-5	13.2	165	17mm	Mison2	15l/min	CMT(1656) Shellite 6.1 2mm DB 1006	10	80			3.5mm/s	1	1	2	12
								13.3	163													
								13.3	164													
								13.1	164													
								13.4	164													
								13.1	164													
								13.1	164													
								13.3	164													
								12.9	165													
								13.6	166													
PM 12.9.2016 (035)																						
TH12G-036	Co-alloy	42CrMo4 (D120, 120mm)	CMT	Weaving	6.0m/min	0%	-5	13.3	162	17mm	Mison2	15l/min	Shellite 6.1.2 (1656) (DB 1006)	1	60			3mm/s	1	1	2	12
TH12G-037	Co-alloy	42CrMo4 (D120, 120mm)	CMT	Weaving	6.0m/min	0%	-5	13.1	161	17mm	Mison2	15l/min	Shellite 6.1.2 (1656) (DB 1006)	1	60			3mm/s	1	1	2	12
PM 7.10.2016 (036-037)																						
TH12G-041	Co-alloy	Cr-steel (D100, 130mm)	CMT	Weaving	6.5m/min	0%	-5	16.4	172	17mm	Mison2	15l/min	Shellite 6.1.2 (1656) (DB 1006)	1	70			3mm/s	1	1	2	12
TH12G-042	Co-alloy	Cr-steel (D100, 130mm)	CMT	Weaving	6.5m/min	0%	-5	15.7	176	17mm	Mison2	15l/min	Shellite 6.1.2 (1656) (DB 1006)	1	70			3mm/s	1	1	2	12
TH12G-043	Co-alloy	Cr-steel (D100, 130mm)	CMT	Weaving	6.5m/min	0%	-5	17.2	172	17mm	Mison2	15l/min	Shellite 6.1.2 (1656) (DB 1006)	1	70			3mm/s	1	1	2	12
TH12G-044	Co-alloy	Cr-steel (D100, 130mm)	CMT	Weaving	6.5m/min	0%	-5	17.1	173	17mm	Mison2	15l/min	Shellite 6.1.2 (1656) (DB 1006)	1	70			3mm/s	1	1	2	12

b) Minutes of TH12G-025 to TH12G-044